DIVIDING ANNULAR/TWO-PHASE FLOW IN HORIZONTAL T-JUNCTIONS

By

JOHN D. BALLYK, B.Sc., B.Eng., M.Eng.

A Thesis

Submitted to the School of Graduate Studies

in Partial Fulfillment of the Requirements

for the Degree

Doctor of Philosophy

McMaster University

DIVIDING ANNULAR/TWO-PHASE FLOW IN HORIZONTAL T-JUNCTIONS

TO MY WIFE CATHERINE AND MY CHILDREN

LAURA, MATTHEW AND MARK

DOCTOR OF PHILOSOPHY (1992) McMASTER UNIVERSITY

(Mechanical Engineering) Hamilton, Ontario

TITLE: Dividing Annular/Two-Phase Flow in Horizontal T-Junctions

AUTHOR: John D. Ballyk, B.Sc. (Memorial University)
B.Eng. (Memorial University)
M.Eng. (McMaster University)

SUPERVISOR: Dr. M. Shoukri

NUMBER OF PAGES (xvii)170

ABSTRACT

The results of an experimental and analytical investigation of the separation phenomenon in dividing annular two-phase flow is presented. Detailed experiments have been carried out with a steam-water loop to isolate the effects of flow split, inlet quality, inlet mass flux and branch diameter on the phase and pressure distribution characteristics in horizontal T-junctions. Through the set of measurements made in the experimental program, the phase separation and pressure distribution characteristics were shown to be strongly interdependent. Based on these measurements, a physical model describing the phase separation mechanism is presented.

This physical model is then developed mathematically. A model to predict the dividing flow characteristics for annular flow in a T-junction is proposed consisting of mixture and vapor phase continuity equations, two pressure change correlations and a closure relationship. The pressure change from the inlet through the run of the T is modelled by way of a balance of axial momentum at the junction based on a separated flow assumption. The branch pressure change is modelled using a balance of mechanical energy for the branching flow consisting of reversible and irreversible components. In the development of the branch model, a new equivalent inlet density for the branching flow (ρ_1^*) and a two-phase multiplier (Φ^*) are defined. The closure relationship links the phase separation characteristics with the junction pressure changes. It involves a balance between pressure and inertia forces

within the junction volume defining a dividing surface for each phase between the run and branch flows. The degree of phase redistribution is then determined using a well defined inlet flow distribution.

The model is capable of predicting the experimentally observed phase separation characteristics from three independent studies of annular/steam-water and air-water flow in dividing T-junctions.

ACKNOWLEDGEMENTS

The patient guidance provided by Professor M. Shoukri throughout the course of this investigation is sincerely appreciated.

Sincere thanks are also extended to the graduate students and technical staff of the Department of Mechanical Engineering. The author is particularly grateful for the thoughtful dialogue with Dr. A. Abdul-Razzak.

The financial support of the Natural Sciences and Engineering Research Council of Canada and the Ontario Graduate Scholarship program is greatly appreciated.

The author is especially grateful to his wife, Catherine, and children, Laura, Matthew and Mark for their love and patience.

TABLE OF CONTENTS

TABLE OF CONTENTS (Continued)

TABLE OF CONTENTS(Continued)

NOMENCLATURE

A	= Cross sectional area	
A_{GE}	= Cross sectional area of gas extracted	
A_{LE}	= Cross sectional area of liquid extracted	
a	= Correlation parameter	(eqn. 2.38)
C	= Contraction coefficient	
D	= Diameter	
DLX	= Run development length	
DLY	= Branch development length	
E	= Equilibrium entrainment ratio	
$\dot{E}$	= Power	
F_d	= Volumetric interfacial drag force	
F_w	= Volumetric wall drag force	
G	= Mass flux	
h	= Enthalpy	
$h(\pi)$	= Bottom film thickness	
$h(\theta)$	= Angular film thickness distribution	
$h'(\theta)$	= Normalized angular film thickness distribution	
j	= Superficial velocity	
k_{1-2}	= Axial momentum correction factor	
$\bar{k}_{1-2}$	= Run loss coefficient	
k_{1-3}	= Branch loss coefficient	
$\dot{m}$	= Mass flow rate	
N	= Photon count	
P	= Pressure	
$(\Delta P_{2-1})_J$	= Run junction pressure differential	
$(\Delta P_{1-3})_J$	= Branch junction pressure differential	
R	= Radius	
s	= Correlation parameter	(eqn. 2.30)
S	= Slip ratio	
u	= Velocity (x-component)	

v = Velocity (y-component)

$\dot{V}$ = Volumetric flow rate

x = Quality

Subscripts

1 = Inlet

2 = Run

3 = Branch

a = Air

c = Condensate

cw = Cooling water

D = Downstream point of intersection of inlet and branch tubes

f = Film

f_c = Centripetal force per unit mass

g = Gas phase

H = Homogeneous

i = In

irrev = Irreversible

j = Junction

l = Liquid

m = Mixer

o = Out

rev = Reversible

s = Separated flow

t = Test section

w = water

Greek Symbols

α = Void fraction

β = Inlet angle of orientation w.r.t. horizontal

γ = Branch take-off angle w.r.t. the inlet axis

ϕ = Branch angle of orientation w.r.t. horizontal

Φ	= Branch two-phase multiplier	
θ	= Correlation parameter	(eqn. 2.1)
θ'	= Correlation parameter	(eqn. 2.34)
μ	= Dynamic viscosity	
π_2	= Correlation parameter	(eqn. 4.1)
ρ	= Density	
ρ'	= Momentum density	(eqn. 2.24)
ρ'''	= Energy density	(eqn. 2.22)
ρ^*	= Inlet density of branching flow	(eqn. 5.21)
σ	= Surface tension	

LIST OF FIGURES

LIST OF TABLES

CHAPTER 1

INTRODUCTION

When a two-phase flow is divided at a flow junction or within a manifold the phases can divide unevenly such that the qualities in the downstream legs are unequal. This phase redistribution and the associated pressure changes are important design criteria for many systems in the power and process industries. Some examples include; loss-of-coolant accident (LOCA) in nuclear reactor safety analysis, wet steam injection systems for enhanced oil recovery and the design of phase separators. Since the behavior of two-phase flows in such situations is not well understood, it is commonly assumed that the quality in all downstream legs of a manifold are equal and therefore equal to the inlet quality. Experimental evidence indicates that this assumption may be significantly in error under most flow conditions.

Experimental studies of this phenomena have shown it to be dependent on a broad range of both flow and geometrical parameters. The extent to which the phases separate can depend on flow regime, mass flux, quality and system pressure as well as branching conduit size, take off angle and orientation. To date, no general method or analytical approach has been advanced to predict the phenomena for parameter ranges extending beyond the data from which they were developed. Due to the large number of parameters involved, empirically based models would be impractical to develop. A more

realistic approach is to model the flow behavior by identifying the governing mechanisms, applying the appropriate conservation laws and closing with experimentally based constitutive relationships.

The present work represents an extension of the work initiated in the Master of Engineering program at McMaster University (Ballyk, 1986). The scope of the previous work included the commissioning of a steam/water loop to collect data on the separation and pressure distribution characteristics for steam/water annular flow in a horizontal T-junction with a branch to inlet diameter ratio of unity. In the present work, the number of test sections used is extended to a total of three representing branch to inlet diameter ratios of 1.0, 0.82 and 0.50. The data is also examined to obtain a physical description of the processes involved in the phase separation phenomenon. This physical model is then developed mathematically and the resultant mathematical model is used to predict the experimental data from the present work as well as that of other investigators. The thesis closes with recommendations for future experimental and analytical work.

CHAPTER 2

LITERATURE SURVEY

2.1 Introduction

Due to a broad range of applications and a relatively superficial understanding of the phenomena, a significant amount of research effort is currently being devoted to the study of two-phase flow division. Within the past few years many publications have appeared that address one or more aspects of this problem. These studies have shown that the separation phenomena results from a complex process involving many interdependent hydrodynamic and geometrical parameters.

Although steam and water is most often the gas/liquid combination of interest, most experimental studies have been carried out with air/water mixtures. These investigations have typically considered isolated T-junctions under fully developed conditions. It is hoped that the more complex geometries and flow conditions encountered in practice can be analyzed once the dominant mechanisms have been identified from these fundamental studies. In the following discussion, the nomenclature used will be as shown in Figure 2.1 with subscripts 1, 2 and 3 referring to the inlet, run and branch respectively. As shown in Figure 2.1, the general problem of flow in a piping junction involves a number of geometrical parameters. These include the inlet, run and branch diameters (D_1, D_2 and D_3 respectively), as

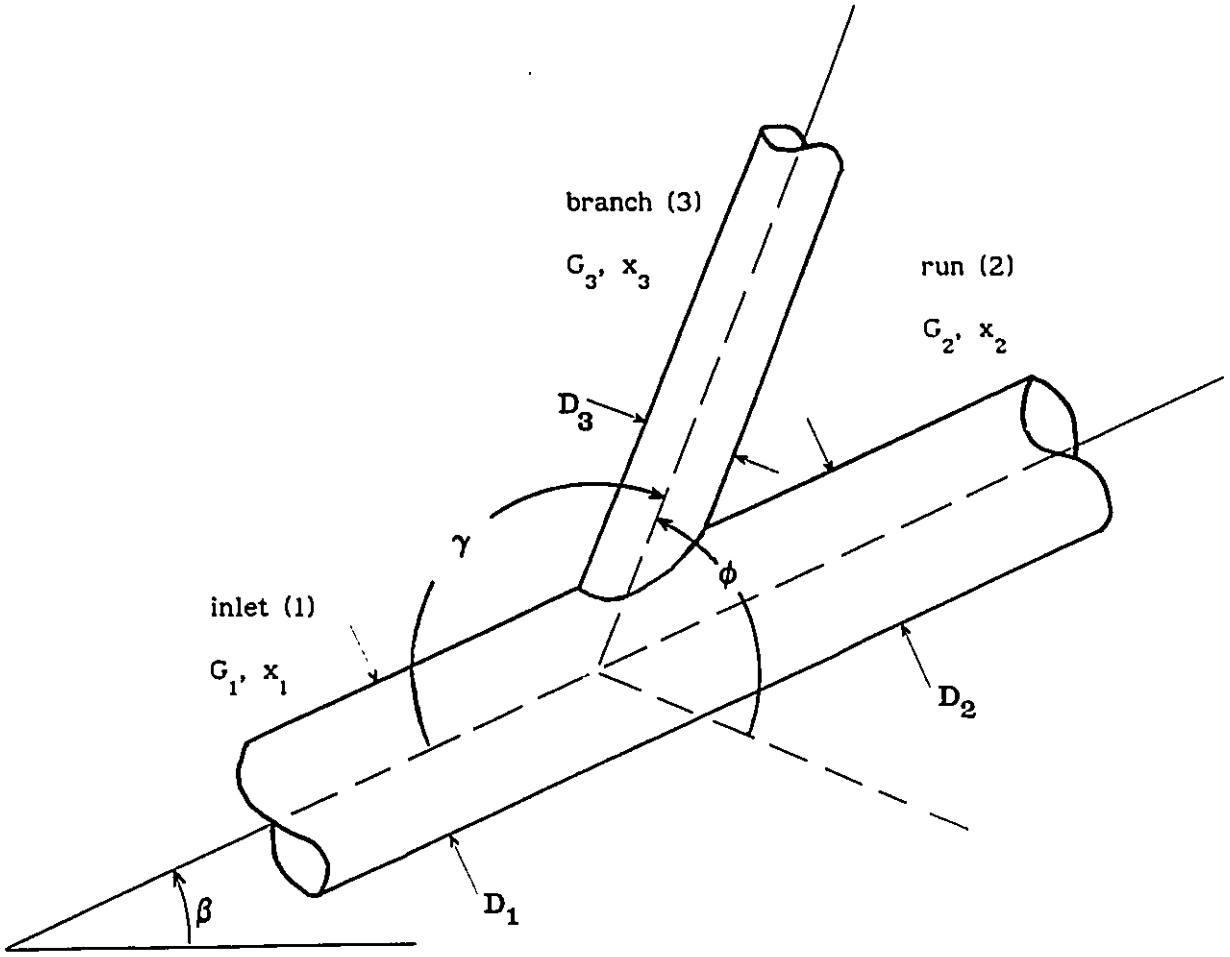

Figure 2.1 Nomenclature use for Two Phase Flow Division

well as the inlet and branch angles of orientation w.r.t. the horizontal (β and ϕ respectively) and the branch take-off angle w.r.t. the inlet axis (γ).

The characteristics of interest in the analysis of dividing two-phase flow are the pressure changes and the redistribution of phases that take place across a flow junction. Under most conditions, when a two-phase flow stream is divided at a junction, the phases will separate with the resultant qualities in the downstream legs varying from the inlet quality. This flow split and phase separation is also associated with junction pressure changes. In general the branching flow experiences a drop in pressure due to high irreversible losses while the remaining flow undergoes a pressure rise as it expands downstream of the junction.

Phase distribution data has typically been presented in two ways. The first is by plotting the fraction of liquid removed through the branch ($\dot{m}_3(1-x_3)/\dot{m}_1(1-x_1)$) against the fraction of gas removed ($\dot{m}_3 x_3/\dot{m}_1 x_1$) . Equal phase distribution ($x_1 = x_2 = x_3$) is then represented by the diagonal corresponding to equal fractions of each phase removed. Figure 2.2 shows a schematic representation of preferential gas and preferential liquid extraction plotted in this manner. The second method is to plot the ratio of branch to inlet quality (x_3/x_1) against the total flow fraction removed through the branch (flow split, $\dot{m}_3/\dot{m}_1$) as shown in Figure 2.3. Equal phase distribution is then represented by the horizontal line at $x_3/x_1 = 1.0$. The complete vapour extraction curve is generated by considering all of the gas phase to be removed through the branch before any of the liquid is extracted. When the value of the flow split is below that of the inlet quality ($\dot{m}_3/\dot{m}_1 < x_1$) complete vapour extraction corresponds to the horizontal line $x_3/x_1 = 1/x_1$ (i.e. $x_3 = 1.0$). When the flow split is above the inlet quality, a mass

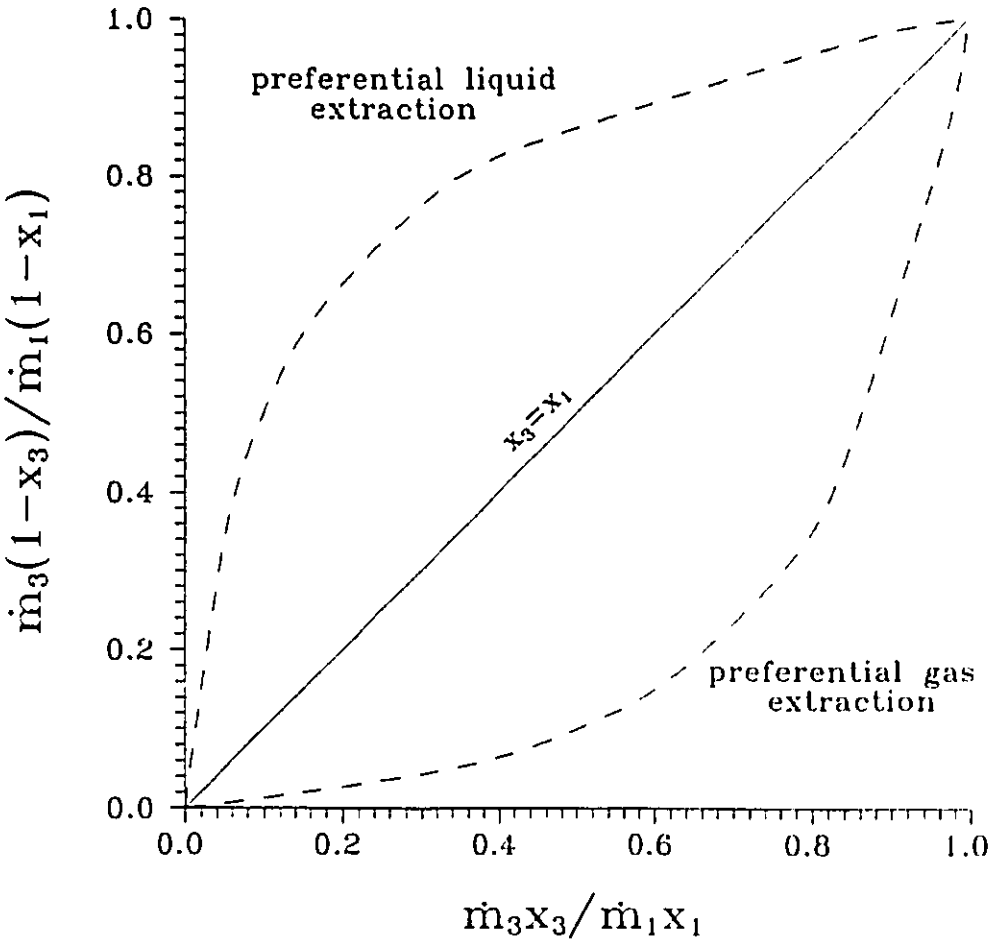

Figure 2.2 Fraction of Liquid Removed Through the Branch versus the Fraction of Gas Removed

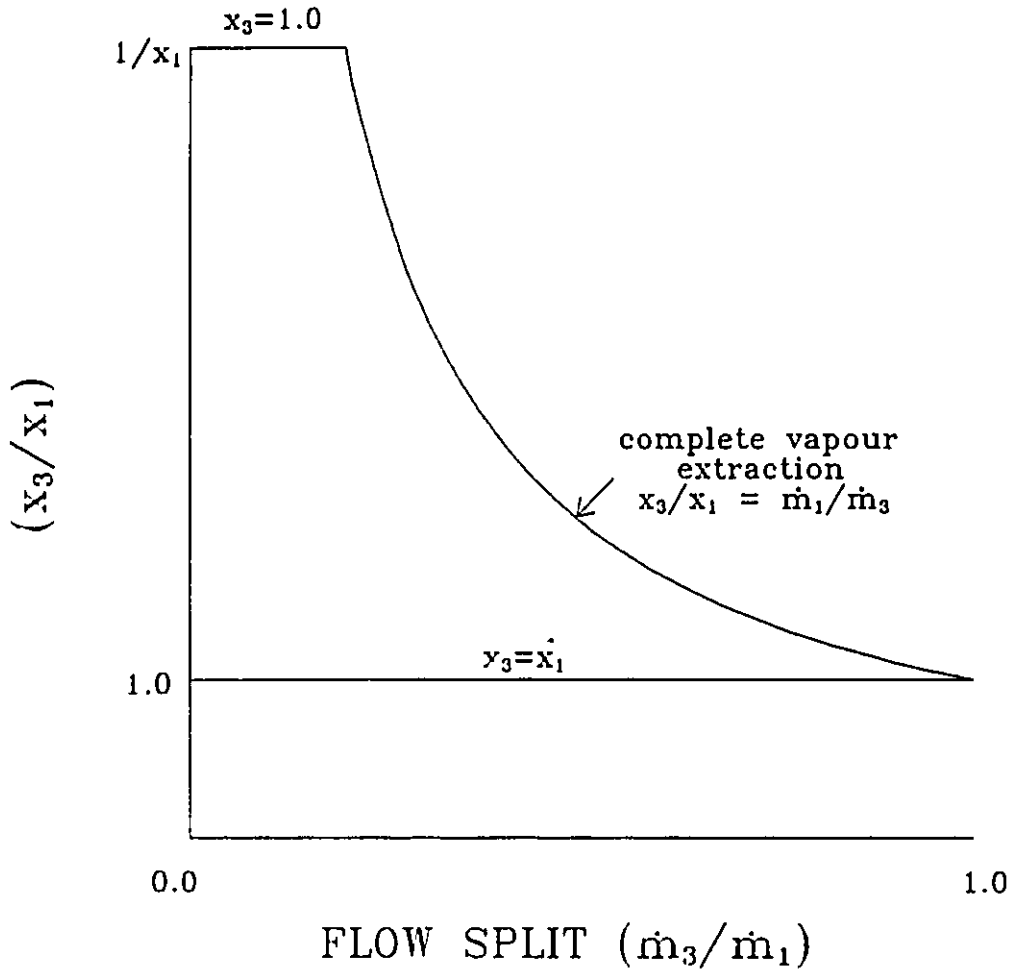

Figure 2.3 Ratio of Branch to Inlet Quality versus Flow Split

balance shows that complete vapour extraction is represented by the inverse of the flow split (i.e. $x_3/x_1 = \dot{m}_1/\dot{m}_3$). When all of the inlet flow is removed through the branch, the branch and inlet qualities are equal, corresponding to the point (1,1) in the Figure.

A typical pressure distribution within a dividing T-junction is shown schematically in Figure 2.4. Measurements are made by way of pressure taps located along each leg of the test section. By extrapolating the fully developed pressure profile in each leg to the junction, the pseudo axial pressure rise, $(\Delta P_{2-1})_j$, and branch pressure drop, $(\Delta P_{1-3})_j$, are obtained as shown.

2.2 Experimental Investigations

Results from one of the early investigations of the separation phenomenon in horizontal T-junctions were presented by Collier (1976). Air-water data for an inlet mass flux of 136 kg/m^{2}s and inlet qualities in the range of 0.02-0.50 were presented. The inlet section was 38 mm I.D. and diameter ratios (D_3/D_1) of 0.667 and 0.333 were used. The data showed significant phase redistribution at the junction with the branching flow receiving most of the gas phase ($x_3 > x_1$). Only for a small portion of inlet conditions and very low flow splits ($\dot{m}_3/\dot{m}_1 < 0.10$) was the branch quality seen to be below that of the inlet. For the higher inlet qualities ($x_1 > 0.25$) separation effects became less severe with increasing quality. This trend reversed for lower inlet qualities. This variation is most likely a flow regime effect.

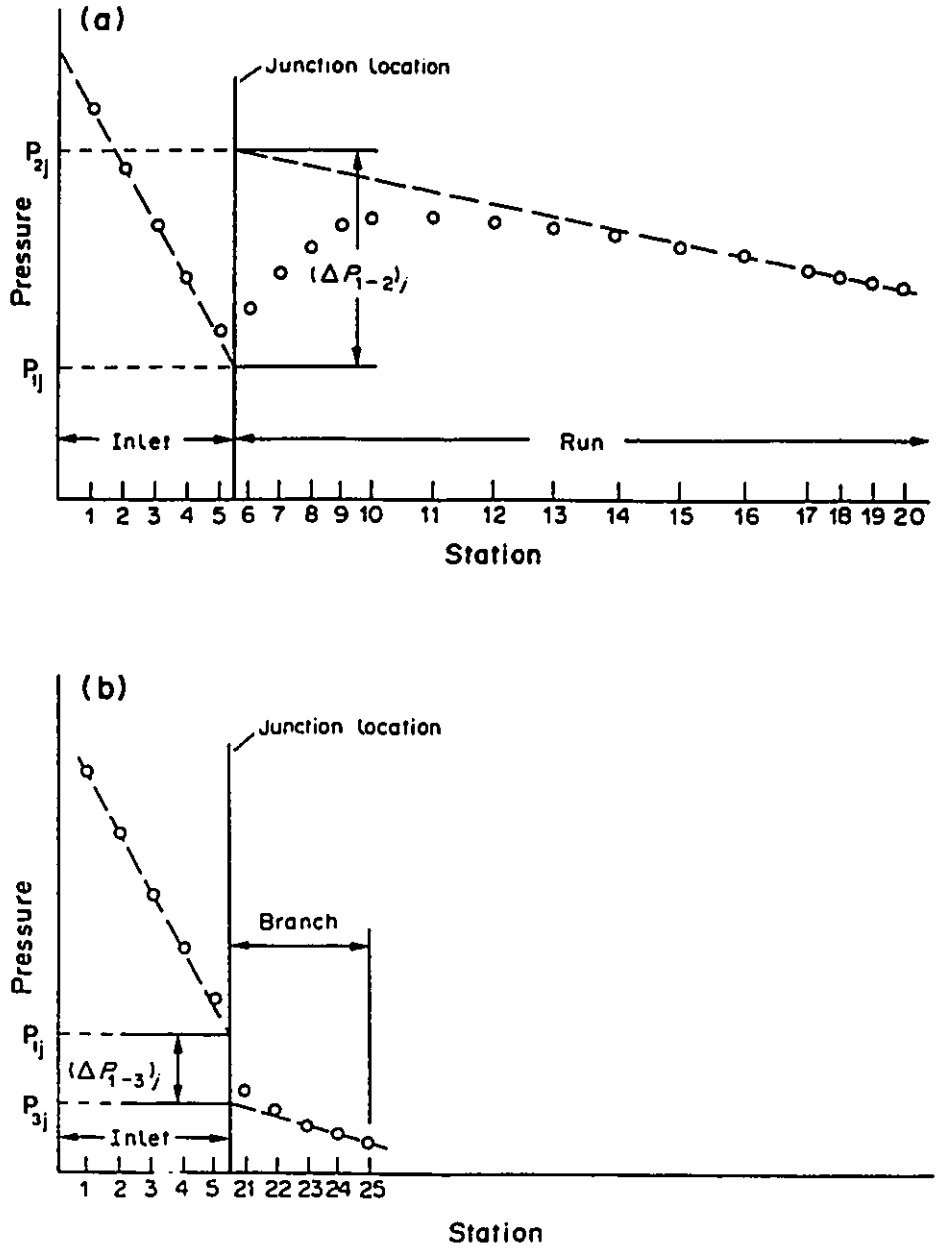

Figure 2.4 Schematic Diagram of a Typical Pressure Distribution in Dividing Flow: (a) Run Pressure Differential $(\Delta P_{2-1})_j$; (b) Branch Pressure Differential $(\Delta P_{1-3})_j$

Hong (1978) presented air/water data in the mass flux and quality ranges of 17-124 kg/m^2s and 0.25-0.97 respectively. The inlet section was horizontal and both branch and inlet were 9.5 mm I.D. Experiments were performed to isolate the effects of inlet flow regime, liquid phase viscosity, branch attitude and the gas and liquid superficial velocities. The data presented showed trends opposite to those of Collier (1976) with the branching flow taking most of the liquid phase. The author also reported no apparent effect of inlet flow regime. Johansen (1979) also examined air/water separation in a horizontal T-junction in the ranges $69 < G_1 < 841$ kg/m^2s and $0.5 < x_1 < 1.0$, covering the stratified to annular flow regimes. His results showed both of the previous trends dependent upon the inlet mass flux. Inlet flow regime effects were not considered.

Honan and Lahey (1980) conducted an air/water investigation with a vertical inlet section and equal branch and inlet diameters (38 mm). In this study, the effects of branch take-off angle (45, 90 and 135^{o}), inlet quality ($0.001 \leq x_1 \leq 0.01$) and inlet mass flux ($1357 \leq G_1 \leq 2714$ kg/m^2s) were considered for bubbly and churn turbulent inlet flows. No less than 30% of the inlet flow was removed through the branch. All experiments showed preferential gas extraction through the branch. The authors reported that the effect of inlet quality was significant with more separation occurring at higher inlet qualities. This supports the lower quality results presented by Collier (1976). The branch take-off angle and inlet mass flux had no apparent effect on the degree of phase separation measured.

Henry (1981) investigated the separation phenomena for annular air/water flow in a horizontal test section with a branch to inlet diameter ratio of 0.2. His data were in the mass flux and quality ranges of $200 \leq G_1 \leq$

850 kg/m^{2}s and 0.1 $\leq x_1 \leq$ 0.6. The data, however, covered a very low range of flow split ratio ($\dot{m}_3/\dot{m}_1 \leq$ 0.06). For this range of flow split, the branch liquid flow rate varied approximately linearly with the branch gas flow rate. The extrapolated data indicated that some limiting value of liquid flow rate could be established in the branch when the branch gas flow rate is reduced to zero. The author suggested that this resulted from the portion of liquid film flowing on the wall of the inlet tube that is intercepted by the branch opening being the first component of flow to be extracted. The data also exhibited trends similar to those presented by Collier (1976) as the separation effects became less severe with increasing inlet quality.

Whalley and Azzopardi (1980) performed experiments on vertical and horizontal T-junctions with air/water annular flow. The inlet tube was 31.8 mm I.D. and the branch tube measured 12.7 mm I.D. ($D_3/D_1 = 0.4$). At most, approximately 20% of the inlet air flow was removed through the branch. Much of the data showed the branch quality below the inlet quality. Supplementary experiments were carried out to measure the film flow rates for each of the inlet conditions tested in vertical flow. The authors found a linear relationship between the air and water removal rates as well as an extrapolated liquid removal rate through the branch for zero gas removal. These findings support those of Henry (1981). An angle, θ, was defined to express the angle over which the liquid film must be removed to generate the branching liquid flow, i.e.

$$\theta = \frac{360(\text{water flow rate in side tube})}{\text{total film flow rate}} \qquad (2.1)$$

or

$$\theta = \frac{360\dot{m}_3(1-x_3)}{\dot{m}_1(1-E)(1-x_1)} \tag{2.2}$$

where E represents the equilibrium entrainment ratio in the inlet tube. For vertical flow, an approximately linear relationship was also found between θ and and the portion of air entering the side tube ($\dot{m}_3 x_3/\dot{m}_1 x_1$).

Azzopardi and Whalley (1982) extended the vertical experiments to include diameter ratios (D_3/D_1) of 0.2 and 0.6. For the larger diameter ratio, up to approximately 70% of the inlet air flow was removed through the branch. Further experiments were performed with churn flow in the inlet section. The authors reported almost a straight line relationship between θ (Equation [2.2]) and the air mass flux in the branch, neglecting data points from inlet conditions with very low film flow rates. The results for churn flow were consistent with the annular flow data when an equivalent film flow rate could be defined.

The authors suggested that the local momentum flux of a fluid (ρu^2) is a measure of its resistance to being diverted to the branch. In annular flow it is then the low momentum flux fluids (gas core; low density, high velocity and liquid film; high density, low velocity) that are most easily diverted to the branch. The momentum flux of the entrained droplets is too high (high density, high velocity) to be readily extracted.

Saba and Lahey (1984) performed air/water experiments in a horizontal T-junction of equal diameters using three values of mass flux, G_1= 1355, 2041 and 2711 kg/m^{2}s and low inlet qualities ($x_1 \leq$ 0.01). These conditions favored stratified and slug flow conditions at the inlet. No less than 30% of the total inlet flow was removed through the branch. These

experiments included measurements of the junction pressure changes determined by the method outlined in Section 2.1. The data presented showed preferential air removal typically in the range of complete vapour extraction.

Seeger et al. (1986) presented data from a T-junction with a horizontal inlet and equal inlet and branch diameters ($D_1 = D_2 = D_3 = 50$ mm). The branch was orientated systematically downward, upward and horizontally. Measurements were made over a broad range of inlet flow conditions and branch flow splits ($\dot{m}_3/\dot{m}_1$) for both air/water and steam/water flow. Simultaneous measurements of the junction pressure changes were also made. The downward branch, in general, showed preferential water removal at low flow splits where gravity effects favor liquid removal by distributing more of the liquid phase on the bottom of the inlet tube. This causes more of the liquid flow to be intercepted by the branch opening enhancing its removal. Under some conditions, particularly at high flow splits, the branch quality was above the inlet quality as the inertia effects became more important. The upward orientated branch yielded severe phase separation (preferential gas extraction) which was relatively independent of the inlet conditions. This is expected since both gravity and inertia act to inhibit liquid removal. The results for the horizontal branch showed preferential gas removal, though not as severe as the vertical branch data. Total separation was approached for high values of branch flow split. The branch quality generally peaked at flow splits ($\dot{m}_3/\dot{m}_1$) of approximately 0.3. The degree of phase separation decreased for both increasing superficial gas velocity and increasing pressure. Both of these conditions correspond to increasing gas phase momentum flux. The resultant decrease in separation is consistent with the

mechanism suggested by Azzopardi and Whalley (1982). No specific difference between air/water and steam/water results were noted.

Rubel (1986, 1988) presented low pressure steam/water data for a horizontal T-junction covering the stratified and wavy flow regimes. He observed the branch quality to be lower than the inlet quality for stratified flow and generally above the inlet quality for wavy and semi-annular flows within the ranges tested.

2.3 Analytical Models

2.3.1 Introduction

Lahey (1986) showed that the various models proposed for quantifying the characteristics of dividing two-phase flow can be considered in terms of the model format used by Saba and Lahey (1982, 1984). That is, describing the complete phenomena for a given junction geometry requires eight parameters to be determined. These are; the mass fluxes in each leg (G_1, G_2, G_3), the qualities in each leg (x_1, x_2, x_3) and the two junction pressure changes, $(\Delta P_{2\text{-}1})_j$ and $(\Delta P_{1\text{-}3})_j$. Three of these must be specified as independent variables or boundary conditions, the remaining five are then dependent variables. Five independent equations are then required to ensure closure. These equations have typically taken the following form;

i) The mixture continuity equation

ii) The vapour phase continuity equation

iii) A run pressure change correlation

iv) A branch pressure change correlation

v) A closure relationship

The mixture and vapour phase continuity equations are respectively,

$$\dot{m}_1 = \dot{m}_2 + \dot{m}_3 \tag{2.3}$$

and, assuming no phase changes

$$\dot{m}_1 x_1 = \dot{m}_2 x_2 + \dot{m}_3 x_3 \ . \tag{2.4}$$

These are straight forward and need not be considered further. The remaining three equations will be discussed in detail in the following sections

2.3.2 Run Pressure Change Correlations

When a single-phase or two-phase flow is divided in a T-junction, the flow in the axial direction through the run of the T experiences a rise in pressure. This results from the diversion of a portion of the flow to the branch and the subsequent deceleration of the remaining flow through the run. For a dividing T-junction, a single-phase axial (x-directed) momentum balance for the control volume shown in Figure 2.5 may be written as

$$\int_{A_1} P_{1j} dA - \int_{A_2} P_{2j} dA = \int_{A_2} \rho u_x u_x dA + \int_{A_3} \rho u_x u_y dA - \int_{A_1} \rho u_x u_x dA, \tag{2.5}$$

where P_{1j} and P_{2j} are the junction inlet and run pressures and u_x and u_y represent the local axial (x-directed) and branching (y-directed) velocities of the fluid. If the inlet and run have equal areas ($A_1 = A_2 = A$) where the average fluid properties are assumed to define the flow, the momentum balance becomes

$$(\Delta P_{2-1})_j = P_{2j} - P_{1j} = \rho(u_1^2 - u_2^2) - \frac{1}{A} \int_{A_3} \rho u_x u_y dA \tag{2.6}$$

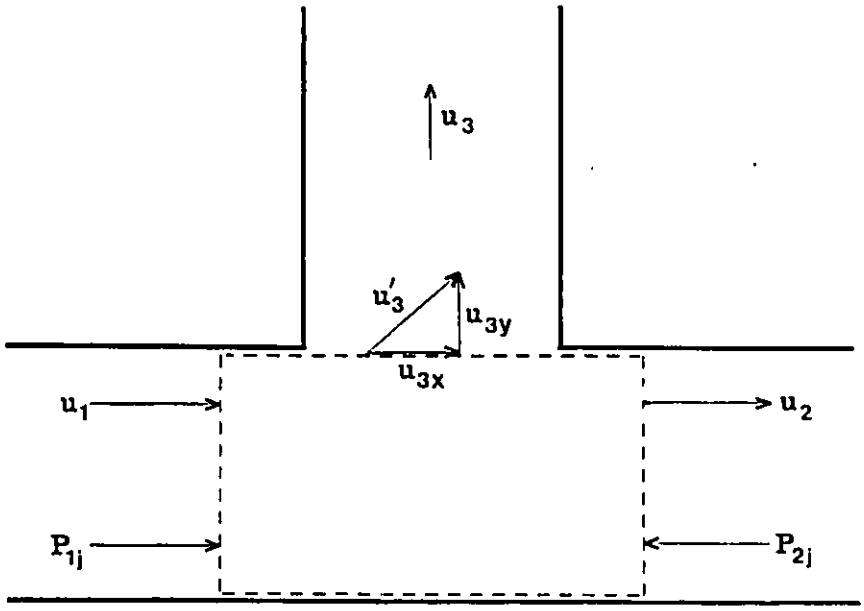

Figure 2.5 Junction Control Volume for Momentum Based Run Pressure Change Correlations

Here, u_1 and u_2 are the average inlet and run velocities respectively. The first term on the r.h.s. of Equation [2.6] accounts for the axial momentum change across the junction while the second term accounts for the axial momentum carried out of the control volume with the branching flow. This term is indeterminate since the value of u_x cannot be estimated. For single-phase flow, this equation is usually simplified to

$$(\Delta P_{2-1})_J = k_{1-2}\rho(u_1^2 - u_2^2) \tag{2.7}$$

where the momentum correction factor (k_{1-2}) accounts for the axial momentum of the branching flow. The value of (k_{1-2}) is generally determined experimentally for a given junction geometry.

Consider an extreme case where the branching flow loses all of its axial momentum before being removed through the branch. Under these conditions, u_x is zero everywhere on A_3 and the momentum correction factor (k_{1-2}) has a value of unity. The other extreme case would have the branching flow losing none of its axial momentum before being extracted through the branch. Fouda (1975) suggested that under these conditions the following mass balance would apply

$$\rho u_y dA = -\rho A du_x. \tag{2.8}$$

Solving for k_{1-2} between Equations [2.6], [2.7] and [2.8] yields an axial momentum correction factor of 0.5 independent of the flow split ($\dot{m}_3/\dot{m}_1$). The author then suggests that the value of k_{1-2} should normally fall between 1.0 and 0.5. Values outside this range have been widely reported in the literature (McNown (1954), Reimann and Seeger (1986), Ballyk et al. (1988)). This suggests that the mass balance of [2.8] may not be valid.

If the extreme case of no loss of axial momentum for the branching

flow is interpreted as $u_x = u_1$ everywhere on A_3, then

$$\frac{1}{A}\int_{A_3}\rho u_x u_y dA = \frac{A_3}{A}\rho u_1 u_3. \tag{2.9}$$

The average branch velocity can be determined from the flow split and area ratio as,

$$u_3 = \frac{\dot{m}_3 A}{\dot{m}_1 A_3}\, u_1. \tag{2.10}$$

Substituting [2.9] and [2.10] into [2.6], the momentum correction factor can be determined from [2.7] as

$$k_{1-2} = 1 - \frac{1}{2 - \dot{m}_3/\dot{m}_1}. \tag{2.11}$$

Most of the published data for single-phase dividing flow yields momentum correction factors with values bounded by Equation [2.11] (no loss of axial momentum) and unity (complete loss of axial momentum).

Alternatively, a loss coefficient, $\bar{k}_{1-2}$, can be defined based on a mechanical energy balance between the inlet and run of the T accounting for reversible and irreversible pressure changes, i.e.

$$(\Delta P_{2-1})_J = P_{2J} - P_{1J} = \frac{\rho}{2}(u_1^2 - u_2^2) - \bar{k}_{1-2}\frac{\rho}{2}u_1^2. \tag{2.12}$$

The first term on the r.h.s. of Equation [2.12] is the reversible run pressure rise and the second term is the irreversible pressure loss modelled in terms of a loss coefficient ($\bar{k}_{1-2}$) acting on the inlet dynamic head.

Another method for correlating the run pressure change was used by Reimann and Seeger (1986). This method is also based on defining two components of change from the inlet through the run of the T. The first component is a reversible pressure change from the inlet to the throat of a

vena contracta located in the run downstream of the junction. The second is an irreversible loss from the vena contracta to a position downstream where the flow is fully developed. This term is modelled in terms of a sudden expansion. For single-phase incompressible flow, with a run contraction coefficient (C_2) representing the area ratio between the vena contracta and the inlet section, the pressure change is derived as

$$(\Delta P_{2\text{-}1})_j = \frac{1}{2}\left(\frac{G_1^2}{\rho} - \frac{G_2^2}{\rho}\right) - \left(\frac{1}{C_2} - 1\right)^2 \frac{G_2^2}{2\rho}. \qquad (2.13)$$

When this equation is compared with the previous single-phase Equations, ([2.7] & [2.12]), it is apparent that it is only capable of correlating flow conditions yielding momentum correction factors ($k_{1\text{-}2}$) less than 0.5 or positive values for the run loss coefficient ($\bar{k}_{1\text{-}2}$). Experimentally determined values outside these constraints are well reported in the literature.

These single-phase models have been extended to two-phase flows in various ways. By considering a two phase flow to be a homogeneous mixture in which the phases have equal velocities, the homogeneous mixture density (ρ_H) and velocity (u_H) may be written as

$$\rho_H = \frac{\rho_G \rho_L}{x\rho_L + (1-x)\rho_G} \qquad (2.14)$$

and

$$u_H = \frac{G}{\rho_H} \qquad (2.15)$$

respectively where G is the total mass flux. These can be combined with the axial momentum balance, Equation [2.7], to generate a homogeneous model for the run pressure rise, i.e.,

$$(\Delta P_{2-1})_j = k_{(1-2)H} \left[(\rho_H u_H^2)_1 - (\rho_H u_H^2)_2\right], \tag{2.16}$$

where $k_{(1-2)H}$ is the homogeneous momentum correction factor.

By considering the momentum of each phase separately at the control volume boundaries and introducing $k_{(1-2)S}$, the separated flow momentum correction factor, the momentum balance becomes

$$(\Delta P_{2-1})_j = k_{(1-2)S} \left[\left(\frac{G_1^2 x_1}{\rho_G \alpha_1} + \frac{G_1^2 (1-x_1)^2}{\rho_L (1-\alpha_1)} \right) - \left(\frac{G_2^2 x_2}{\rho_G \alpha_2} + \frac{G_2^2 (1-x_2)^2}{\rho_L (1-\alpha_2)} \right)\right]. \tag{2.17}$$

Here, the average velocities of each phase are assumed to be characteristic of the flow and are determined through the void fraction (α).

Madden and St. Pierre (1969/70) carried out air/water experiments on a vertical slot type distributor with various slot to inlet area ratios (0.0255 - 0.619). Inlet conditions were varied over the ranges $271 \leq G_1 \leq 678$ kg/m^{2}s and $0.2 \leq x_1 \leq 0.7$ at approximately 340 kPa favoring annular inlet flows. The axial pressure rise across the slot was determined by an extrapolation technique similar to that described in section 2.1. The data was reduced in terms of the separated flow model (Equation [2.17]) with the required void fractions determined from the Lockhart-Martinelli correlation. The value of the separated flow momentum correction factor was seen to be approximately unity independent of the slot geometry. This suggests that the axial momentum of the branching flow is insignificant relative to the momentum change across the junction.

Fouda (1975) and Fouda and Rhodes (1974) investigated annular air/water flow in a 50.8 mm diameter inlet tube with a 25.4 mm vertical branch. The data obtained was reduced by way of both the homogeneous and

separated flow models. The authors suggested that the separated flow model (Equation [2.17]) be used for simple T-junctions with a momentum correction factor $k_{(1-2)S}$=0.533. It should be noted that the axial pressure rise was not determined by an extrapolation technique but from a pair of pressure taps, one upstream and one downstream of the junction. Depending upon the tap locations, the measured pressure rise can be quite arbitrary and will always be underestimated. This is the most likely source of the discrepancy.

Saba and Lahey (1982, 1984) conducted air/water experiments with low quality ($x_1 \leq 0.01$) stratified and slug flow conditions in a horizontal T-junction. The axial pressure rise data was reduced in terms of run linear momentum equations very similar to Equations [2.16] and [2.17]. The authors reported good agreement between the experimental data and the homogeneous model with a correction factor ($k_{(1-2)H}$) equal to the single-phase correction factor (k_{1-2}) determined experimentally from the corresponding single-phase equation. The value of k_{1-2} obtained from their single-phase experiments showed a dependence on inlet Reynolds number and no flow split dependence. This is the opposite of what has typically been observed experimentally.

The model presented by Reimann and Seeger (1986) (Equation [2.13]) was applied to a separated two-phase flow by assuming fully developed conditions both upstream and downstream of the vena contracta in order to determine the local slip ratios ($S_i = u_{Gi} / u_{Li}$, i = 1,2) from appropriate correlations. At the throat of the vena contracta, the flow was assumed well mixed (i.e. $S_{C2} = 1.0$). The contraction coefficient (C_2) was derived from the single-phase value based on the same volumetric flow split as,

$$C_2 = \left[1+\left(\frac{\rho_{H1}}{\rho_{H2}}\right)^{0.5} \frac{\dot{V}_1}{\dot{V}_2} \sqrt{\bar{k}_{1-2}}\right]^{-1} . \qquad (2.18)$$

Here, $\bar{k}_{1-2}$ is the single-phase loss coefficient defined by Equation [2.12] and $\dot{V}_1$ and $\dot{V}_2$ represent the inlet and run volumetric flow rates respectively. Based on these assumptions, the following relationship was obtained for the run pressure change,

$$-(\Delta P_{1-2}) = \frac{\rho_{H2}}{2\rho_L^2}\left\{\frac{G_2^2}{C_2^2}\left[x_2\left(\frac{\rho_L}{\rho_G}\right)+\left(1-x_2\right)\right]^2 - G_1^2\left[x_1\left(\frac{\rho_L}{\rho_G}\right)+S_1\left(1-x_1\right)\right]^2\left[x_2+\frac{1-x_2}{S_1^2}\right]\right\}$$

$$+\frac{G_2^2}{\rho_L}\left\{\left[x_2\left(\frac{\rho_L}{\rho_G}\right)+S_2\left(1-x_2\right)\right]\left[x_2+\frac{1-x_2}{S_2^2}\right]\frac{1}{C_2}\left[x_2\left(\frac{\rho_L}{\rho_G}\right)+\left(1-x_2\right)\right]\right\} \quad (2.19)$$

The authors reported reasonable agreement between the model and experimental values for both steam/water and air/water flow with various inlet flow patterns.

2.3.3 Branch Pressure Change Correlations

The branching portion of a dividing flow generally experiences a drop in pressure due to high irreversible losses which typically exceed any associated Bernouli type pressure rise. For single-phase flow, the resulting pressure change, $(\Delta P_{1-3})_j$, has been correlated in various ways. The most common is a balance of mechanical energy between the inlet and branch made up of reversible and irreversible components. This method yields an equation similar to Equation [2.12] derived for the run flow, i.e.

$$(\Delta P_{1-3})_j = P_{1j} - P_{3j} = \frac{\rho}{2}(u_3^2-u_1^2) + k_{1-3}\frac{\rho}{2}u_1^2 \quad (2.20)$$

where the first term on the r.h.s. of Equation [2.20] is the reversible pressure change and the second term is the irreversible change modelled in

terms of the inlet dynamic head. The value of the loss multiplier (k_{1-3}) is determined experimentally.

Saba and Lahey (1982, 1984) suggested that, for separated two-phase flow, this equation may be written as

$$(\Delta P_{1-3})_J = \frac{\rho_{H3}}{2}\left(\frac{G_3^2}{(\rho_3''')^2} - \frac{G_1^2}{(\rho_1''')^2}\right) + k_{1-3}\frac{G_1^2}{2\rho_L}\Phi_S \ . \tag{2.21}$$

Here, k_{1-3} is the single-phase loss coefficient, Φ_S is a separated flow two phase multiplier and the energy density (ρ''') is defined by

$$\frac{1}{(\rho''')^2} = \left[\frac{x^3}{\rho_G^2\alpha^2} + \frac{(1-x)^3}{\rho_L^2(1-\alpha)^2}\right] \ . \tag{2.22}$$

The authors suggested that a separated two-phase flow multiplier could be used in the form,

$$\Phi_S = \frac{\rho_L}{\rho_1'} \ , \tag{2.23}$$

where ρ' is the momentum density defined by

$$\frac{1}{\rho'} = \left[\frac{x^2}{\rho_G\alpha} + \frac{(1-x)^2}{\rho_L(1-\alpha)}\right] \ . \tag{2.24}$$

A homogeneous model for the branch pressure change was then obtained by replacing the momentum and energy densities in Equations [2.21] and [2.23] with the appropriate homogeneous densities from Equation [2.14], i.e.

$$(\Delta P_{1-3})_J = \frac{\rho_{H3}}{2}\left[\frac{G_3^2}{\rho_{H3}^2} - \frac{G_1^2}{\rho_{H1}^2}\right] + k_{1-3}\frac{G_1^2}{2\rho_L}\Phi_H \ . \tag{2.25}$$

Here,

$$\Phi_H = \frac{\rho_L}{\rho_{H1}} \tag{2.26}$$

The authors reported good agreement between the homogeneous model and experimental values for stratified and slug inlet flows.

Reimann and Seeger modelled the branch pressure change in the same way as the run pressure change. That is, in terms of a reversible component from the inlet to the throat of the vena contracta located in the branch and an irreversible component from the throat to the fully developed region. The resulting equation was then reduced based on a homogeneous flow assumption (i.e. $S_1 = S_3 = S_{C3} = 1.0$) and defining the branch contraction coefficient (C_3) from the single-phase loss coefficient (k_{1-3}) as,

$$C_3 = \left(1 + \frac{\dot{V}_1}{\dot{V}_3} \sqrt{k_{1-3}} \right)^{-1} . \tag{2.27}$$

Based on these assumptions, the homogeneous model then takes the form,

$$(\Delta P_{1-3})_J = \frac{\rho_{H3}}{2} \left(\frac{G_3^2}{\rho_{H3}^2} - \frac{G_1^2}{\rho_{H1}^2} \right) + k_{1-3} \frac{G_1^2}{2\rho_L} \frac{\rho_L \rho_{H3}}{\rho_{H1}^2} . \tag{2.28}$$

This model is similar to Saba and Lahey's homogeneous model with a two-phase multiplier defined by

$$\Phi_H = \frac{\rho_L \rho_{H3}}{\rho_{H1}^2} . \tag{2.29}$$

The authors reported that the measured data was better represented by the above homogeneous model than that presented by Saba and Lahey (1982, 1984). Agreement was particularly improved in the low flow split ranges.

Recently, Kalkach-Navarro et. al. (1988) performed a 3 dimensional numerical simulation of low pressure flow in a dividing horizontal T-junction

using the PHOENICS code. The authors applied a two-fluid model valid for adiabatic two-component flows. The inlet conditions considered in this study where stratified, the T had all legs of equal diameter and the branch was assumed to be orientated vertically upward, downward and horizontally. When The results were compared with previously published data, the model was reported to predict the observed extrapolated pressure changes within ± 10%.

2.3.4 Closure Relationships

The closure relationship must relate the degree of phase separation (or branch quality) to one or more of the remaining flow or geometrical parameters. These relationships have taken many different forms. One of the first predictive tools suggested was from Hong (1978) in the form of nomographs based on his experimental work. Due to the large number of parameters involved in the separation process and the complicated geometries encountered in practice, this method is of limited value for general application.

Henry (1980) suggested that phase division is not a strong function of pressure gradients within the junction. He therefore suggests that any solution method for a two-phase pipe network must include a relationship between the branch phase flow rates and those in the inlet which does not include the local pressure gradients. His observation of a linear dependence of the branch water flow rate on the branch gas flow rate formed the basis for an empirical correlation of the form

$$x_3 = \frac{1}{s+1}\left(1 - \frac{G_i}{G_3}\right) \tag{2.30}$$

Here, G_i represents the extrapolated branch liquid mass flux when the branch gas flow rate is reduced to zero and s is the slope of the linear relationship between the branch phasic flow rates. These were fit empirically with the following dimensional equations

$$s\left(\frac{x_1}{1-x_1}\right) = 8.1\text{x}10^{-7}(G_1 x_1)^3 \tag{2.31}$$

and

$$G_i\left(\frac{x_1}{1-x_1}\right) = 0.00007(G_1 x_1 - 10)^3 \ . \tag{2.32}$$

These relationships were developed from experimental data for a specific junction geometry and flow conditions. Since they are not based on the flow dynamics, it is unlikely that they may be extrapolated for application beyond these conditions.

Azzopardi and Whalley (1982) identified the axial momentum flux of a flow component (ρu^2) as a measure of its resistance to being diverted to the branch. For the vertical annular flows considered in their experimental program, the momentum flux of the liquid film is much closer to that of the gas than it is to that of the entrained droplets. The gas and liquid film extracted through the branch are then assumed to come from the segment of the inlet tube defined by θ (Equation [2.2], the angle over which the liquid film is extracted). The relationship between the portion of gas removed and θ is then,

$$\frac{\dot{m}_3 x_3}{\dot{m}_1 x_1} = \frac{1}{2\pi} (\theta - \sin\theta) \tag{2.33}$$

Azzopardi and Freeman-Bell (1983) extended this work to include a wider range of diameter ratios. They noted that the effect of branch diameter was best represented by

$$\frac{\theta}{\theta'} = 1.2 \left(\frac{D_3}{D_1} \right)^{0.4} \tag{2.34}$$

when the portion of gas removed is given by

$$\frac{\dot{m}_3 x_3}{\dot{m}_1 x_1} = \frac{1}{2\pi} (\theta' - \sin\theta') \ . \tag{2.35}$$

This indicates higher branch qualities with smaller branch diameters. The authors reported that most of their data was predicted to within ±30% with results from higher inlet qualities deviating most significantly. Extending this model to horizontal inlet flows requires knowledge of the angular distribution of film thickness in the inlet section. The horizontal predictions were best for low gas extraction rates.

Saba and Lahey (1984) suggested that it was the relatively low inertia of the vapour phase which allowed it to be preferentially removed through the branch. They therefore used a vapour phase linear momentum equation as a closure relationship of the form

$$-\alpha \frac{dp}{dx} = \alpha F_d + \alpha \rho_G u_G \frac{du_G}{dz} + \alpha F_w + \rho_g \alpha \sin \gamma_{1-3} \ . \tag{2.36}$$

Here, F_d and F_w are the volumetric interfacial and wall drag forces respectively. For a horizontal branch, $\gamma_{1-3} = 0$. With the help of empirical

correlations developed by the authors and those of other investigators, this equation was integrated along a branching streamline to obtain a closure equation. The authors reported that agreement between the model predictions and measured data where within the data uncertainty limits when a homogeneous assumption was employed.

Seeger et. al. (1986) presented a simple empirical correlation to fit their data of the form,

$$\frac{x_3}{x_1} = 5\left(\frac{\dot{m}_3}{\dot{m}_1}\right) - 6\left(\frac{\dot{m}_3}{\dot{m}_1}\right)^2 + 2\left(\frac{\dot{m}_3}{\dot{m}_1}\right)^3 + a\left(\frac{\dot{m}_3}{\dot{m}_1}\right)\left[1 - \frac{\dot{m}_3}{\dot{m}_1}\right]^4. \qquad (2.37)$$

The parameter 'a' relates the peak of the phase separation curve, $(x_3/x_1)_{max}$, to the ratio of the gas to liquid momentum flux $(\rho_G u_G^2/\rho_L u_L^2)$ in the inlet section. From their experiments, equal separation was approached as the ratio of momentum fluxes approaches unity. The value of 'a' was determined from an empirical fit of their data as, a = 14.6 for bubbly flow and

$$a = 13.9\left[\left(\frac{\rho_G S_1^2}{\rho_L}\right)^{-0.26} - 1.0\right] \qquad (2.38)$$

for all other flow patterns.

The model presented by Shoham et al. (1987) assumed the existence of dividing streamlines for both the gas and liquid phases through a cross-section at the mid-plane of the junction. The location of these streamlines at the junction inlet defined the segments of the inlet tube from which the branching flow of each phase is extracted. The gas phase streamline was assumed to follow a circular arc through the junction volume. The segment from which the liquid was removed was shifted from that of the gas through the net centripetal force per unit mass (f_c) acting on liquid

that was assumed to follow the gas phase streamline, i.e.

$$f_c = \frac{\rho_L u_L^2 - \rho_G u_G^2}{\rho_L r_o} \tag{2.39}$$

where r_o is the radius of curvature of the gas phase dividing streamline. This model was extended to reduced T-junctions ($D_3/D_1 < 1.0$) by Shoham et al. (1989).

The Hwang et al. (1988) model was also based on an assumption of dividing streamlines defining segments of the inlet tube from which the branching flows were extracted. The authors considered the point of intersection of the run and branch tubes at the mid plane of the junction. This was the point where the dividing streamlines for the gas and liquid phases cross. Here, the pressure forces were assumed balanced by centrifugal and interfacial drag forces such that the angle of intersection could be determined. A power law function, satisfying appropriate boundary conditions, was then assumed to describe the streamlines within the junction volume. Empirical correlations were derived that allow the dividing streamlines for each phase to be determined separately. The branch quality could then be determined, assuming the lateral distribution of the phases in the inlet was known. The authors reported good agreement between the model predictions and all available data from other investigators. This model was extended to include impacting wyes and tees by Hwang et al. (1989).

CHAPTER 3

EXPERIMENTAL ARRANGEMENTS

3.1 Experimental Facility

3.1.1 Steam/Water Loop

The steam/water loop used in the experimental program is shown schematically in Figure 3.1. The system consists of a two horsepower Moyno progressive cavity pump (Model 1L4, SSF ACC) capable of delivering water at a rate of 0.6 l/s at a differential pressure of 500 kPa. Water is supplied to the pump from a 450 l hot water storage tank. The inlet water flow is controlled by way of valves located in the main water line and loop bypass. From the pump, the water flows to a 6 kw Chromalox circulation heater. To protect the equipment and measuring instruments from impurities in the water it is then passed through a filter (GAF, Model RBXAS-HD) capable of removing particles to 10 μm diameter. From the filter, the water flows through a check valve to the two-phase mixer.

Steam is taken from the main supply at approximately 700 kPa and passed through a filter identical to that for the inlet water. This section of the steam line is also equipped with an inverted bucket steam trap (Spirax Sarco, Model 1/2 NPT-BIX125) to collect any condensate that may be present. The steam pressure is then reduced to the desired pressure through a Spence,

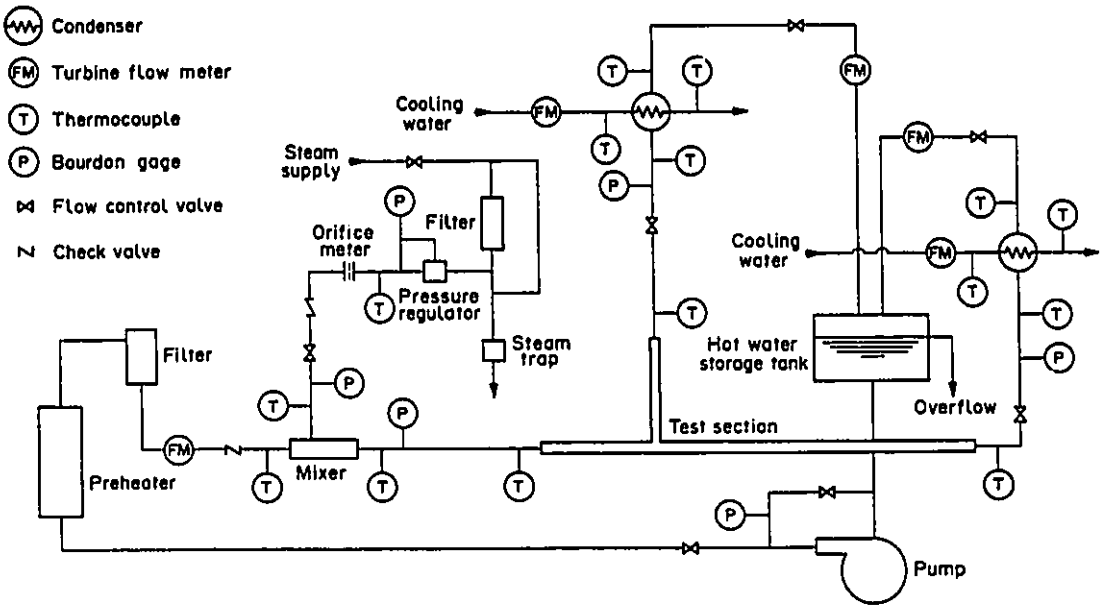

Figure 3.1 Schematic Diagram of the Steam/Water Loop

Type EC, 12.7 mm (1/2 inch) pressure regulator. The steam flow rate is measured by way of an orifice plate assembly described in detail in section 3.2.2. From the orifice meter, the flow passes through a check valve and a flow control valve to the two-phase mixer where it is combined with the inlet water.

The steam and water are well mixed within the two-phase mixer. From the mixer, the flow becomes fully developed and reaches thermodynamic equilibrium through a 3.6 m long section of 25.4 mm (1 inch) sch. 40 stainless steel pipe before reaching the test section.

The test sections used for the experiments presented herein were 90° T-junctions with all legs in the horizontal plane. The test sections are described in detail in section 3.1.3. At the junction, the flow is split into two streams; one in the axial direction through the run of the T, the other in the radial direction through the branch. At the outlet from each leg, the steam/water mixture enters a 50 kilowatt, multi pass, shell and tube condenser (American Standard P/N 5-030-05-014-004) exiting as single-phase water. Two flow control valves, one upstream and one downstream of the condenser, were used in each leg to adjust flow distribution. Cooling water is supplied to the condensers from the mains at approximately 6-10 degrees celsius. The condensate from each branch is delivered back to the storage tank. The water level in the tank is kept constant by means of an open overflow. The entire loop and tank are insulated to minimize heat losses with Micro Lok fiberglass pipe or blanket insulation.

3.1.2 Two-Phase Mixer

The mixer design, shown schematically in Figure 3.2, is similar to that used by Shoukri (1980). The mixer is approximately 0.44 m long and is made up of two concentric stainless steel tubes and a reducing section. The inner and outer tubes are nominal 50.8 mm (2 inch) sch. 40 and nominal 25.4 mm (1 inch) sch. 40 stainless steel pipes respectively. The outer tube is fitted with two 1 inch nipples on opposite sides connecting to the inlet steam supply. The reducing section is tapered at 15° to the axis and welded to the downstream end of the outer tube. The flow exits from the mixer through a nominal 25.4 mm (1 inch) stainless steel nipple.

3.1.3 Test Sections

Three test sections were used in the experimental program. Each consisted of a horizontal inlet tube with one horizontal branch carefully machined and fixed at 90° to ensure a sharp edged opening. The main tube used for all test sections was constructed of 31.75 mm O.D. 25.65 mm I.D. stainless steel tubing. Three branch sizes were used corresponding to branch to inlet diameter ratios (D_3/D_1) of 1.0, 0.82 and 0.50. A schematic diagram of the test section with a branch to inlet diameter ratio of 1.0 is shown in Figure 3.3. At the entrance to the test section, a 0.15 m long section of transparent tubing (TPX) was used for identification of the inlet flow regime.

For all of the test sections used, the inlet and branch sections were the same length (610 mm) with 5 pressure taps in each located

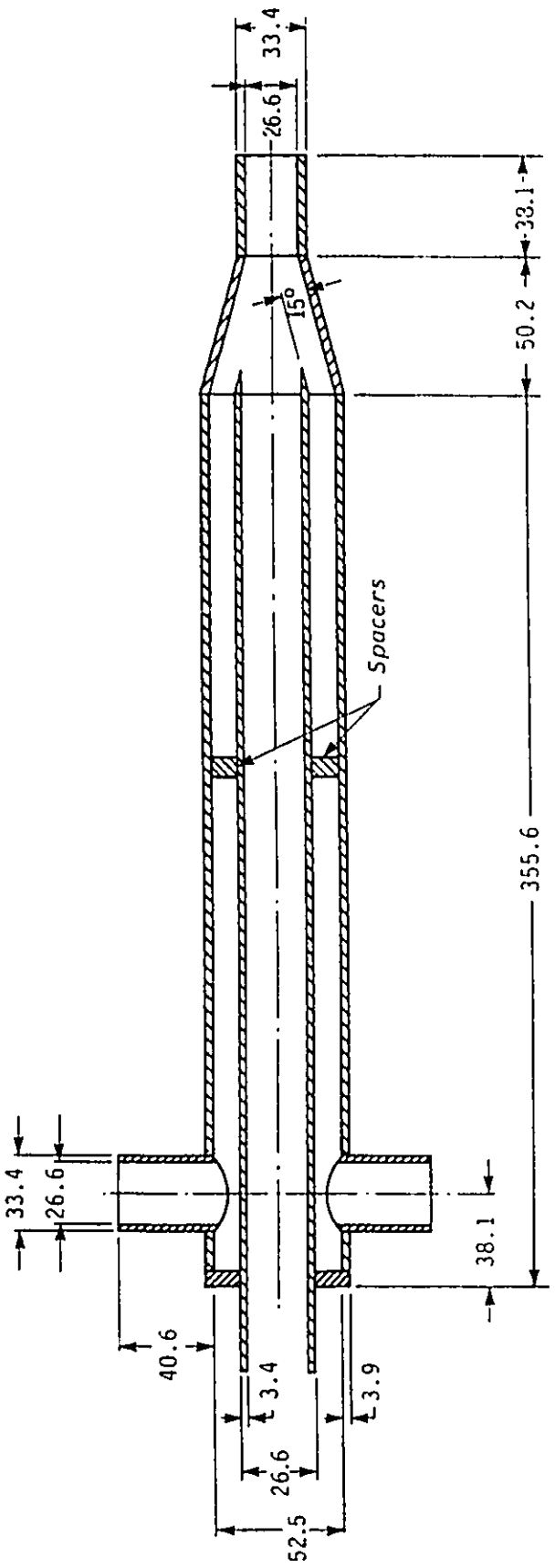

Figure 3.2 Two-Phase Mixer

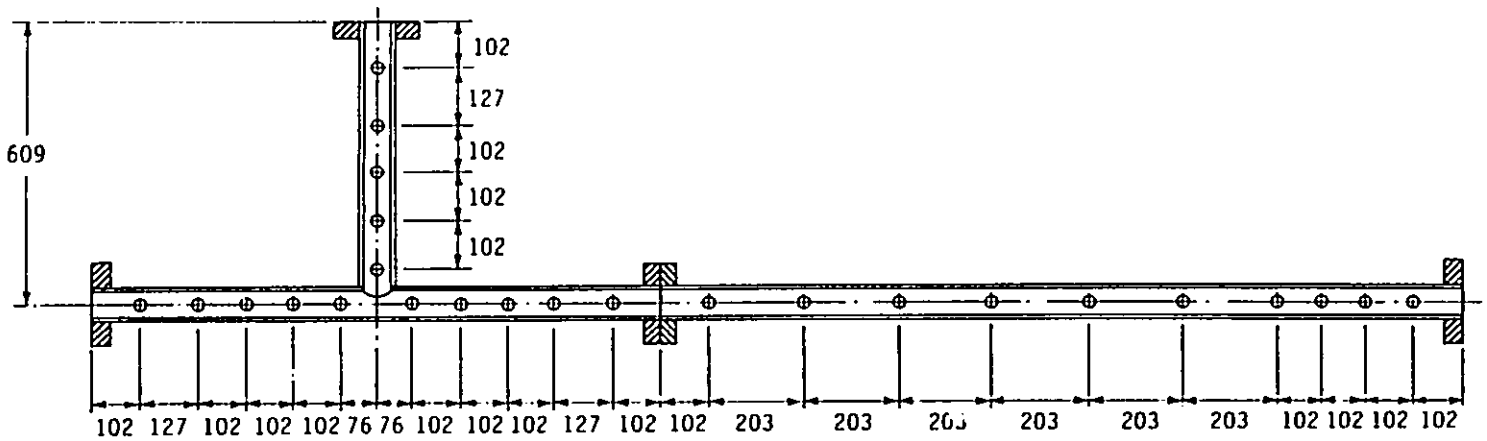

Figur 3.3 Test Section Schematic - $D_3/D_1 = 1.0$

symmetrically about the junction. Due to a slower flow development, the run contained up to 15 pressure taps over approximately 2300 mm to ensure that a fully developed pressure profile was measured. At each tap location, a 1.6 mm hole was drilled through the tube wall and polished to ensure no burrs protruded into the flow area. All taps were located on the bottom of the test section to inhibit steam from entering the pressure lines. The taps were connected to the pressure measurement system using Tygon tubing. The end of each leg was flanged so that subsequent test sections may be easily installed in the loop.

3.2 Measurements and Calibration

3.2.1 Water Flow Rate Measurements

Water flow rates were measured with turbine flow meters at five locations throughout the loop as listed below (see Figure 3.1).

Location	Model	Range
Mixer Inlet	ITT Barton, No. 806	0.15-1.8 l/s
Run Condenser Exit	ITT Barton, No. 806	0.15-1.8 l/s
Branch Condenser Exit	Flow Technology, FT-8N10-LJC	0.06-0.6 l/s
Run Cooling Water	Flow Technology, FT-8N10-LJC	0.06-0.6 l/s
Branch Cooling Water	Flow Technology, FT-8N10-LJC	0.06-0.6 l/s

In order to capture the phase separation detail with the smallest diameter

branch (D_2/D_1 = 0.5), a lower range flow meter (.03-0.3 l/s) was installed in parallel with the larger meter for low flow split measurements. All meters were calibrated by the manufacturers. The higher range meters (ITT Barton, No. 8086) operate accurately to within 1% of reading over the entire flow range. The lower range meters are accurate to 0.5% of reading over the measurement range. All meters were equipped with magnetic pickup coils and the output signals were connected to frequency channels in the data acquisition system.

3.2.2 Steam Flow Rate Measurements

Steam flow rates were measured using an orifice plate assembly. The system consists of an orifice plate (19 mm bore diameter) installed in the 25.4 mm (1 inch) nominal sch. 40 steam line downstream of the pressure regulator. The plate is held in place with a 300 lb orifice flange union. Both plate and union were supplied by Cantrols Equipment Ltd.

To ensure that the pressure lines to the transducer remain vapour free, the assembly was equipped with two condensing chambers mounted above the orifice meter as shown in Figure 3.4. The condensing chambers were fabricated in the departmental machine shop from 225 mm sections of 50.8 mm (2 inch) sch. 40 stainless steel pipe. Each was fitted with plain blanks on both ends and three 19.1 mm (3/4 inch) bosses around the centre of the pipe. The upper bosses were fitted with ball valves allowing the chambers to be vented. Those located at 45° down from horizontal were fitted with 6.4 mm (1/4 inch) tubing connecting one chamber to the upstream flange tap and the

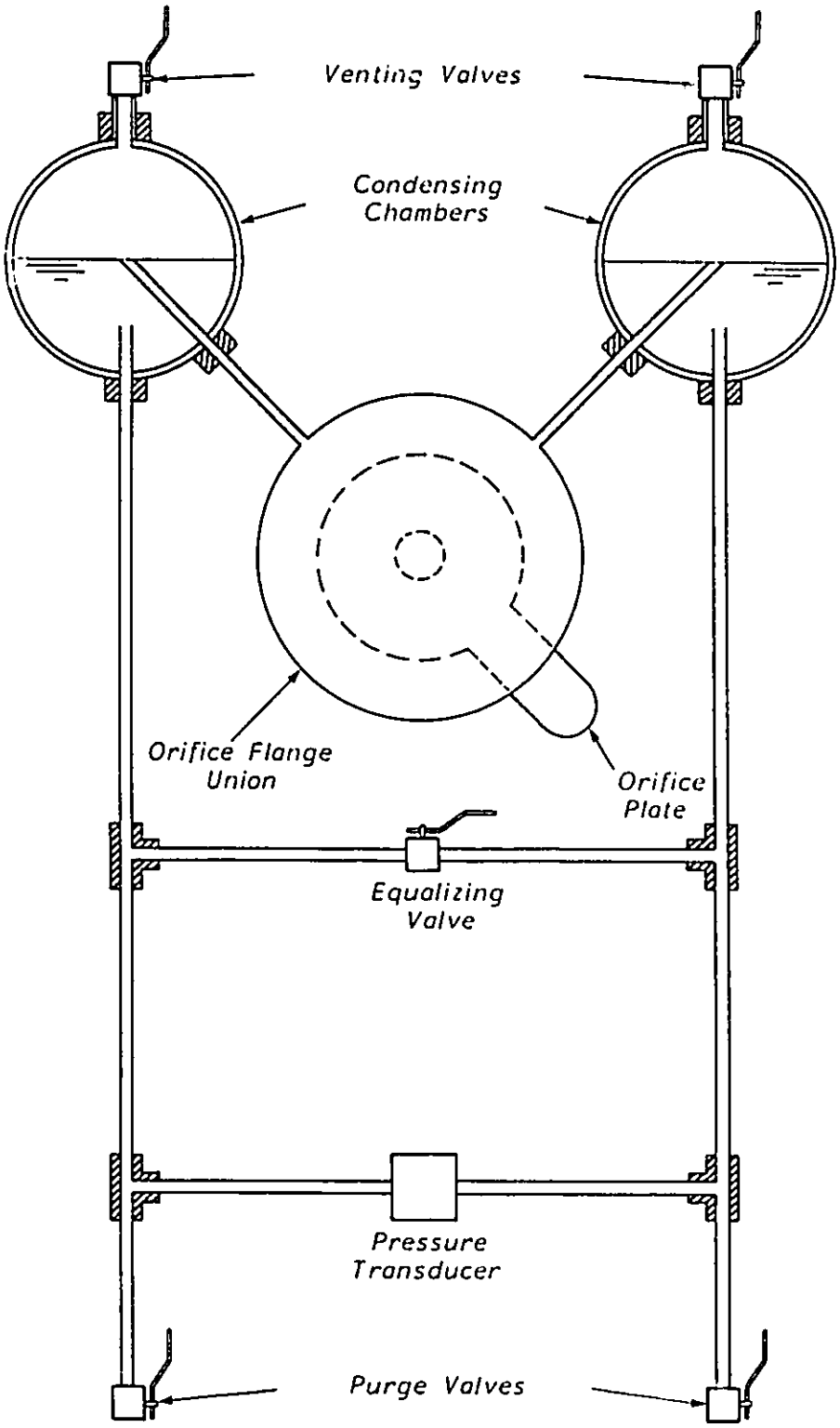

Figure 3.4 Orifice Meter Assembly

other chamber to the downstream flange tap. These tubes protruded through the wall to the centre of the chambers. The bosses located on the bottom of the chambers were fitted with 1/4 inch tubing passing through the wall to about 1/4 of the chamber height. These tubes extended downward and were connected through an equalizing line which could valved out. The pressure signals were then delivered to the appropriate side of a differential pressure transducer (Validyne, Model DP15-36) in the range 0-35 kPa. The transducer is excited at 5 volts, 5kHz by a Carrier demodulator (Model CDC 101). This unit demodulates the transducer output providing a +/- 10 volt DC signal which is delivered to the data acquisition system.

As the branch diameter was decreased, there was a corresponding increase in the system pressure which limited steam flow. As a result, higher pressures were then required upstream of the orifice plate. Accordingly, the orifice meter was calibrated on line for three upstream pressures (300, 375 and 450 kPa(a)) by direct weighing of the condensate. Calibration details were presented in Ballyk (1986).

3.2.3 Temperature Measurements

Temperature measurements were made using standard E type thermocouples at 15 locations throughout the loop as listed below (see Figure 3.1).

- Steam inlet to the two-phase mixer
- Water inlet to the two-phase mixer
- Two-phase mixer exit
- Test section inlet

- Test section exit (run)
- Run condenser inlet
- Run condenser outlet
- Test section exit (branch)
- Branch condenser inlet
- Branch condenser exit
- Cooling water inlet (run)
- Cooling water exit (run)
- Cooling water inlet (branch)
- Cooling water exit (branch)
- Steam line upstream of orifice

All measurements were referenced to zero by way of an ice/water bath. The analog signals from all thermocouples were delivered directly to the data acquisition system.

3.2.4 Pressure Distribution Measurements

A schematic diagram of the pressure measurement system is shown in Figure 3.5. The first upstream pressure tap in the inlet section (tap #1) is used as a reference. Its signal was split with one branch connected to the high side of a differential pressure transducer (Validyne, Model DP 15-46, 0-350 kPa). The low side of this transducer was open to atmosphere to measure system pressure. The other branch was connected to the high side of a bank of two differential pressure transducers, one high range and one low range, used for measuring the pressure difference between station #1 and subsequent stations. The signals from all other pressure taps are delivered

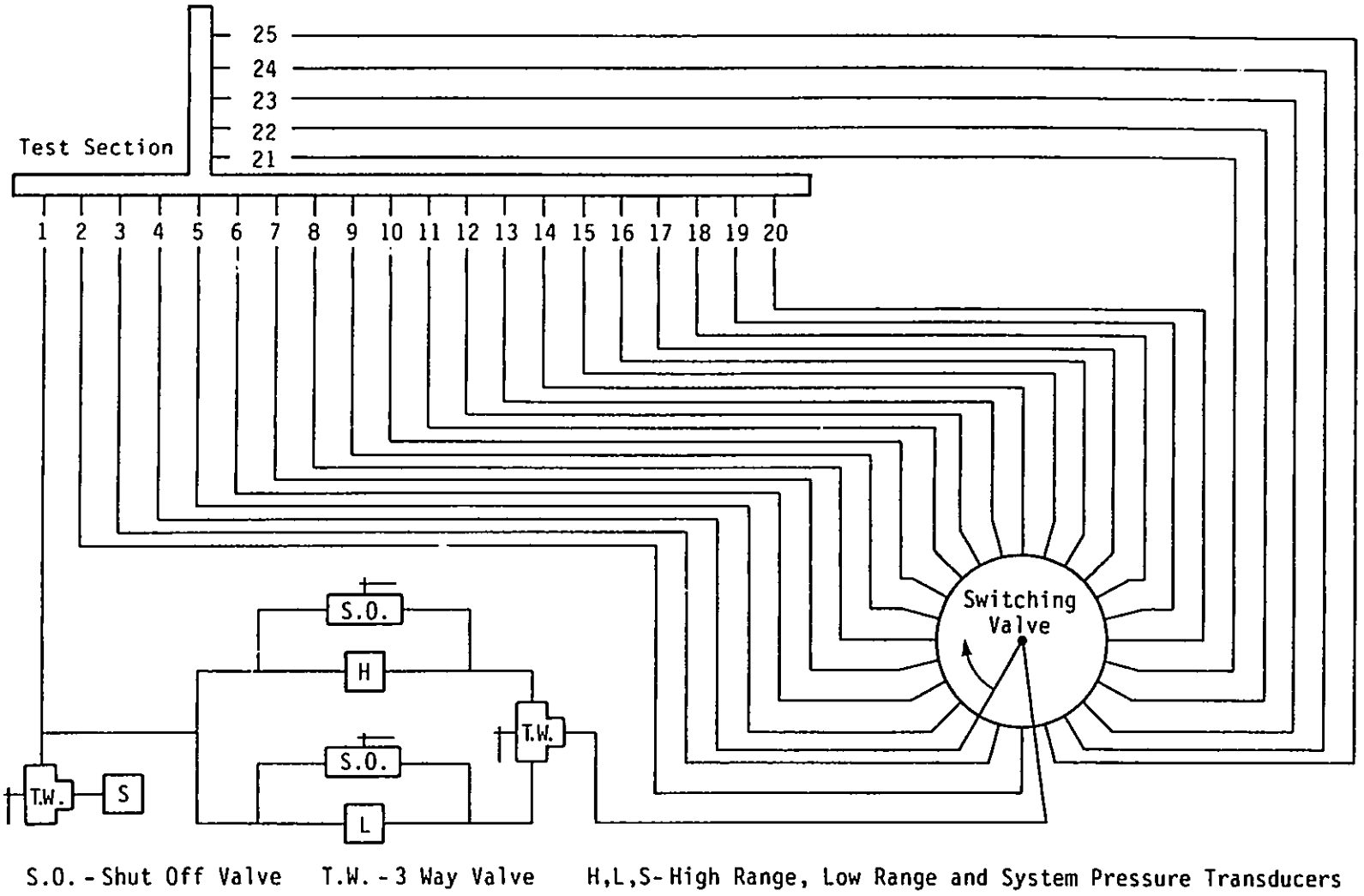

Figure 3.5 Schematic Diagram of Pressure Measurement System

individually to the low side of the transducer bank through a 24 channel switching valve (Scanivalve Model W02). These signals can be directed to the high or low range transducer through a series of valves as shown.

Pressure lines from the taps to the transducer bank were made of transparent Tygon tubing. After installation, all lines were thoroughly purged to ensure no air remained in the system. The transparent tubing allowed a visual check for air or steam that may have become trapped in the lines.

For all experimental runs the high range transducer used was a Validyne Model DP15-38 of the range 0-55kPa. For single and two-phase runs the low range transducers used were Validyne Models DP103-20 (0-.55 kPa) and Model DP103-28 (0-5.5 kPa) respectively. The transducers are excited at 5 volts, 5 kHz by a demodulators identical to that for the orifice meter transducer (see section 3.2.2).

Transducer calibration details were presented in Ballyk, 1986.

3.2.5 Void Fraction Measurements

Void fraction measurements were made at various locations throughout the test section with a single beam gamma densitometer. The system consisted of a 75 mCi cobalt 57 sealed source contained in a stainless steal casket and located above the test section. The gamma beam was defined by two sets of 12 stainless steel collimating plates (127 X 127 X 19.1 mm plates, 50.3 X 12.7 mm aperture) one set above and one bellow the test section. The signal was received by a 76.2 mm cubic NaI(Tl) scintillator and standard signal processing equipment (see Figure 3.6). The processed signal

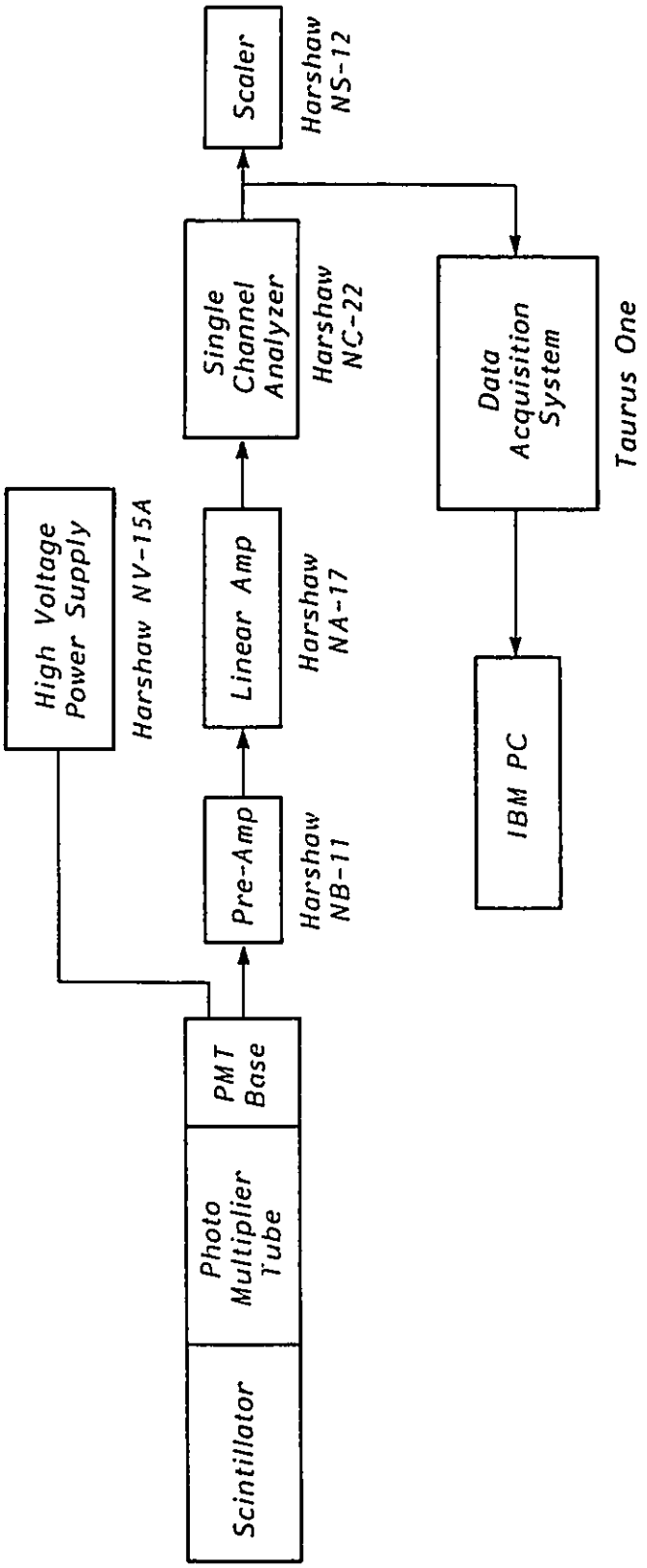

Figure 3.6 Signal Processing System for Void Fraction Measurements

was delivered to two cascaded counters in the data acquisition system. In order to maintain a high sensitivity to test section void, the aperture of the collimating plates was reduced for measurements with the smallest diameter branch. This was done by inserting stainless steel rods on either side of the aperture both above and below the test section. The source, collimating plates and scintillator were housed in a carriage capable of scanning the test section on a traversing table. Void fraction measurements were made at 17 stations throughout the test section as shown in Figure 3.7. Measurements at stations 1 through 11 and 13 through 17 were made with the traversing system. It was experimentally observed that certain flow conditions did yield fully developed void fraction profiles at the furthest downstream station in the run. For this reason, a single fixed densitometer stand was added at station 12 far downstream of the junction.

The system was calibrated daily by a taking full and zero void counts at each station ($N_{(\alpha=1)_i}$ and $N_{(\alpha=0)_i}$ respectively, i= 1-17). The test void fraction (α_i) was determined from the test count ($N_{\alpha i}$) using the linear interpolation equation, i.e.,

$$\alpha_i = \frac{N_{\alpha i} - N_{(\alpha=0)_i}}{N_{(\alpha=1)_i} - N_{(\alpha=0)_i}} \tag{3.1}$$

Further design and calibration details were presented in Ballyk (1986).

3.2.6 Data Acquisition System

All signals from the flow meters, thermocouples, pressure transducers and the gamma densitometer were directed to a Taurus One

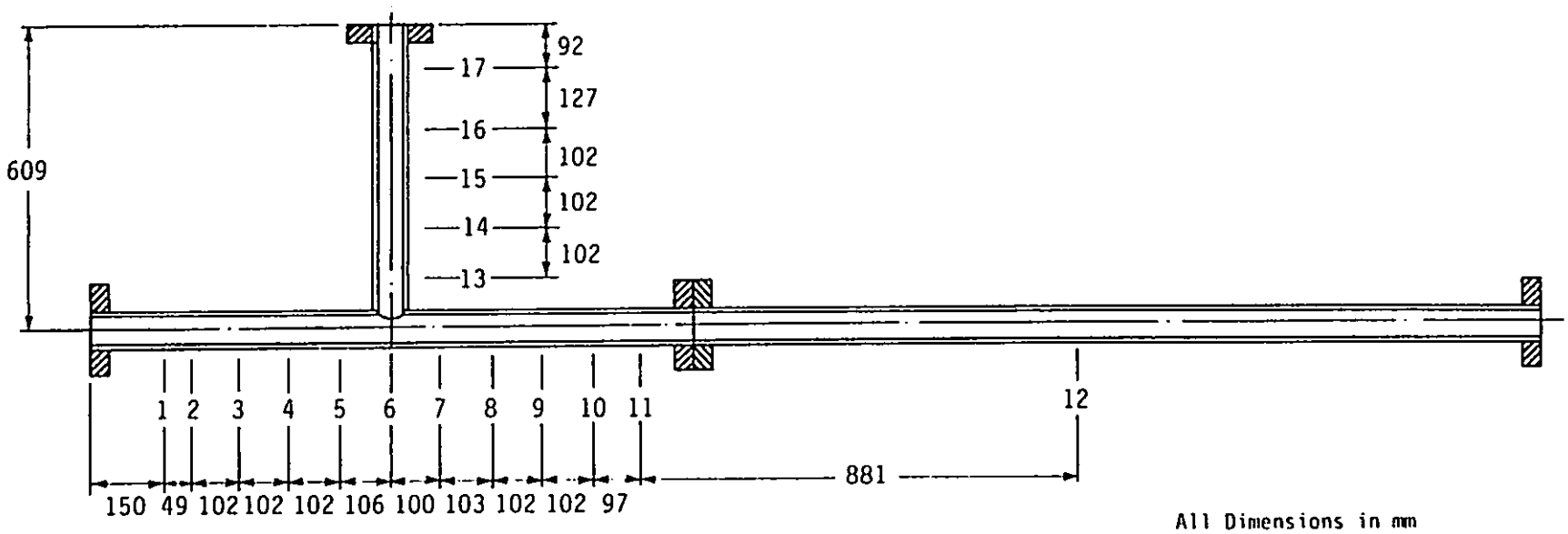

Figure 3.7 Void Fraction Measurement Stations

acquisition system manufactured by Tarus Computer Products Inc. The Taurus One is a Z80A based microcomputer with its own firmware based operating system and an input/output bus for installing various I/O modules. The present system is equipped with two Input/Output modules (T-10470 and T-3732T) yielding 4 frequency channels 3 event counters and 32 analog input channels. Since the number of frequency channels was one less than the number of flow meters, the two cooling water meters were connected to a single channel by way of a switch. The system was hosted by an IBM PC.

3.3 Experimental Procedure

3.3.1 Start-up Procedure

Following is a step by step description of the procedure used to calibrate the gamma densitometer and prepare the loop for experimental measurements. This procedure was carried out at the beginning of each day.

1. Open all transducer equalizing valves and the condensing chamber exhaust valves. Check and correct for any transducer zero shift. Close the condensing chamber exhaust and orifice meter equalizing valves.
2. Open the loop bypass and main water line valves. Start the pump and open both flow control valves in each leg. Close the bypass valve and turn on the preheater.
3. Open both cooling water valves to about 50% full flow. Open the main steam supply valve, then slowly open the steam flow control valve to 100% full flow.

4. Monitor the loop temperature distribution and adjust the cooling water flow rates to maintain condensate temperatures of approximately 75° C.
5. When the inlet water temperature reaches 70°C, close the steam flow control valve and cooling water supplies.
6. At this point only water is flowing in the loop. Put the gamma source in place and unclamp the densitometer carriage from the traversing table. Take and record zero void counts at each void fraction measuring station for 30 seconds.
7. Open both cooling water valves to approximately 50% full flow and slowly open the steam flow control valve to 100% full flow.
8. Turn off the preheater, slowly open the loop bypass valve and close the main water supply valve removing the water from the loop.
9. Adjust cooling water flow rates to maintain condensate temperatures below 80°C. Allow steam to flow through the test section for approximately 10 minutes to ensure no water remains.
10. Take full void counts at each void fraction measuring station for 30 seconds.
11. Open the main water line valve and slowly close the loop bypass valve to re-establish a two-phase flow within the system.

3.3.2 Test Procedure

The independent flow parameters for each experimental run were the nominal values of inlet mass flux, inlet quality and flow split. These were set by adjusting flow rates of water and steam to the mixer and the flow

control valves in the run and branch of the T. The flow conditions throughout the loop were monitored at the computer terminal while adjusting the flow valves. At this point, all of the conditions on the screen were those based on a single data sweep of the temperature and flow measurement systems. The process of establishing the desired flow conditions was iterative as small changes in one control valve could affect the flow through others. Once the desired conditions were obtained, the system was allowed to run for approximately 30 minutes to ensure that a steady state was reached.

At steady state, data sweeps of the flow conditions were taken and averaged with previous sweeps. Once the fluctuations had been averaged out (approximately 15-20 sweeps) the final test conditions were determined. If these were acceptable, the inlet flow regime was recorded and the pressure and void fraction distributions were obtained. If not, the flow was adjusted and the process repeated.

Pressure measurements began by directing the pressure signal from station #1 to the high side of the system pressure transducer (S in Figure 3.5). The demodulator output signal was sampled for 30 seconds at a rate of 100 samples per second. These values were averaged to determine the system pressure at tap #1. The transducer bank valves were set such that the signal from the switching valve was directed to the high range transducer (H in Figure 3.5). The switching valve was then set to measure the pressure differential between taps #1 and #2. The signal from the high range transducer was then sampled for 2 seconds at a rate of 100 samples per second. If the average reading was less than 4.5 kPa the operator was prompted to set the valves to deliver the signal to the low range transducer otherwise the valve settings remained unchanged. The appropriate channel was

then sampled for 30 seconds at 100 samples per second to measure the pressure drop between stations #1 and #2.

Once this pressure drop was determined, a sweep of the flow conditions was made and averaged with the preceding readings. The updated conditions were sent to the printer and displayed on the screen along with the previous 3 updates. If no significant or monotonic variation in the conditions was noted that would nullify the test run, the operator proceed to measure pressure drop between taps #1 and #3. A similar procedure was followed for the rest of the pressure taps. At the end of the pressure measurements, all transducer equalizing valves were set open.

Void fraction measurements were made by locating the gamma densitometer traversing carriage at each measurement station in turn and recording a 30 second count. The void fraction was computed and both the count and void fraction was recorded. Between each measurement, a sweep of the loop flow conditions was made and averaged with the preceding measurements as for pressure drop measurements.

At the end of the void fraction measurements, the data acquisition for the test run was complete.

3.3.3 Shut-down Procedure

Following is a step by step description of the procedure used to shut-down the loop at the end of each day.

1. Slowly close the steam flow control valve and main steam supply valve.
2. Turn off the preheater. Close both cooling water supply valves.

3. Fully open the loop bypass valve and close the run and branch control valves on the condensate side. Turn off the pump.
4. Clamp the densitometer carriage in place. Return the source to the storage locker.

3.3.4 Data Reduction

The data collected from all experimental runs was reduced to determine a total of 11 parameters. These are;

- The mass flow rate in each leg ($\dot{m}_1$, $\dot{m}_2$, and $\dot{m}_3$)
- The flow quality in each leg (x_1, x_2, and x_3)
- The fully developed void fraction in each leg (α_1, α_2, and α_3)
- The run and branch junction pressure differentials (ΔP_{1-2} and ΔP_{1-3}) respectively.

The mass flow rate at the test section inlet ($\dot{m}_1$) is the sum of the mixer flows of steam and water,

$$\dot{m}_1 = \dot{m}_{Gm} + \dot{m}_{Lm} \tag{3.2}$$

The mass flow rates in the run and branch ($\dot{m}_2$ and $\dot{m}_3$) were determined directly from the appropriate turbine flow meter.

The quality in the inlet section (x_1) is the thermodynamic equilibrium quality based on the mixer conditions and the test section saturation conditions determined from pressure tap #5, the closest inlet tap to the junction. Previous estimates for the test section saturation conditions (Ballyk (1986) and Ballyk (1988)) were based on the average temperature between the test section inlet and the exit temperatures in the run and branch. As the branch diameter was decreased, the pressure losses

through the branch became very significant (both junction losses and branch frictional losses). This resulted in relatively low temperatures at the branch exit which were not considered consistent with junction conditions. The inlet quality is given by,

$$x_i = \frac{\dot{m}_{Gm} h_{Gm} + \dot{m}_{Lm} h_{Lm} - \dot{m}_i h_{Lt}}{\dot{m}_i (h_{Gt} - h_{Lt})} . \qquad (3.3)$$

In the run and branch of the T, the qualities were determined from an energy balance at the appropriate condenser i.e.

$$x_i = \frac{\dot{m}_i h_{ci} + [\dot{m}_{cw} (h_{cwo} - h_{cwi})]_i - \dot{m}_i h_{Lt}}{\dot{m}_i (h_{Gt} - h_{Lt})} \qquad i = 2, 3 . \qquad (3.4)$$

The fully developed void fraction in each leg of the test section was determined directly from measurements. In general, these values were the furthest upstream measurement in the inlet section and the furthest downstream measurements in the run and branch sections.

The junction pressure differentials were determined by extrapolating the fully developed pressure profile in each leg of the T to the junction. The required differential is then the difference between the two extrapolated values as discussed in section 2.2.

The correlations used for the saturated fluid properties in the test section (from Shoukri, 1980) are shown in Appendix A. The required sub cooled liquid properties are determined from a table look up of saturated properties based on temperature. At the mixer inlet, the steam was slightly superheated and the enthalpy was determined from steam tables.

3.3.5 Test Conditions

Experiments with all three test sections were carried out under both single-phase water and two-phase steam/water conditions. Single-phase water tests were carried out at room temperature with 4 values of inlet mass flux. The flow split through the branch was varied ($0.1 \leq \dot{m}_3/\dot{m}_1 \leq 1.0$) and the pressure distribution for each condition was measured. The single-phase test conditions are shown in Table 3.1

Two-phase flow tests were carried out with the same nominal values of inlet mass flux that were used in the single-phase tests. The inlet quality was varied from 0.02 to 0.15 and the inlet flow conditions were always annular. The two-phase test conditions are shown in Table 3.2. The range of the present data was compared with that of other investigators by Muller and Reimann (1991) as shown in Figure 3.8. When compared with the flow regime map of Mandhane et. al (1974), Figure 3.9, the data is generally within the annular flow regime. For lower inlet quality conditions ($x_2 \cong 0.02$), the data maps close to annular/slug flow transition. Various flow splits were used for each inlet condition and test section. The flow splits were chosen to ensure that, where possible, the phase separation and pressure distribution detail was captured over the entire flow split range. The experimental results for both single-phase and two-phase experiments are shown in Appendix B.

TABLE 3.1: SINGLE-PHASE TEST CONDITIONS

Flow Split	Inlet Mass Flux (G_1)[kg/m^{2}s]			
($\dot{m}_3/\dot{m}_1$)	450	600	900	1200
0.1	X	X	X	X
0.3	X	X	X	X
0.5	X	X	X	X
0.7	X	X	X	X
0.9	X	X	X	X*
1.0	X	X	X	X*

* D_3/D_1 = 0.82 and 0.50 only

TABLE 3.2: TWO-PHASE TEST CONDITIONS

Inlet Quality	Inlet Mass Flux (G_1)[kg/m^{2}s]			
	450	600	900	1200
0.020		1	1,3	1,3
0.045	1,3	1,2,3	1,3	
0.080		1,2,3		
0.150	1,2			

1, 2 and 3 represent D_3/D_1= 1.0, 0.82 and 0.50 respectively

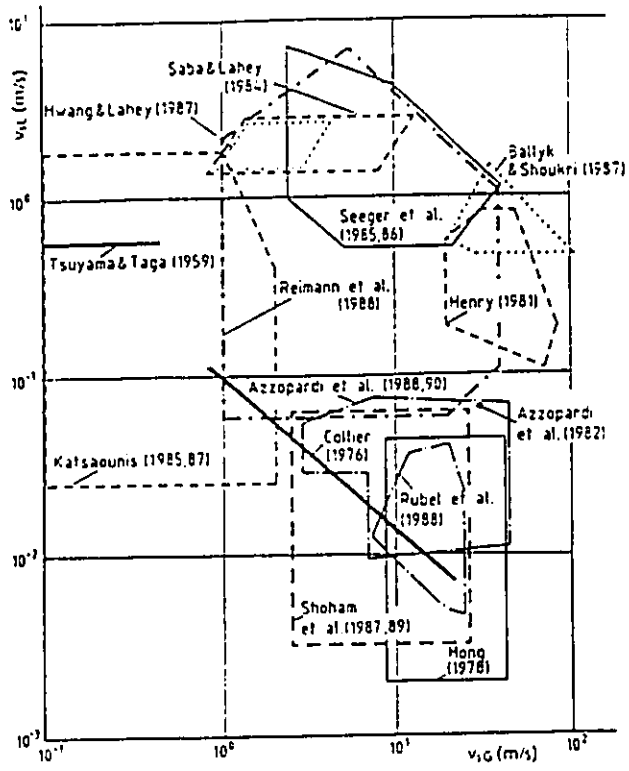

Figure 3.8 Range of Inlet Conditions for Dividing Two-Phase Flow Experiments with Horizontal Inlets (from Muller and Reimann, 1991)

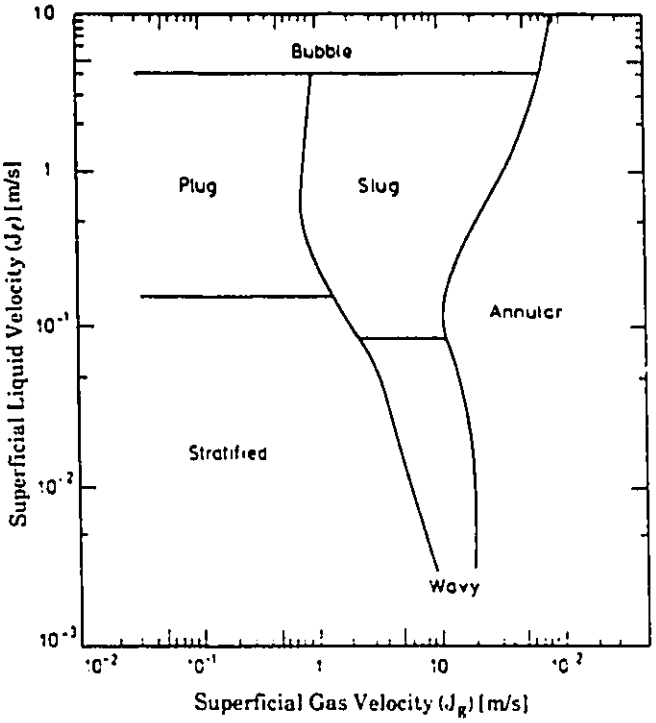

Figure 3.9 Flow Regime Map from Mandhane et. al. (1974)

3.3.6 Phase and Energy Balances

Of the 64 two-phase experimental runs with equal branch and inlet diameters, 44 had condensate flow rates that were within the linear range of both the run and branch flow meters. For these runs, comparing the total condensate flows with the total mixer flows of steam and water showed that 95% of the data satisfied mass continuity within ±1.5%. Based on these results, it was considered reasonable to use a mass balance in the cases where one of the condensates fell below the linear range of the meter.

The rate at which energy is convected into the test section is determined from the mixer flows as;

$$\dot{E}_{in} = \dot{m}_{Gm} h_{Gm} + \dot{m}_{Lm} h_{Lm} \quad . \tag{3.5}$$

The flow rate of energy leaving the test section can be determined from the condensate and cooling water flows as;

$$\dot{E}_{out} = \dot{m}_2 h_{c2} + [\dot{m}_{cw}(h_{cwo} - h_{cwi})]_2 + \dot{m}_3 h_{c3} + [\dot{m}_{cw}(h_{cwo} - h_{cwi})]_3. \tag{3.6}$$

Comparing these two values for all experimental runs showed that 90% of the data satisfied the energy balance within ±1.6%.

The flow of each phase at the test section inlet was determined from an assumption of thermodynamic equilibrium (Equation [3.3]). The flow of each phase exiting the test section was determined from energy balances at the condensers (Equation [3.4]). When these values were compared for all runs, 90% of the data satisfied continuity to within ±9.0% and ±1.3% for steam and water respectively.

CHAPTER 4

RESULTS AND DISCUSSION

4.1 Phase Separation

4.1.1 Introduction

For annular two-phase flow, three distinct components of flow can be identified. These are, a relatively low velocity liquid film flowing along the walls of the tube, a high velocity gas core and high velocity liquid droplets entrained within the gas core. From the present and previous experimental results, it appears that this flow structure strongly affects the distribution of the phases within a flow junction.

The phase separation data are first presented by plotting the branch quality, normalized with respect to the inlet quality (x_3/x_1), against the branch flow split ($\dot{m}_3/\dot{m}_1$) as discussed in section 2.1. Figure 4.1 shows typical results for a horizontal T junction with $D_3 = D_1$ for a fixed inlet mass flux ($G_1 = 600$ kg/m^{2}s) and inlet quality ($x_1 = 0$ .045). This figure shows how unevenly the phases can be distributed in the downstream legs of the T. An assumption of equal phase distribution would have all data points falling on the horizontal line at $x_3/x_1 = 1.0$. Clearly, this assumption does not approximate the measured data in any region. The branch quality is higher than the inlet quality over most of the flow split range. Only at low flow

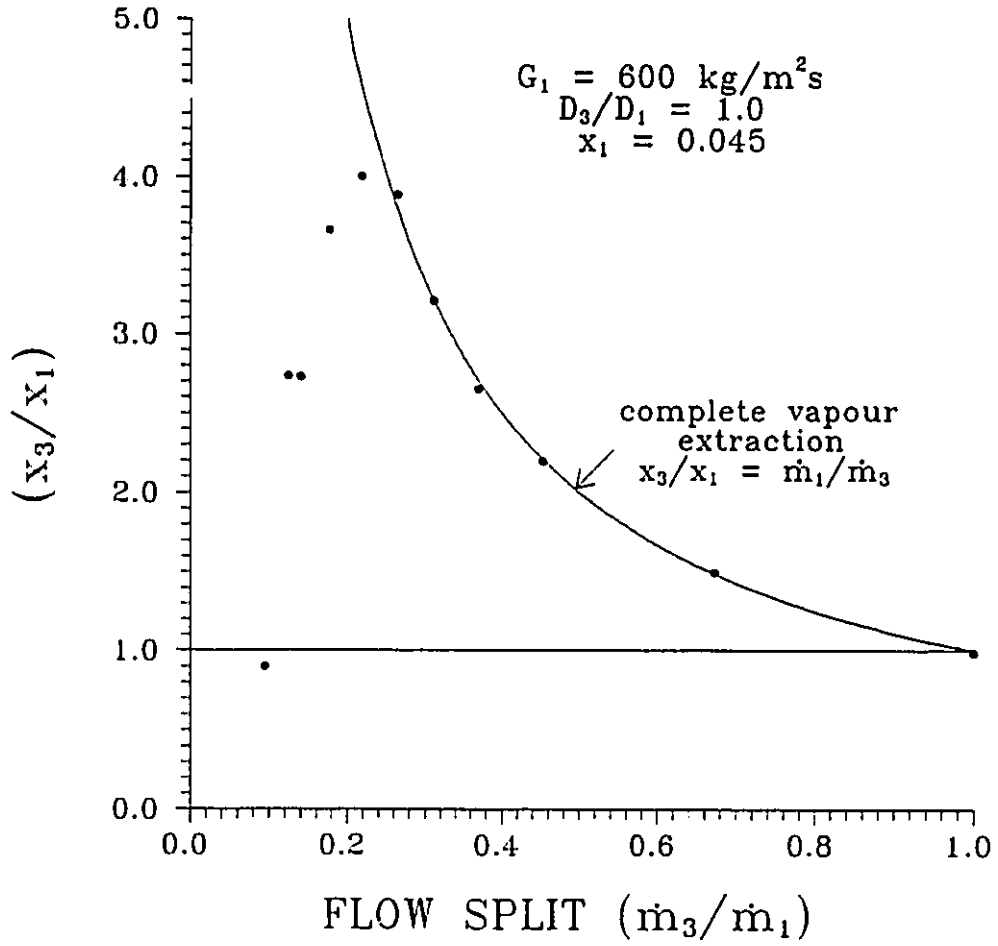

Figure 4.1 Typical Phase Separation Characteristics

G_1= 600 kg/m^{2}s, x_1= 0.045, D_3/D_1= 1.0

splits ($\dot{m}_3/\dot{m}_1 < .1$) is the branch quality below that of the inlet. This is a result of the component of flow most readily available for extraction being a portion of the liquid film intercepted by the branch opening. Extrapolating the data in this region to the axis suggests that a limiting value of water flow would exist in the branch when the branch gas flow is reduced to zero. This supports the findings of Henry (1981) and Azzopardi and Whalley (1982).

Once this local liquid film has been depleted, the next flow component which is easily extracted is the low density gas core. It has been suggested that the momentum flux (ρu^2) of a flow component represents a measure of the fluids resistance to being diverted to the branch. For typical inlet conditions considered in the experimental program, the relative momentum flux between the gas, liquid film and entrained droplets was approximately 1:20:1250. Because of its relatively low momentum flux the gas core can respond to the junction pressure forces that drive it toward the branch. This portion of the curve is initially characterized by a very steep increase in branch quality with flow split, crossing the equal distribution line ($x_3/x_1 = 1.0$) at close to 90°.

As the flow split is further increased, the curve ultimately levels off as the incremental portions of flow removed approach the existing branch quality. At this point the data is close to the complete vapour extraction curve representing all of the gas phase flowing in the branch and the run carrying single-phase water. Once complete vapour extraction is reached, any further increase in flow split reduces the branch quality along the complete vapour extraction curve as the flow is being removed from the liquid film flowing further away from the branch opening and the high velocity droplets entrained within the gas core.

4.1.2 Effect of Inlet Quality

The effect of inlet quality on the phase separation characteristics is demonstrated in Figures 4.2 through 4.4. Each figure shows results for a fixed diameter ratio ($D_3/D_1 = 1$), a fixed value of inlet mass flux and varying inlet quality. In all cases, an increase in inlet quality reduces the peak of the curve and increases the flow split at which complete separation takes place. It has been suggested that the reduction in the peak of the curve results from the effect of quality variations on the distribution of the phases within the inlet tube and the relative distribution of axial momentum between the flow components.

Consider first the distribution of the phases in the inlet tube. In horizontal annular flow, the liquid film is asymmetrically distributed around the tube wall with the film being thicker on the bottom than on the top of the tube. Butterworth (1972) identified 5 mechanisms responsible for the angular variation of liquid film thickness as:

i) Gravity drainage;

ii) Spreading of the film by wave motion;

iii) Transfer of liquid by net entrainment/deposition of droplets;

iv) Spreading by secondary circumferential shear forces;

v) Spreading by surface tension forces.

Laurinat (1982) and Laurinat et al. (1985) modelled the film distribution accounting for each of these mechanisms. The authors concluded

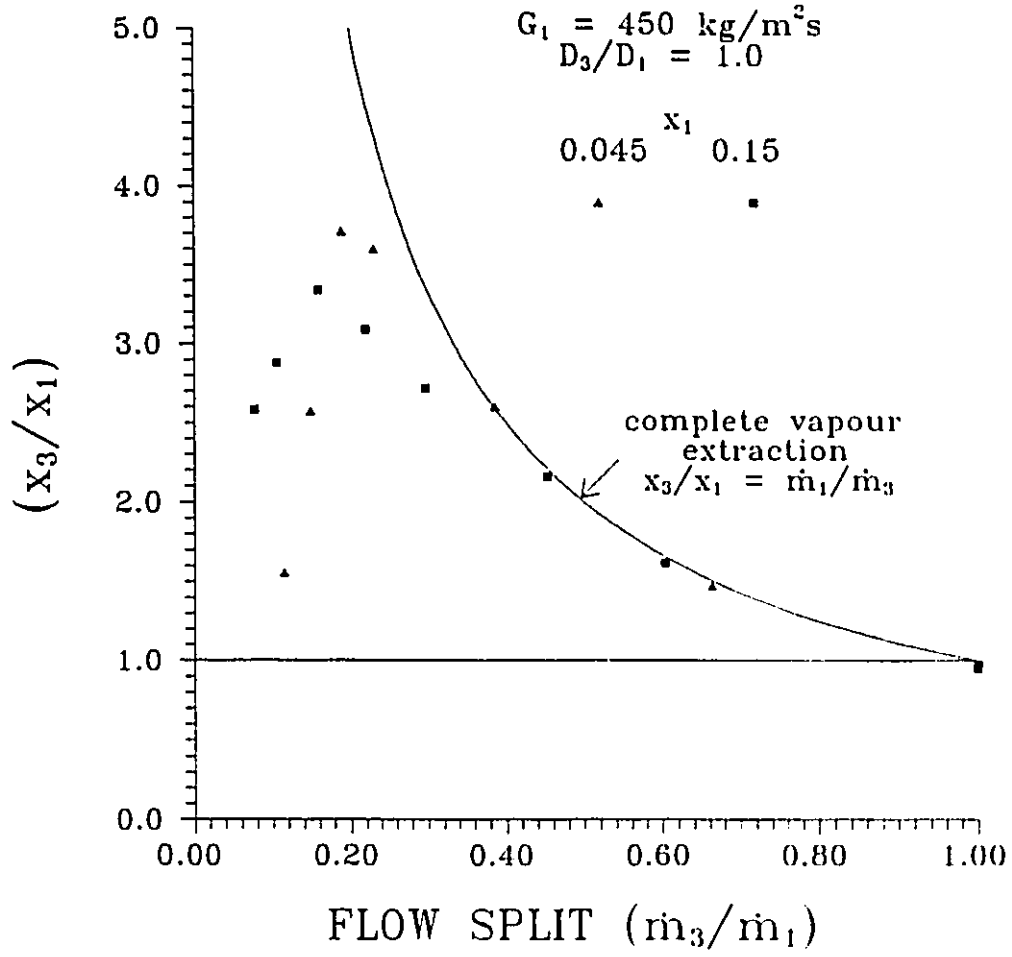

Figure 4.2 Effect of Inlet Quality on Phase Separation Characteristics

G_1= 450 kg/m^{2}s D_3/D_1= 1.0

x_1= 0.045 and 0.15

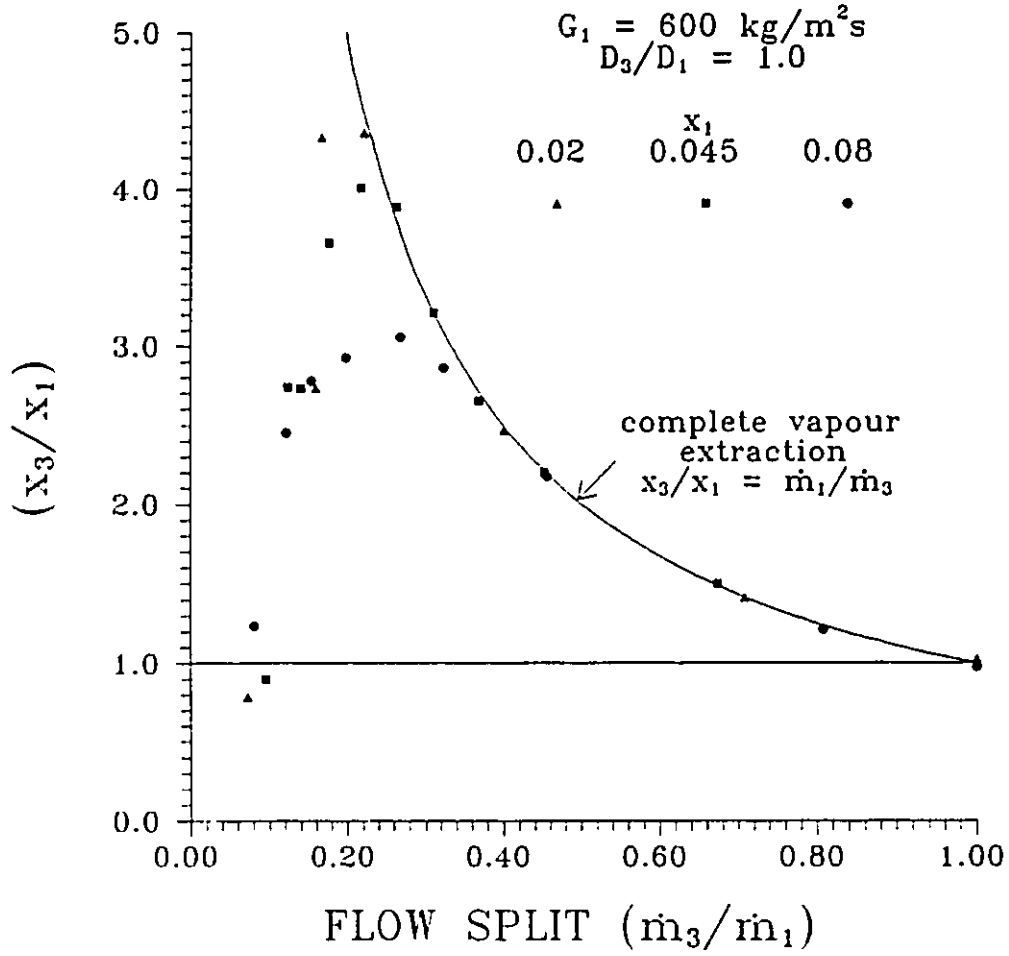

Figure 4.3 Effect of Inlet Quality on Phase Separation Characteristics

G_1= 600 kg/m^{2}s D_3/D_1= 1.0

x_1= 0.02, 0.045 and 0.08

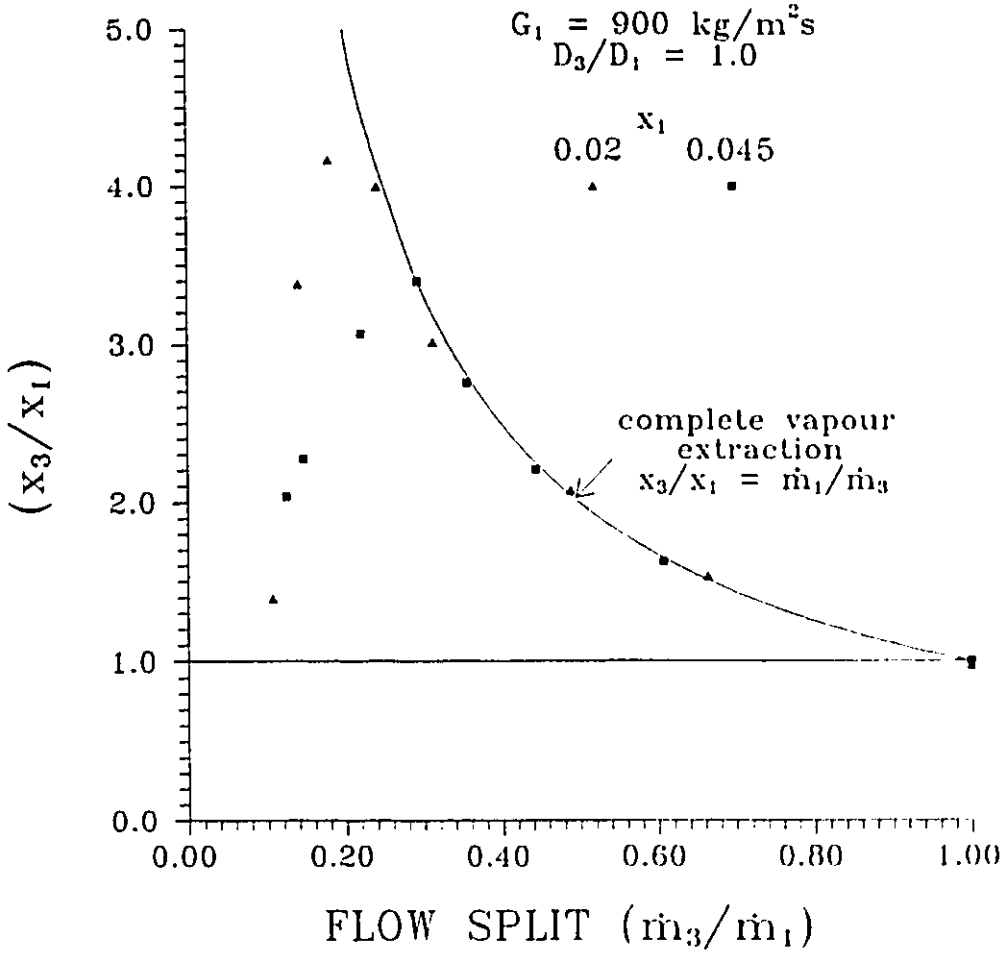

Figure 4.4 Effect of Inlet Quality on Phase Separation Characteristics

G_1= 900 kg/m²s D_3/D_1= 1.0

x_1= 0.02 and 0.045

that the surface tension effects are negligible for the pipe sizes considered in the present investigation. Lin et al. (1985) considered the remaining 4 mechanisms and concluded that gravity drainage, net entrainment/deposition and secondary shear forces are the dominant mechanisms affecting the liquid film distribution in horizontal annular two-phase flow.

The local circumferential component of the gravity force causes the liquid film to have a circumferential component of velocity which drains liquid from the upper potion of the tube towards the bottom. This tends to increase the film thickness at the bottom of the tube relative to the top.

As discussed earlier, a portion of the liquid flow is carried downstream in the form of droplets entrained within the high velocity gas core. There is a continuous exchange of liquid between the film and gas core as droplets are entrained from the film surface and then deposited back onto the surface further downstream. The dominant mechanism for entrainment in annular two-phase flow is the shearing off of roll wave crests from the liquid film by the streaming gas flow (Kataoka et al., 1983). Hewitt and Lacey (1965) indicated that the interfacial wave roughness increases as the averaged film thickness increases. Accordingly, more liquid is entrained from the bottom of the tube where the film is thicker as opposed to the top. Two mechanisms by which the droplets are returned to the film have been identified by James et al. (1987) as the droplet interactions with the gas phase turbulent eddies and by direct result of the velocity they acquire on their ejection from the liquid film. In general, the asymmetries in both the local entrainment and deposition rates tend to favor the transfer of liquid from the bottom of the tube to the top thereby counteracting the effects of gravity drainage.

The interfacial roughness between the liquid film and gas core is larger on the bottom of the tube than at the top as shown by Hewitt and Lacey (1965). Accordingly, there is more hydraulic resistance to the gas flow in the axial direction at bottom of the tube. This region is then associated with a net production of turbulence within the gas core. Hinze (1967) stated that in a region of net turbulence production there is an influx of turbulence-poor fluid and an efflux of turbulence-rich fluid. This favors the transfer of gas from the centre of the core towards the bottom liquid/vapour interface and up along the side of the interface creating a secondary vapour flow pattern as shown in Figure 4.5. This secondary flow yields an upward shear stress on the liquid film which helps to wet the upper portion of the tube again counteracting the effects of gravity drainage.

Increasing quality at constant mass flux in the annular flow, which corresponds to increasing vapour superficial velocity, causes more of the liquid film to be swept up the sides of the tube from the thick layer of liquid on the bottom. This results from an increased contribution to the film distribution by both net entrainment/deposition and secondary vapour flow. Consequently, more of the liquid film can be intercepted by the branch opening and is easily extracted.

This effect is exaggerated by the method of presenting the data in Figures 4.2 through 4.4. As x_1 increases, the maximum value of x_3/x_1 decreases ($(x_3/x_1)_{max} = 1/x_1$). This reduces the peak of the envelope which can enclose the data with increasing inlet quality (see section 2.1). By plotting the fraction of liquid removed through the branch, $\dot{m}_3(1-x_3)/\dot{m}_1(1-x_1)$, against the fraction of vapour removed, $\dot{m}_3 x_3/\dot{m}_1 x_1$, as shown in Figures 4.6 through 4.8, the effect of film distribution is seen to

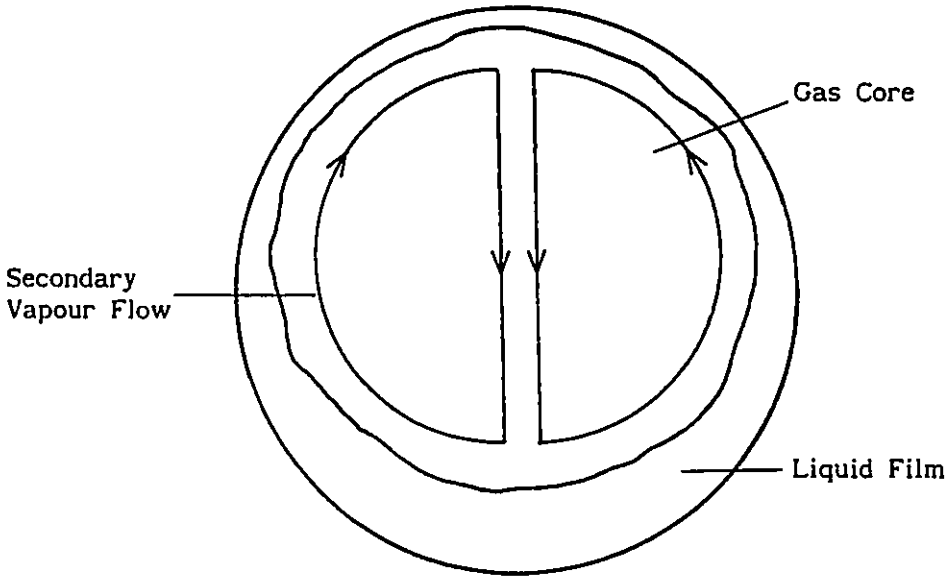

Figure 4.5 Annular Flow Film Distribution and Secondary Vapour Flow

be more subtle. The higher inlet quality data from the region of the peak in the previous curves show a slightly higher fraction of liquid removed through the branch for the same fraction of vapour removed.

Another effect of inlet quality competes with the film distribution and acts to decrease the portion of liquid removed with increasing inlet quality. As quality is increased, the time averaged portion of liquid that is carried as entrained droplets within the gas core increases. The ratio of the mass flow rate of entrained droplets to the total liquid mass flow rate is the equilibrium entrainment ratio (E). As this ratio increases, the lower momentum flux liquid film is depleted resulting in a smaller portion of liquid removed through the branch for a given portion of gas removed.

For a two-phase flow, a critical velocity exists below which no droplet entrainment takes place. Steen (1964), as presented by Wallis (1969), suggested the following criterion for the onset of entrainment:

$$\frac{j_G \mu_G}{\sigma} \left(\frac{\rho_G}{\rho_L} \right)^{1/2} = \pi_2 > 2.46 \times 10^{-4}. \qquad (4.1)$$

For only 3 inlet conditions considered was this criteria exceeded and only significantly for $G_1 = 450$ kg/m^{2}s with $x_1 = 0.15$ ($\pi_2 = 5.06 \times 10^{-4}$). For this condition, the correlation by Wallis (1968) predicts that almost 40% of the liquid is carried as entrained droplets. Figure 4.6 Shows the effect that this level of entrainment can have on the separation characteristics. Particularly at low flow splits, the higher inlet quality condition (having the higher equilibrium entrainment ratio) shows a smaller portion of liquid extracted for the same portion of gas extracted as compared to the lower inlet quality case.

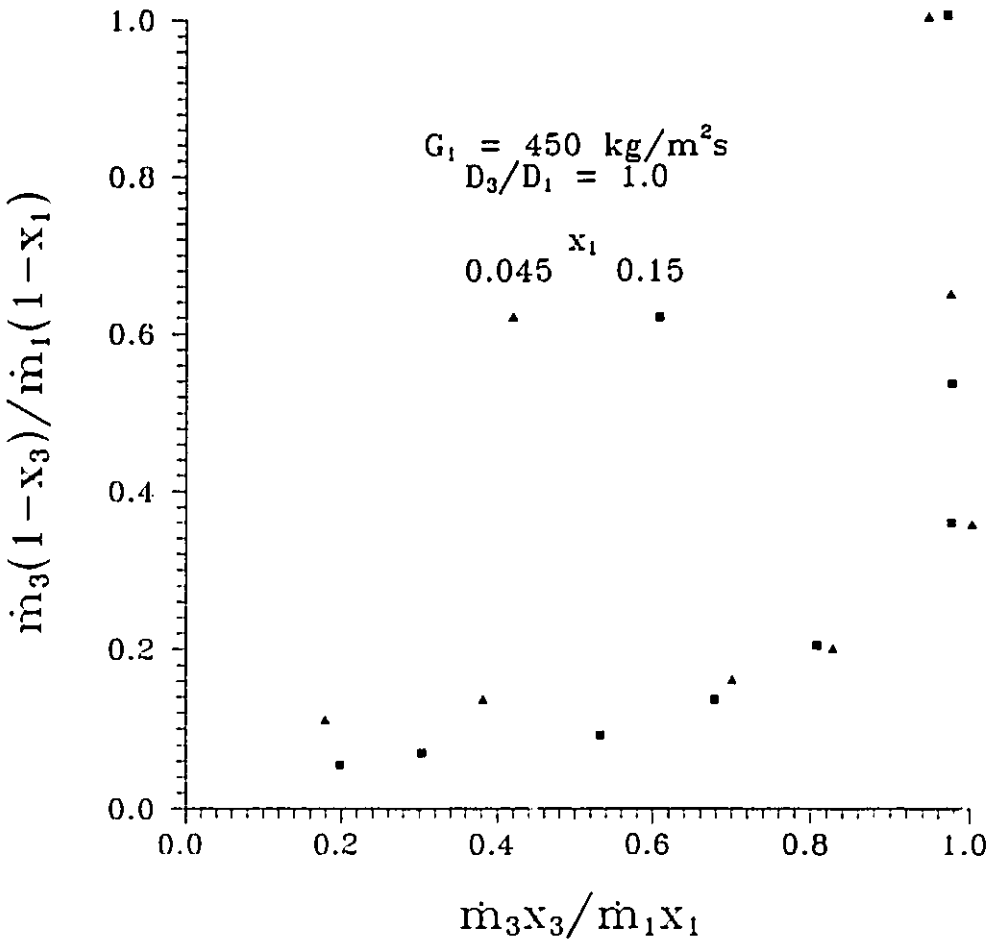

Figure 4.6 Effect of Inlet Quality on Phase Separation Characteristics

Fraction of Liquid vs. Fraction of Gas Extracted

G_1 = 450 kg/m²s D_3/D_1 = 1.0

x_1 = 0.045 and 0.15

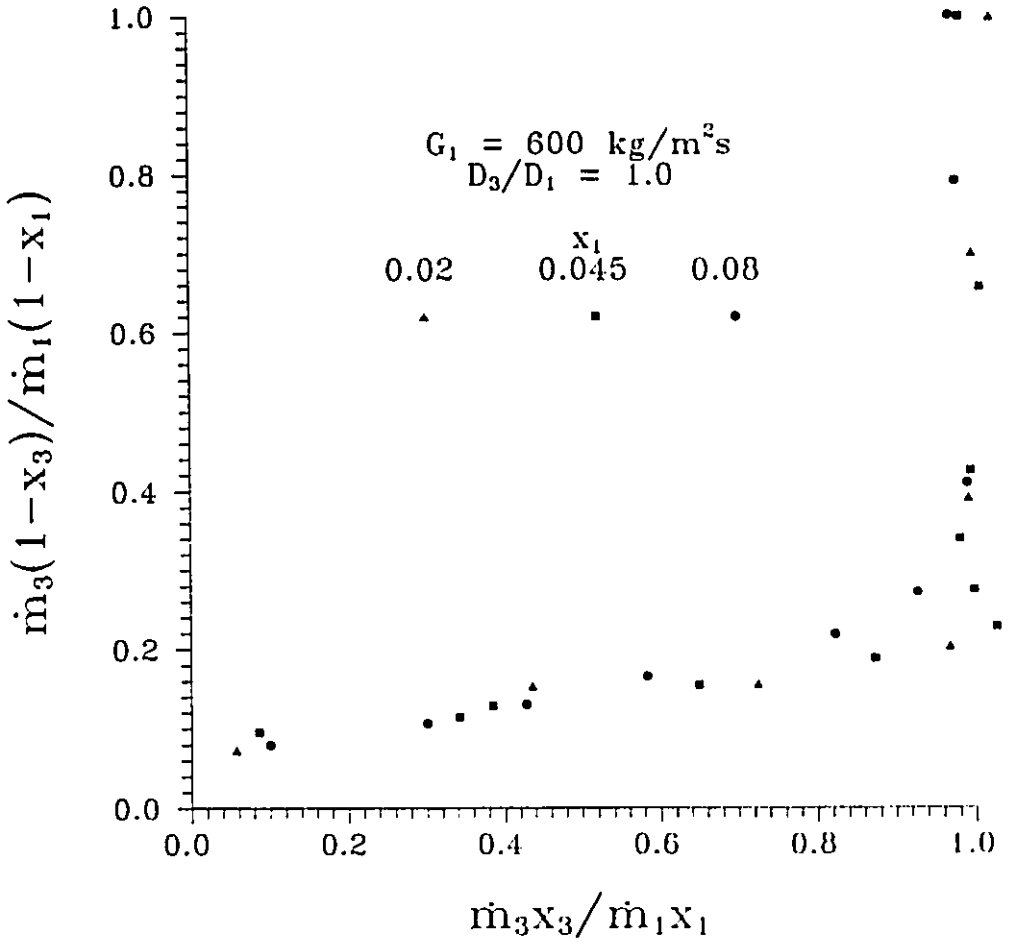

Figure 4.7 Effect of Inlet Quality on Phase Separation Characteristics

Fraction of Liquid vs. Fraction of Gas Extracted

G_1= 600 kg/m²s D_3/D_1= 1.0

x_1= 0.02, 0.045 and 0.08

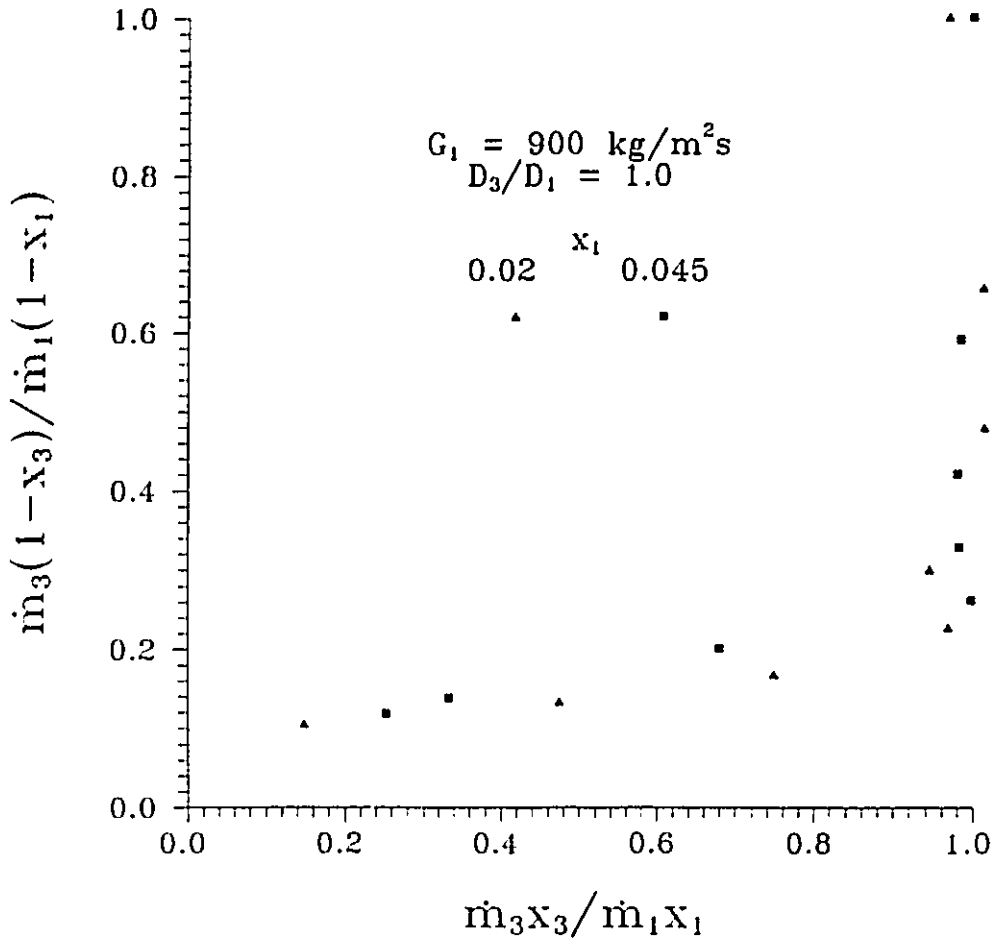

Figure 4.8 Effect of Inlet Quality on Phase Separation Characteristics

Fraction of Liquid vs. Fraction of Gas Extracted

G_1= 900 kg/m^{2}s D_3/D_1= 1.0

x_1= 0.02 and 0.045

4.1.3 Effect of Inlet Mass Flux

Figures 4.9 and 4.10 show the effect of inlet mass flux. Both figures represent data taken at a fixed inlet quality and various values of inlet mass flux (D_3/D_1= 1.0). For the range of inlet conditions tested, the effect of mass flux on the separation characteristics demonstrated trends consistent with those identified for inlet quality variations. Increasing mass flux at constant quality results in an increase in vapour velocity. This may yield a more uniform liquid film distribution through the mechanisms of net entrainment/deposition and or secondary vapour flow as discussed in the previous section. The more uniform film causes more of the liquid to be intercepted by the branch opening thereby reducing the branch quality for a given flow split. This effect is quite subtle for this range of data but the results shown in Figures 4.9 and 4.10 tend to support it, particularly for the highest mass flux cases in each figure.

4.1.4 Effect of Branch Diameter

Figures 4.11 through 4.14 show the effect of diameter ratio on the phase separation characteristics. Each figure is for fixed values of inlet mass flux and quality with the various curves representing different branch diameters. The curves indicate that separation becomes more severe with a reduction in branch diameter as characterized by a higher branch quality at all flow splits before complete vapour extraction. The smaller branch also requires a lower flow split for complete vapour extraction to be reached.

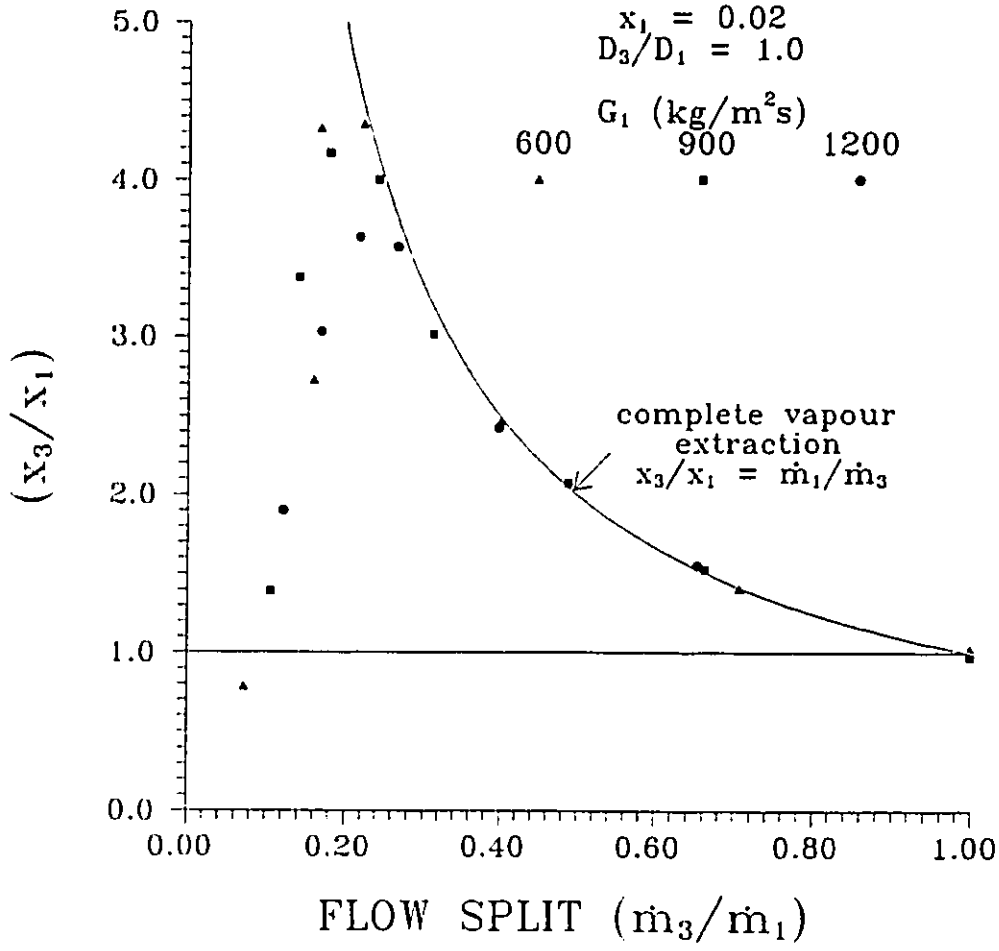

Figure 4.9 Effect of Inlet Mass Flux on Phase Separation Characteristics

x_1 = 0.02 D_3/D_1 = 1.0

G_1 = 600, 900 and 1200 kg/m^{2}s

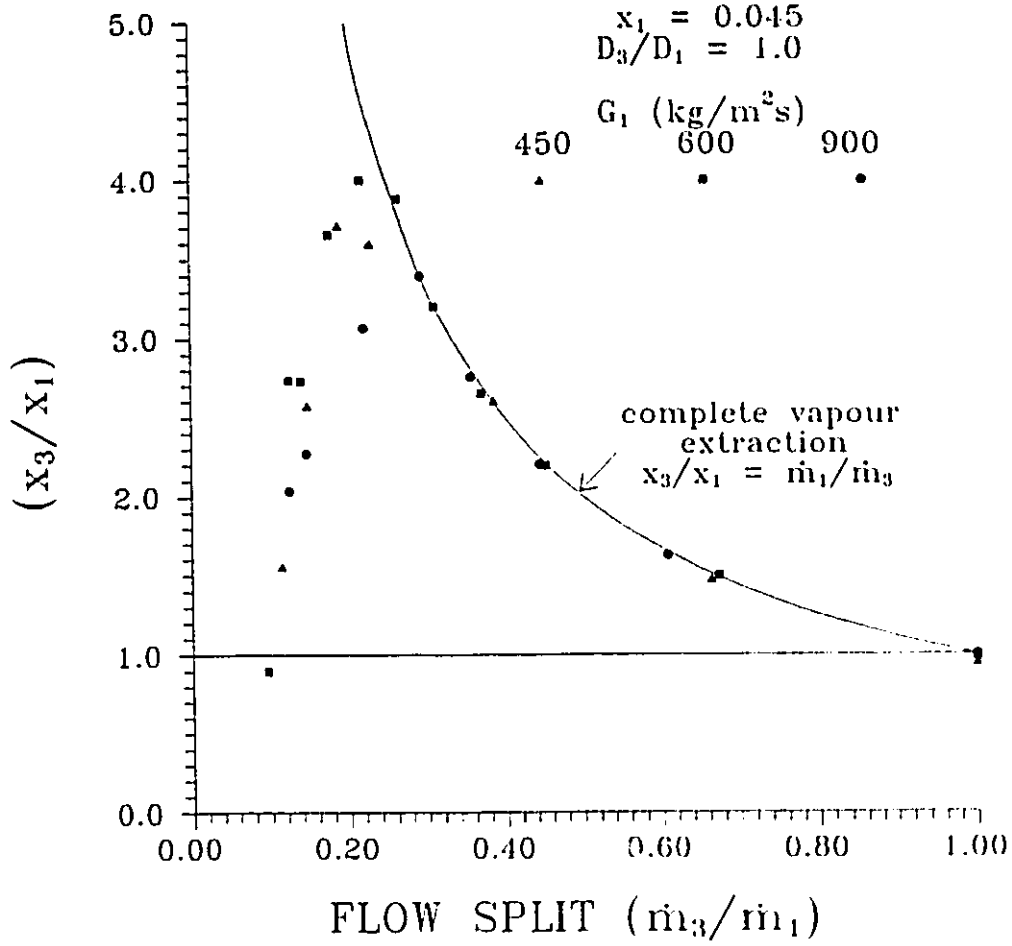

Figure 4.10 Effect of Inlet Mass Flux on Phase Separation Characteristics

x_1= 0.045 D_3/D_1= 1.0

G_1= 450, 600 and 900 kg/m^{2}s

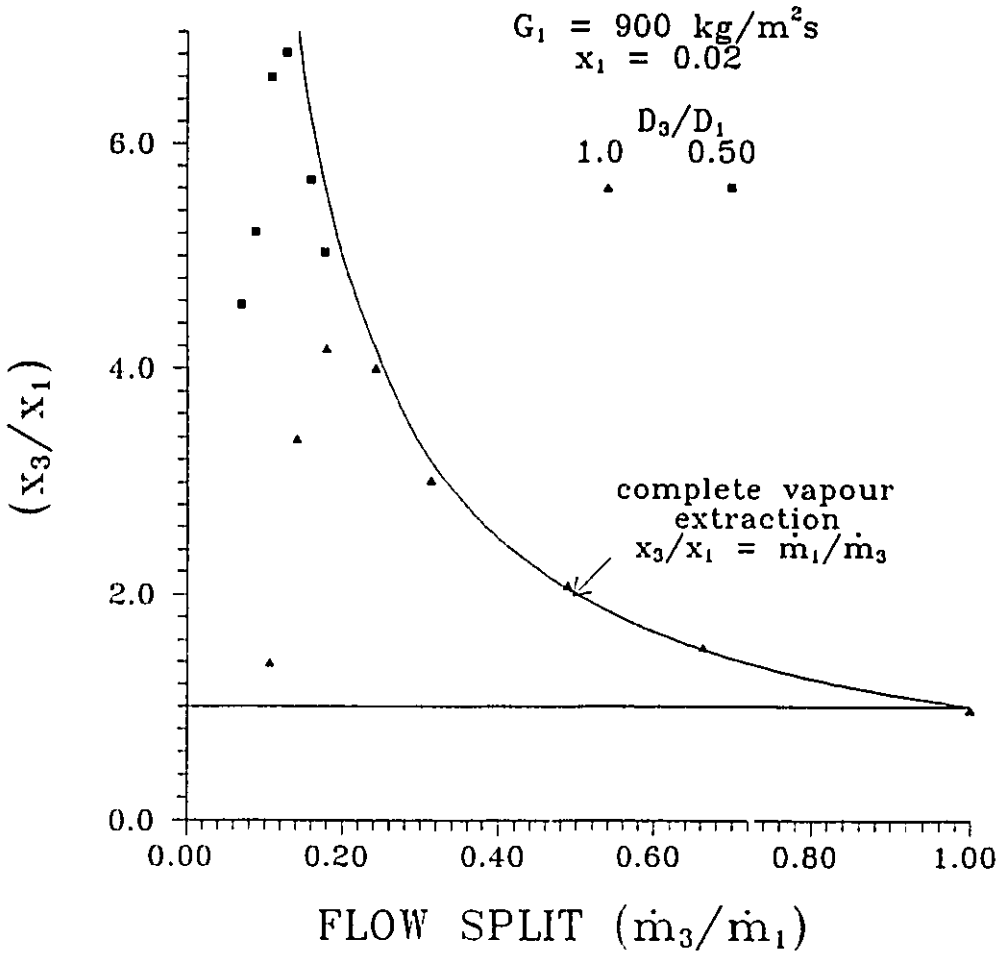

Figure 4.11 Effect of Branch Diameter on Phase Separation Characteristics

G_1 = 900 kg/m^{2}s x_1 = 0.02

D_1 = 1.0 and 0.50

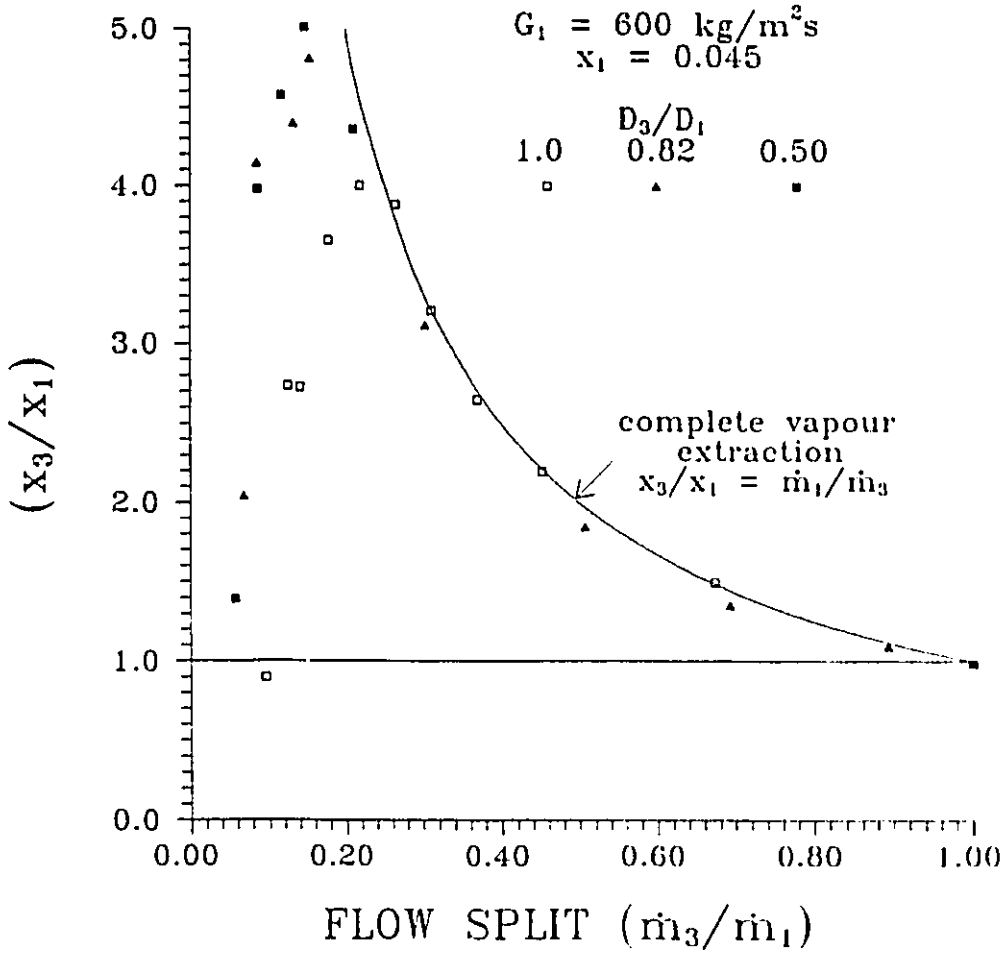

Figure 4.12 Effect of Branch Diameter on Phase Separation Characteristics

G_1= 600 kg/m^{2}s x_1= 0.045

D_1= 1.0, 0.82 and 0.50

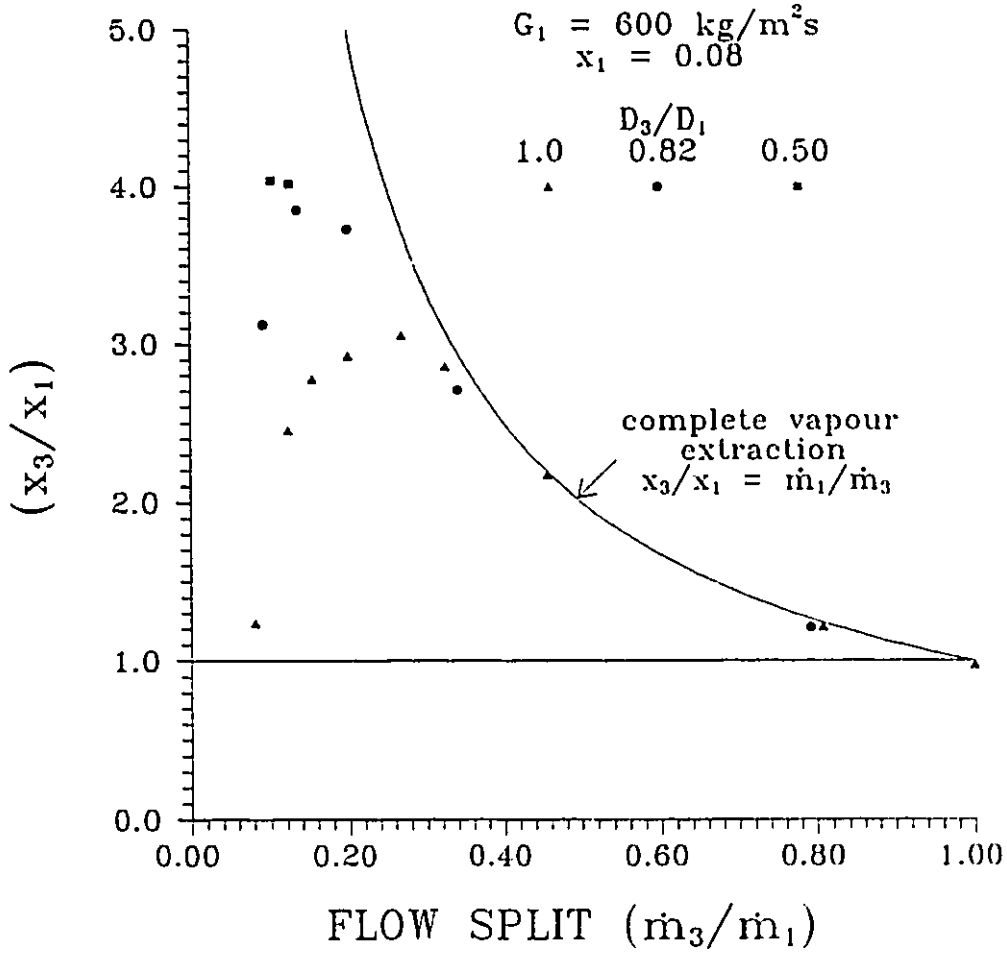

Figure 4.13 Effect of Branch Diameter on Phase Separation Characteristics

G_1= 600 kg/m²s x_1= 0.08

D_1= 1.0, 0.82 and 0.5

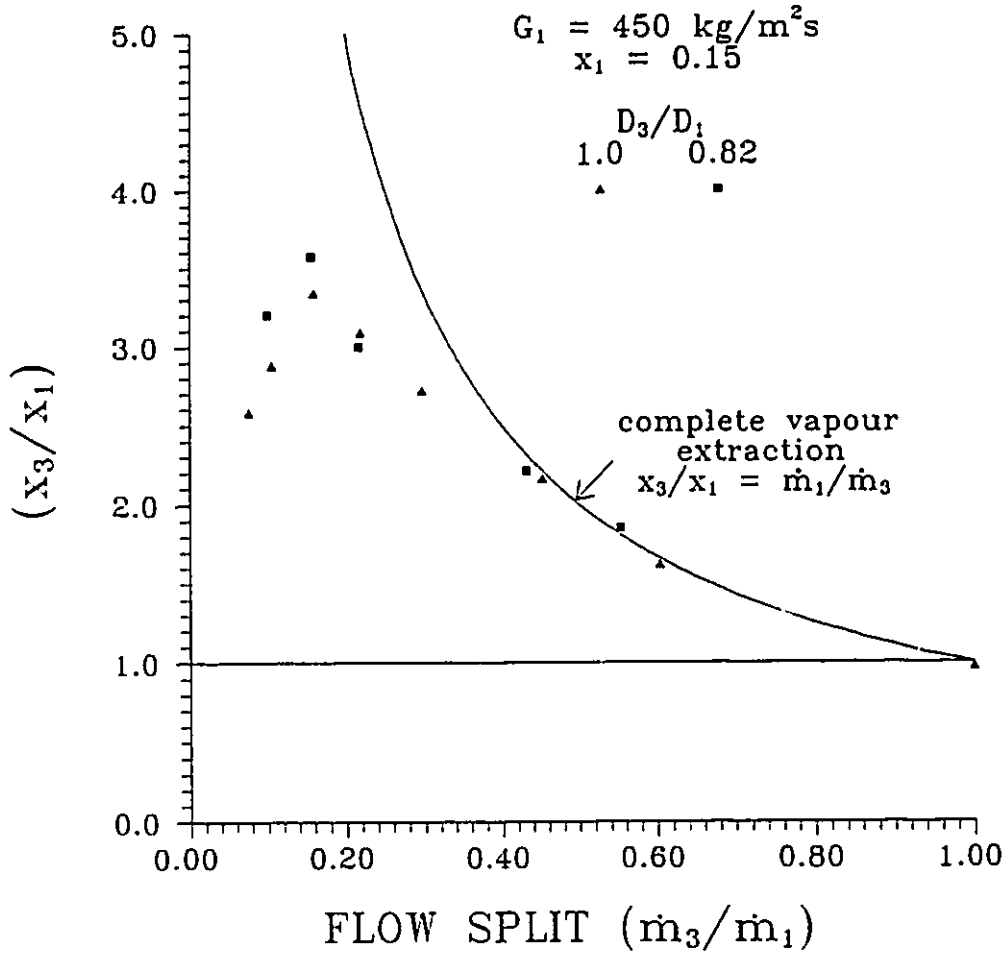

Figure 4.14 Effect of Branch Diameter on Phase Separation Characteristics

G_1= 450 kg/m^{2}s x_1= 0.15

D_1= 1.0 and 0.82

One factor contributing to the higher branch qualities is a reduction in the portion of the liquid film that is easily extracted through the branch while the vapour phase continues to be easily extracted because of its relatively low axial momentum. As the branch diameter is reduced, the liquid film in the inlet flowing above or below the branch opening cannot be extracted directly through the branch. The extraction of these portions of the liquid film is governed by the Bernoulli effect. The high velocity of the gas portion entering the branch causes a local underpressure in the vicinity of the branch opening. The liquid film can then move toward the branch opening in response to the pressure gradient developed. If this pressure gradient is sufficient, a portion of the liquid film will be entrained into the branch by the streaming gas.

Figures 4.12 and 4.13 show that the effect of branch diameter becomes less pronounced as the branch diameter is decreased. The data for a branch to inlet diameter ratio (D_3/D_1) of 0.82 is closer to the data for D_3/D_1= 0.5 than it is to that for D_3/D_1= 1.0. As discussed in previous sections, horizontal annular flow has an asymmetrical film distribution with a thicker liquid layer on bottom. As the branch to inlet diameter ratio is reduced from unity, the incremental portions of liquid film lost to direct extraction on the bottom is greatest at higher branch to inlet diameter ratios. Further, as the branch diameter is decreased, the branching acceleration and velocity of the gas phase must increase for the same portion of gas to be removed. This enhances the carry over mechanism (Bernoulli and entrainment effects discussed above) particularly for the smallest branch diameter (D_3/D_1= 0.5). This may tend to offset the loss of liquid film to direct extraction reducing the extent of separation.

4.2 Two-Phase Pressure and Void Fraction Distribution

Figures 4.15a and 4.15b show typical void fraction profiles through the test section for similar inlet conditions at different flow split ratios. These correspond to a value below that required for total separation ($\dot{m}_3/\dot{m}_1$=0.18) in 4.15a and a condition where almost total phase separation takes place ($\dot{m}_3/\dot{m}_1$=0.31) in 4.15b. These data are for G_1= 600 kg/m^{2}s $x_1 \cong$ 0.045 and D_3/D_1= 1.0. The corresponding pressure distribution data is shown in Figures 4.16a and 4.16b. The drastic drop in the fully developed run void fraction between Figures 4.15a and 4.15b was associated with a flow regime transition from the annular towards slug/plug flow as total separation was approached. This was verified by plotting the run flow conditions on a flow regime map (Mandhane et al. 1974)). Under these conditions, the void fraction through the run remained relatively high for some distance downstream of the junction (Figure 4.15b). Figure 4.16b shows a steep positive pressure gradient in this portion of the run. These measurements suggest the presence of significant phase redistribution and vapour recirculation in the run as the vapour responds to the adverse pressure gradient. This explains the need for a long recovery length in the run, as reported by Saba and Lahey (1984) and observed in the present work.

The variation in some of the measured parameters with branch flow split for typical inlet conditions is shown in Figure 4.17. Increasing the flow split can be considered a direct result of increasing the pressure drop through the branch of the T making it a more favorable flow passage. Accordingly, the branch pressure drop, $(\Delta P_{1\text{-}3})_j$, is seen to increase with increasing flow split in Figure 4.17a. At low flow splits, this is

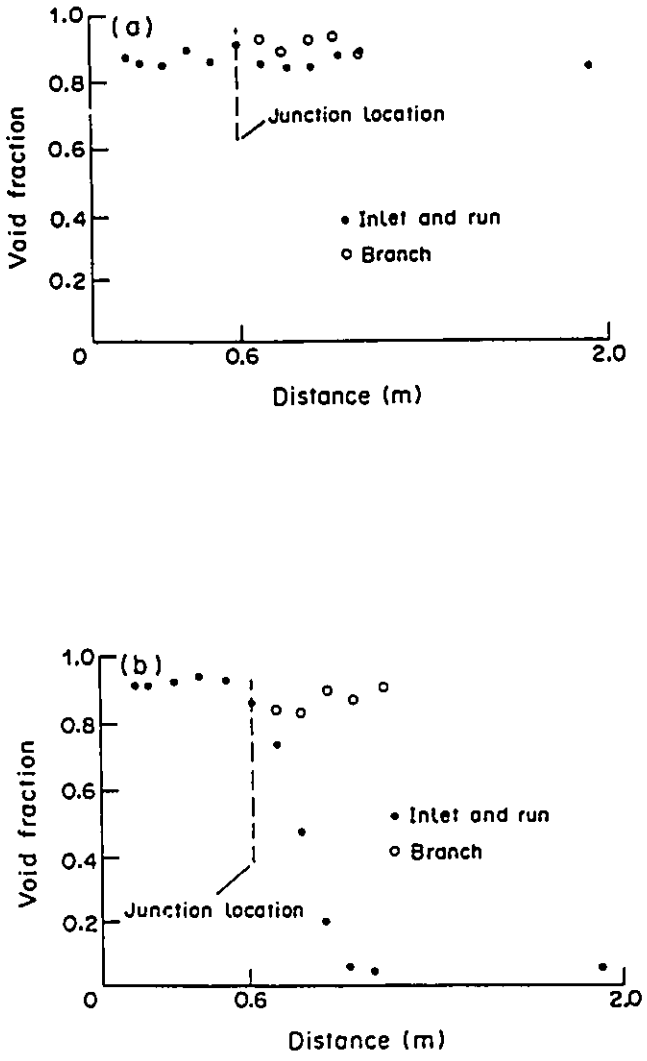

Figure 4.15 Typical Void Fraction Distributions Near Total Separation

(a) $G_1 = 600$ kg/m^{2}s, $x_1 = 0.045$, $\dot{m}_3/\dot{m}_1 = 0.18$

(b) $G_1 = 600$ kg/m^{2}s, $x_1 = 0.050$, $\dot{m}_3/\dot{m}_1 = 0.31$

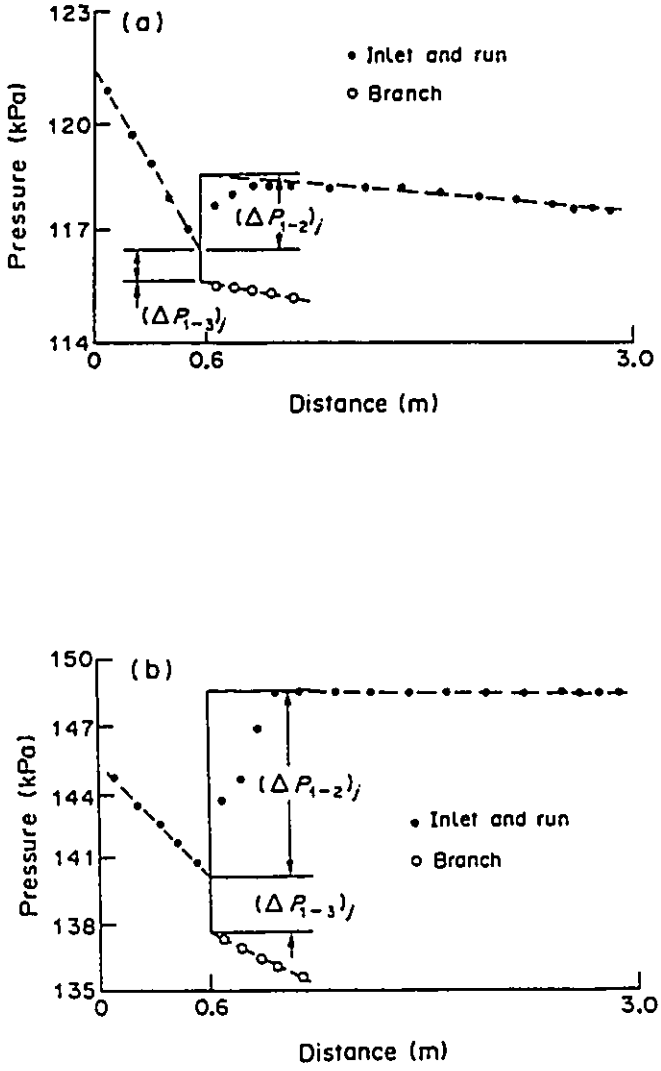

Figure 4.16 Typical Pressure Distributions Near Total Separation

(a) G_1= 600 kg/m^{2}s, x_1= 0.045, $\dot{m}_3/\dot{m}_1$= 0.18

(b) G_1= 600 kg/m^{2}s, x_1= 0.050, $\dot{m}_3/\dot{m}_1$= 0.31

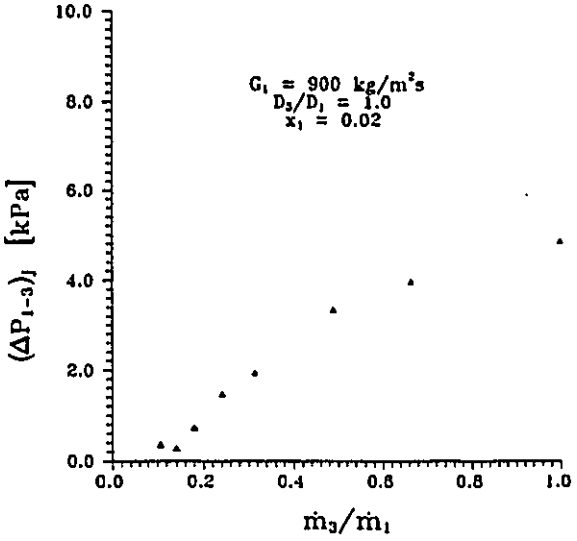

a) Branch Pressure Drop vs. Flow Split

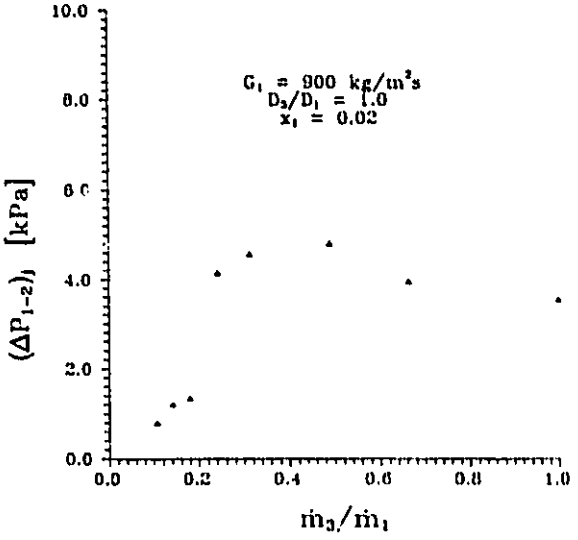

b) Run Pressure Rise vs. Flow Split

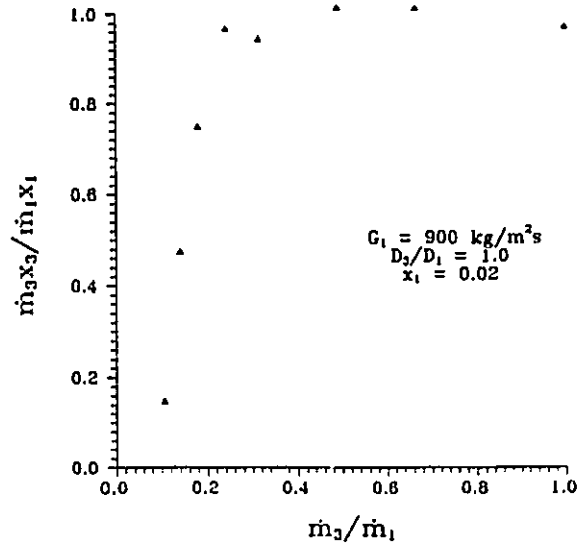

c) Fraction of Gas Extracted vs Flow Split

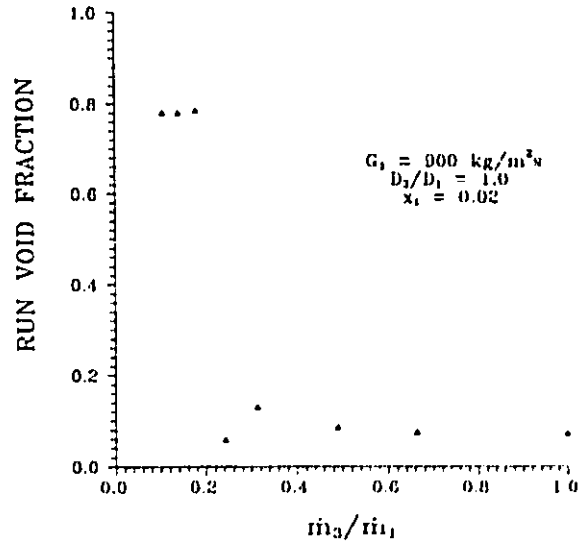

d) Run Void Fraction vs. Flow Split

Figure 4.17 Typical Flow Characteristics in Dividing Two-Phase Flow

simultaneously associated with an increase in the run pressure rise, $(\Delta P_{2\text{-}1})_J$, due to expansion of the flow downstream of the junction as shown in Figure 4.17b. This adverse pressure gradient in the run of the T yields an additional driving force for the flow into the branch. The gas phase responds more readily to the pressure gradients due to its lower momentum as indicated by a steep increase in the fraction of gas removed in Figure 4.17c. As the gas flow through the run is depleted, annular flow cannot be supported and transition towards the lower void fraction (lower momentum) slug\plug flows takes place. This is indicated by a sharp drop in the fully developed run void fraction in 4.17d and is simultaneously associated with a large increase in the run pressure rise (Figure 4.17b).

4.3 Physical Model Formulation

A curve showing typical phase separation characteristics is again shown in Figure 4.18. Based on the measurements described above, it is perceived that the physical situation within the junction can be summarized as follows. At low extraction rates, flow is first diverted to the branch of the T as a result of a small but favorable pressure gradient along the branch. At low flow splits, the branching flow is made up of liquid from the portion of liquid film that is intercepted by the branch opening. This flow component has a relatively low momentum flux (ρu^2) and is well situated for easy extraction. This portion of the curve is represented by zone 1 in the Figure and is characterized by a branch quality below the inlet quality.

The portion of liquid film that is easily extracted is quickly depleted. The next flow component that is readily available for extraction

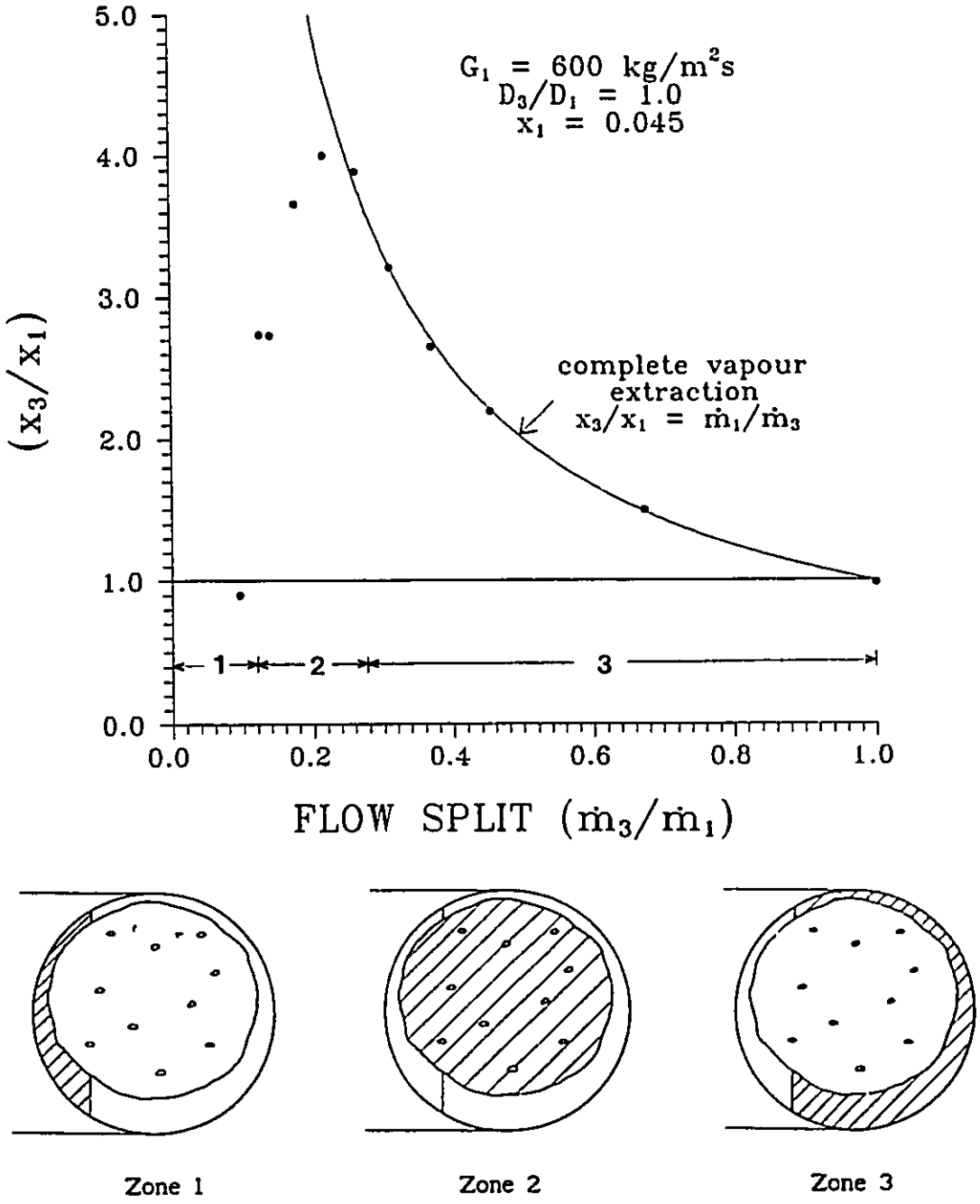

Figure 4.18 Typical Phase Separation Characteristics and Physical Model

is the low density gas core. Due to its low density, this component has a higher acceleration toward the branch in response to the pressure gradients within the junction. This portion of the curve is represented by zone 2 in Figure 4.18 and is characterized by a steep increase in branch quality with flow split. The curve ultimately approaches the complete vapour extraction curve as the gas core becomes depleted. Near complete vapour extraction, the flow in the run undergoes a flow regime transition with a significant reduction in the fully developed run void fraction. The flow momentum through the run is then greatly reduced with a resultant increase in the run pressure rise. At this point the pressure increase through the run represents a significant adverse pressure gradient aiding in the extraction of the remaining flow components (liquid film and entrained droplets).

With all of the gas core diverted to the branch, measurements indicate a very steep positive pressure gradient and negative void fraction gradient through the run of the T (Figures 4.15 and 4.16). Based on these measurements, the physical situation encountered near the point of total separation is depicted schematically in Figure 4.19. It is perceived that the branching flow is extracted from the liquid film intercepted by the branch opening and the high velocity, low density gas core. A vapour/liquid interface may form in the run downstream of the junction, under the influence of the adverse pressure gradient, forming a boundary for a vapour recirculation zone. In the presence of this pressure gradient, condensation can also take place at the vapour/liquid interface. Small vapour bubbles may break off at the interface and continue flowing in the run as shown.

This analysis identifies several factors that are important in establishing the level of phase separation, particularly at low extraction

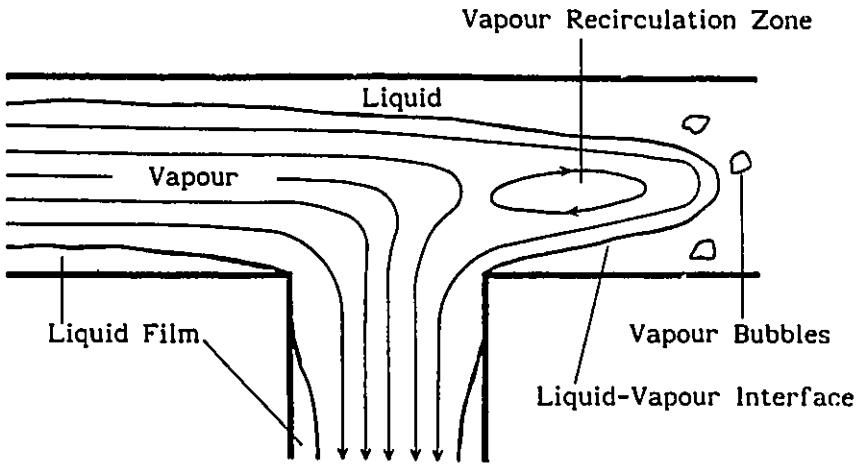

Figure 4.19 Postulated Flow Characteristics Near Total Separation

rates. These include, the distribution of the phases in the inlet tube relative to the branch opening, the junction geometry (branch diameter), the junction pressure distribution and the relative momentum of the flow components. A mathematical formulation of this physical model has been developed in order to predict the degree of phase separation for annular flow in a dividing T junction. This model is presented in Chapter 6.

CHAPTER 5

JUNCTION PRESSURE CHANGES

5.1 Single Phase Pressure Changes

5.1.1 Run Pressure Change

The axial pressure rise at the junction results from the diversion of a portion of the flow to the branch and the subsequent axial deceleration of the remaining flow. This process is similar to that which takes place in a sudden flow expansion which is successfully modelled using axial momentum balance models as discussed by Delhay (1981).

All of the single-phase run pressure change data collected for the three test sections were reduced to a momentum correction factor (k_{1-2}) using a balance of axial momentum at the junction (Equation 2.7), i.e.,

$$(\Delta P_{2-1})_j = k_{1-2}\rho(u_1^2 - u_2^2). \tag{5.1}$$

Figure 5.1 shows the results obtained with varying inlet mass flux for the test section with equal inlet and branch diameters ($D_3/D_1 = 1.0$). The momentum correction factor is seen to decrease with increasing flow split. At higher flow splits, more of the branch flow is removed from the core region of the inlet where the axial momentum of the flow is higher. At higher flow splits, the average axial momentum of the branching flow before

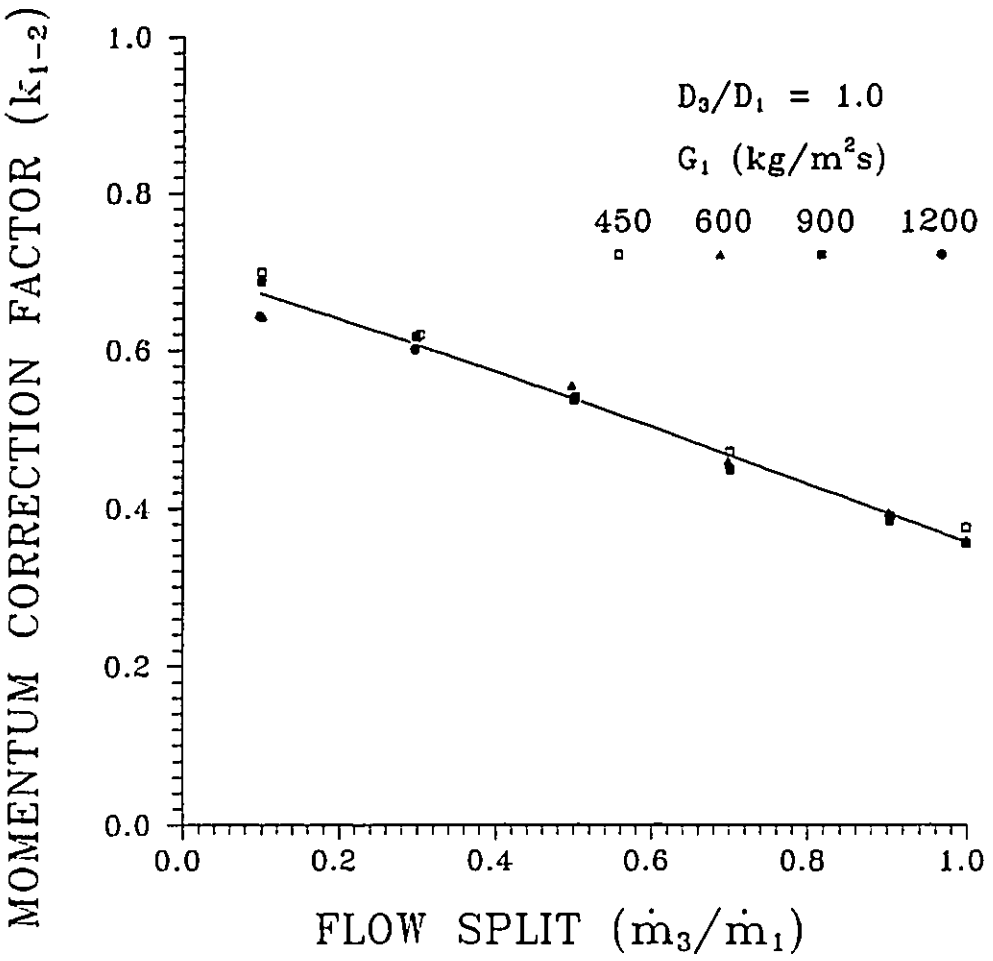

Figure 5.1 Single-Phase Momentum Correction Factor (k_{1-2}) vs. Flow Split

D_3/D_1= 1.0

extraction is then higher. Consequently, the flow is capable of carrying more axial momentum to the branch. As discussed in Section 2.3.2, an increase in the branching flow axial momentum is indicated by a reduction in the momentum correction factor as demonstrated by the data.

The results in Figure 5.1 also show that the mass flux has no appreciable effect on the value of the momentum correction factor for the range of data tested. These findings are consistent with previous published results (e.g. NcNown, 1954 and Collier, 1976).

Figure 5.2 shows the effect of branch diameter on all of the single phase data collected. Over most of the flow split range, the general trend is for the correction factor to decrease with branch diameter at a given flow split. Solving for k_{1-2} between Equations 2.6 and 2.7 yields

$$k_{1-2} = 1 - \frac{1}{A\rho(u_1^2 - u_2^2)} \int_{A_3} \rho u_x u_y dA. \tag{5.2}$$

Assuming average values for u_x and u_y on A_3 (i.e. $u_y = u_3$ and $u_x = u_{3x}$), Equation 5.2 may be written as

$$k_{1-2} = 1 - \frac{u_{3x}/u_1}{2 - \dot{m}_3/\dot{m}_1}. \tag{5.3}$$

As the branch diameter is decreased for a given flow split, a smaller portion of the branch flow will be taken from the slower moving fluid at the walls of the inlet tube. More fluid is then removed from the higher velocity core region which would increase the average axial velocity of the branching flow (u_{3x}). Equation 5.3 suggests that this would yield a lower value of k_{1-2} as demonstrated by the data.

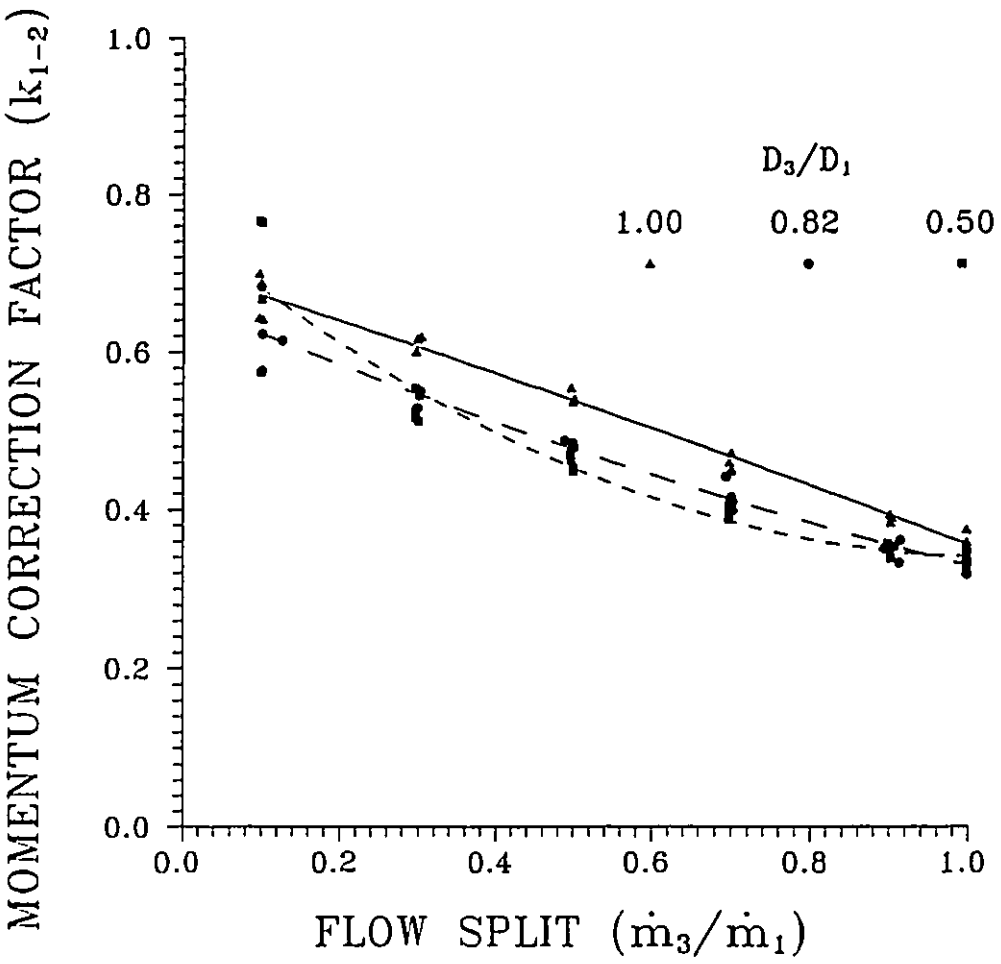

Figure 5.2 Single-Phase Momentum Correction Factor (k_{1-2}) vs. Flow Split

Effect of Branch Diameter

The data shows clearly that a unique relationship exists between the momentum correction factor and flow split, for a given junction geometry, independent of mass flux. Using least squares, the present data was correlated by

$$k_{1-2} = 0.703 - 0.312 \left(\frac{\dot{m}_3}{\dot{m}_1}\right) - 0.035 \left(\frac{\dot{m}_3}{\dot{m}_1}\right)^2, \text{ for } D_3/D_1 = 1.0 \qquad (5.4)$$

$$k_{1-2} = 0.664 - 0.415 \left(\frac{\dot{m}_3}{\dot{m}_1}\right) + 0.080 \left(\frac{\dot{m}_3}{\dot{m}_1}\right)^2, \text{ for } D_3/D_1 = .82 \qquad (5.5)$$

$$k_{1-2} = 0.756 - 0.798 \left(\frac{\dot{m}_3}{\dot{m}_1}\right) + 0.382 \left(\frac{\dot{m}_3}{\dot{m}_1}\right)^2, \text{ for } D_3/D_1 = .50. \qquad (5.6)$$

At very low flow splits the branching flow will be taken from the slow moving fluid at the walls of the tube. Since this fluid has a low axial momentum in the inlet, it is expected that under these conditions the average axial velocity of the branching flow (u_{3x}) will be small. As ($\dot{m}_3/\dot{m}_1$) approaches zero, u_{3x} should also approach zero. From Equation 5.3, the limit for k_{1-2} should then be unity as the flow split is reduced to zero. Equations 5.4 - 5.6 represent the best fit of the data in the range $0.1 \leq \dot{m}_3/\dot{m}_1 \leq 1.0$ and as a result do not demonstrate this limiting trend.

5.1.2 Branch Pressure Change

All of the single-phase branch pressure change data collected for the three test sections were reduced to a branch loss coefficient (k_{1-3}) by way of a mechanical energy balance between the inlet and branch (Equation 2.20), i.e.,

$$(\Delta P_{1-3})_j = P_{1j} - P_{3j} = \frac{\rho}{2}(u_3^2 - u_1^2) + k_{1-3}\frac{\rho}{2}u_1^2. \qquad (5.7)$$

Here, the first term on the r.h.s. of Equation 5.7 represents the reversible pressure change and the second term the irreversible change modelled in terms of a loss coefficient (k_{1-3}) acting on the inlet dynamic head. Figure 5.3 shows the results obtained with varying inlet mass flux for the test section with equal inlet and branch diameters ($D_3/D_1 = 1.0$). The loss coefficient is seen to be dependent upon the branch flow split but demonstrates no significant mass flux dependency.

When the single phase data from all of the test sections was reduced in terms of equation 5.7, the results are as shown in Figure 5.4. The branch loss coefficient is seen be dependent upon junction geometry (D_3/D_1) as well as flow split. The data shows that the pressure losses through the branch increase significantly as the branch diameter is reduced. This results from the corresponding higher radial acceleration required for the same flow fraction to be removed through the smaller diameter branches. These findings are consistent with previous published results (e.g. NcNown, 1954 and Collier, 1976). The data for the three test sections were correlated by;

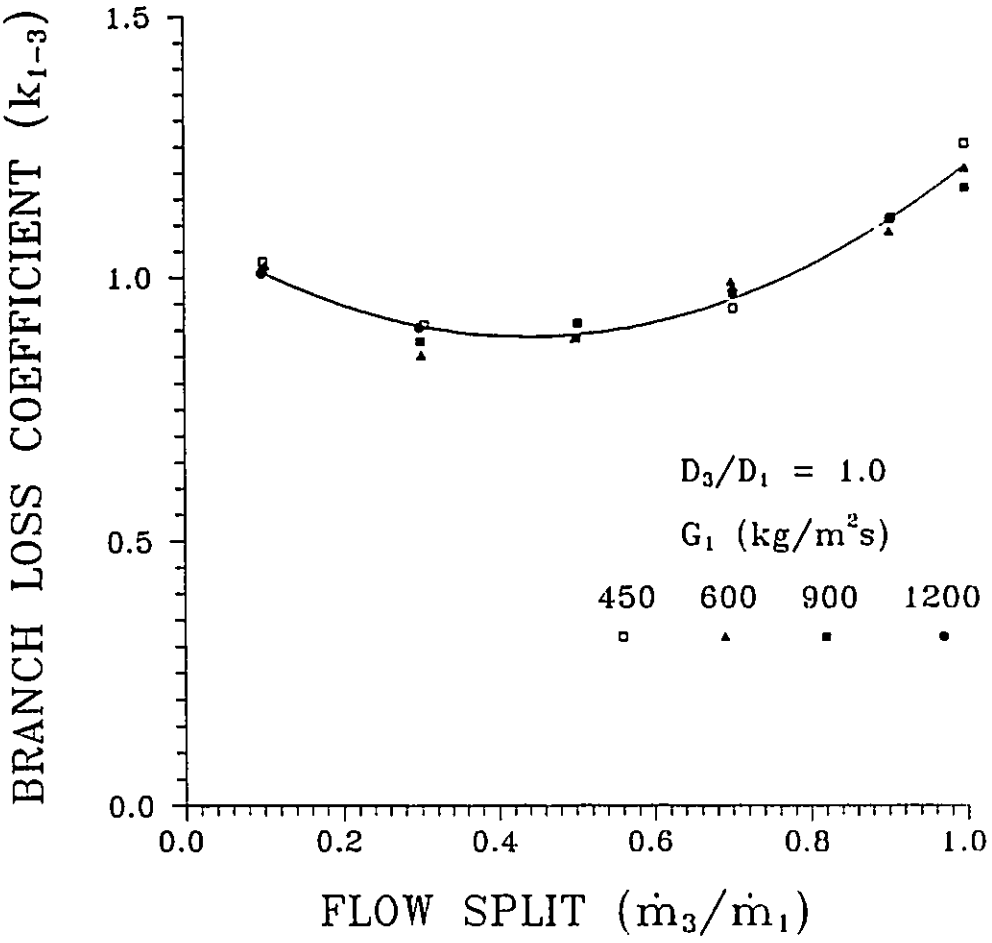

Figure 5.3 Single-Phase Branch Loss Coefficient (k_{1-3}) vs. Flow Split

D_3/D_1= 1.0

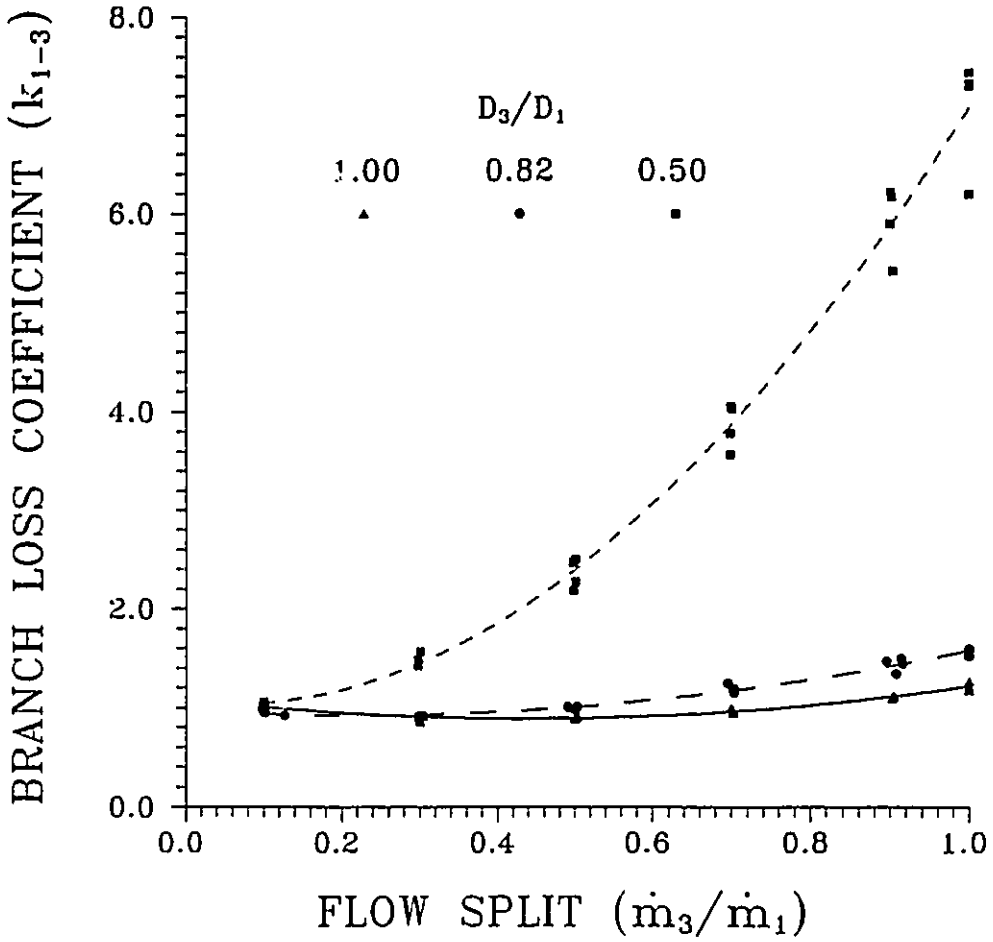

Figure 5.4 Single-Phase Branch Loss Coefficient (k_{1-3}) vs. Flow Split

Effect of Branch Diameter

$$k_{1-3} = 1.091 - 0.921 \left(\frac{\dot{m}_3}{\dot{m}_1}\right) + 1.045 \left(\frac{\dot{m}_3}{\dot{m}_1}\right)^2, \text{ for } D_3/D_1 = 1.0 \qquad (5.8)$$

$$k_{1-3} = 0.974 - 0.478 \left(\frac{\dot{m}_3}{\dot{m}_1}\right) + 1.081 \left(\frac{\dot{m}_3}{\dot{m}_1}\right)^2, \text{ for } D_3/D_1 = .82 \qquad (5.9)$$

$$k_{1-3} = 1.042 - 0.649 \left(\frac{\dot{m}_3}{\dot{m}_1}\right) + 6.688 \left(\frac{\dot{m}_3}{\dot{m}_1}\right)^2, \text{ for } D_3/D_1 = .50. \qquad (5.10)$$

5.2 Two-Phase Pressure Distribution

5.2.1 Run Pressure Change

All of the two-phase run pressure change data collected has been reduced in terms of the models outlined in Section 2.3.2. Figure 5.5 shows the results obtained with the homogeneous model (Equations 2.14 - 2.16) for the test section with equal branch and inlet diameters ($D_3/D_1 = 1.0$), a mass flux of 600 kg/m^{2}s and various inlet qualities. The homogeneous model yielded a momentum correction factor ($k_{(1-2)H}$) that was dependent upon both inlet quality and branch flow split. For each inlet condition, the correction factor also shows a sudden increase in the range of flow splits associated with complete separation ($0.2 < \dot{m}_3/\dot{m}_1 < 0.3$). This range of flow splits was always associated with a significant drop in the fully developed run void fraction and a significant increase in the run pressure rise. Without considering the change in slip ratios on both sides of the junction, the homogeneous model is unable to account for the associated momentum changes.

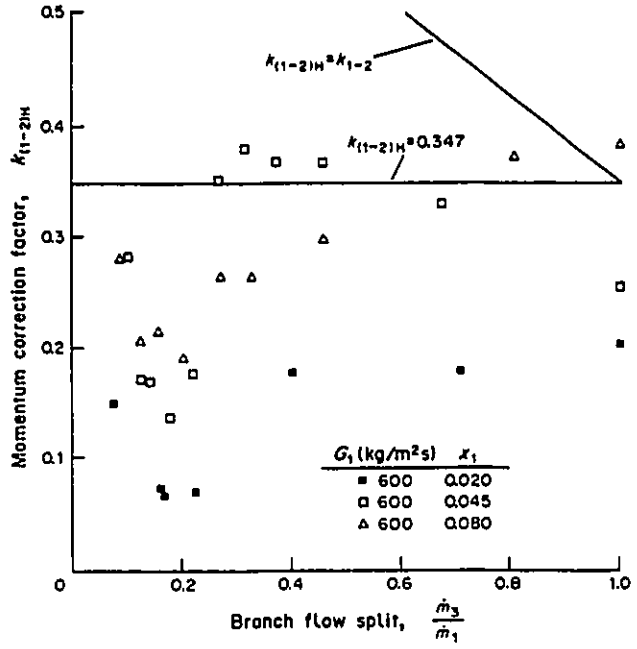

Figure 5.5 Homogeneous Momentum Correction Factor ($k_{(1-2)H}$) vs. Flow Split

$D_3/D_1 = 1.0$, $G_1 = 600$ kg/m^{2}s

Saba and Lahey (1984) suggested that the single-phase momentum correction factor (k_{1-2}) be used to predict the two-phase pressure changes with the homogeneous model. For the data presented herein, the single-phase correction factor was generally higher than the corresponding two-phase value as shown in Figure 5.5. The data from the Saba and Lahey investigation involved lower quality inlet flows than in the present study ($x_1 \leq 0.01$) which may account for the difference. Fouda and Rhodes (1974) suggested that a constant value of 0.347 be used for the homogeneous momentum correction factor. This value is again typically higher than that observed in the present analysis.

The data obtained with the 25.65 mm I.D. branch (D_3/D_1=1.0) was also compared with the Reimann and Seeger model (1986), i.e. Equations [2.18] and [2.19]. The empirical correlations suggested by the authors as well as the experimentally measured values of inlet and run void fraction were used to reduce the data. The level of agreement was similar for both approaches. Figure 5.6 shows the results obtained with the recommended void correlations. Agreement between the model and the present data was seen to be poor, particularly for low flow splits.

When all of the annular flow data collected for the test section having equal branch and inlet diameters (D_3/D_1= 1.0) was reduced in terms of the separated flow model (Equation 2.17) , i.e.;

$$(\Delta P_{2\text{-}1})_j = k_{(1\text{-}2)S}\left[\left(\frac{G_1^2 x_1}{\rho_G \alpha_1} + \frac{G_1^2(1-x_1)^2}{\rho_L(1-\alpha_1)}\right) - \left(\frac{G_2^2 x_2}{\rho_G \alpha_2} + \frac{G_2^2(1-x_2)^2}{\rho_L(1-\alpha_2)}\right)\right]. \qquad (5.11)$$

the result is as shown in Figure 5.7. The separated flow momentum correction factor was seen to scatter about a value of unity independent of flow split

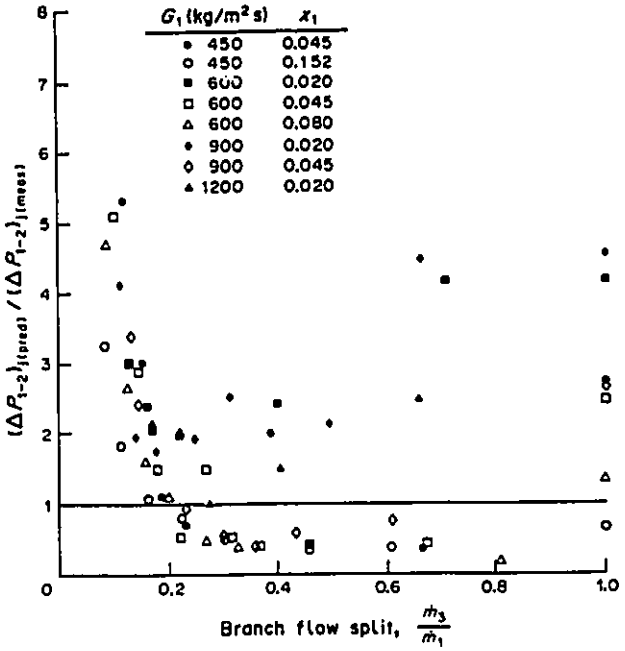

Figure 5.6 Comparison of Predicted (Reimann & Seeger, 1986 model) and Measured Run Pressure Changes - $D_3/D_1 = 1.0$

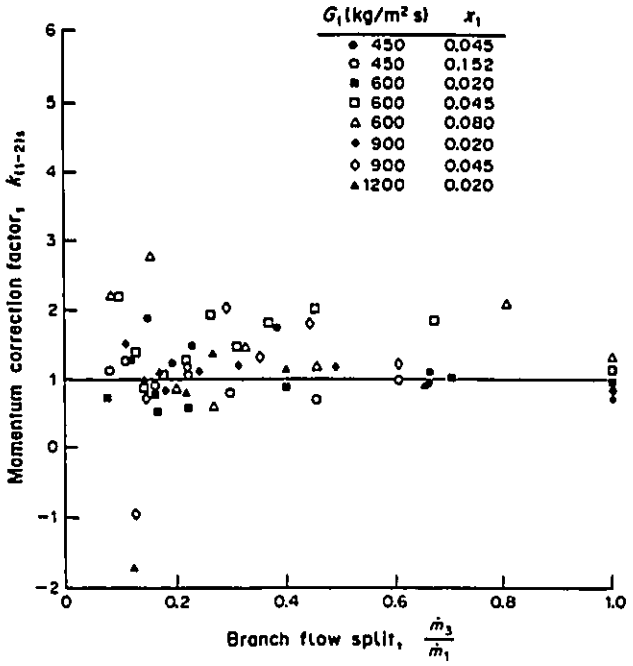

Figure 5.7 Separated Flow Momentum Correction Factor ($k_{(1-2)S}$) vs. Flow Split - $D_3/D_1 = 1.0$

and inlet conditions. This suggests that the axial momentum carried by the branching flow is insignificant relative to the momentum change across the junction.

5.2.1-1 The Effect of Branch Diameter

When all of the annular flow data collected to date for the horizontal branch and three branch diameters was reduced in terms of Equation [5.11], the result is as shown in Figure 5.8. The separated flow momentum correction factor is seen to again scatter about a value of approximately unity independent of flow split, inlet conditions (mass flux and quality) and junction geometry. This result is consistent with the annular air-water measurements of Madden and St. Pierre (1969/70) for various slot distributor geometries.

Obvious scatter around $k_{(1-2)S}$= 1.0 was present at low flow splits particularly for the higher inlet quality runs. At low flow splits, annular flow existed both upstream and downstream of the branch. Consequently, the flow momentum was relatively high in both the inlet and run. The comparatively small pressure rise at low flow splits is then inferred from a difference between two large values. This, coupled with the measurement errors associated with high void fractions (low liquid volume fractions, $(1-\alpha)$, in Equation [5.11]) is expected to cause the data scatter since the liquid phase carries most of the momentum in and out of the control volume. Similar results, with a reduction in the low flow split scatter, were obtained when the data was reduced using known void fraction correlations (Smith, 1969) as shown in Figure 5.9.

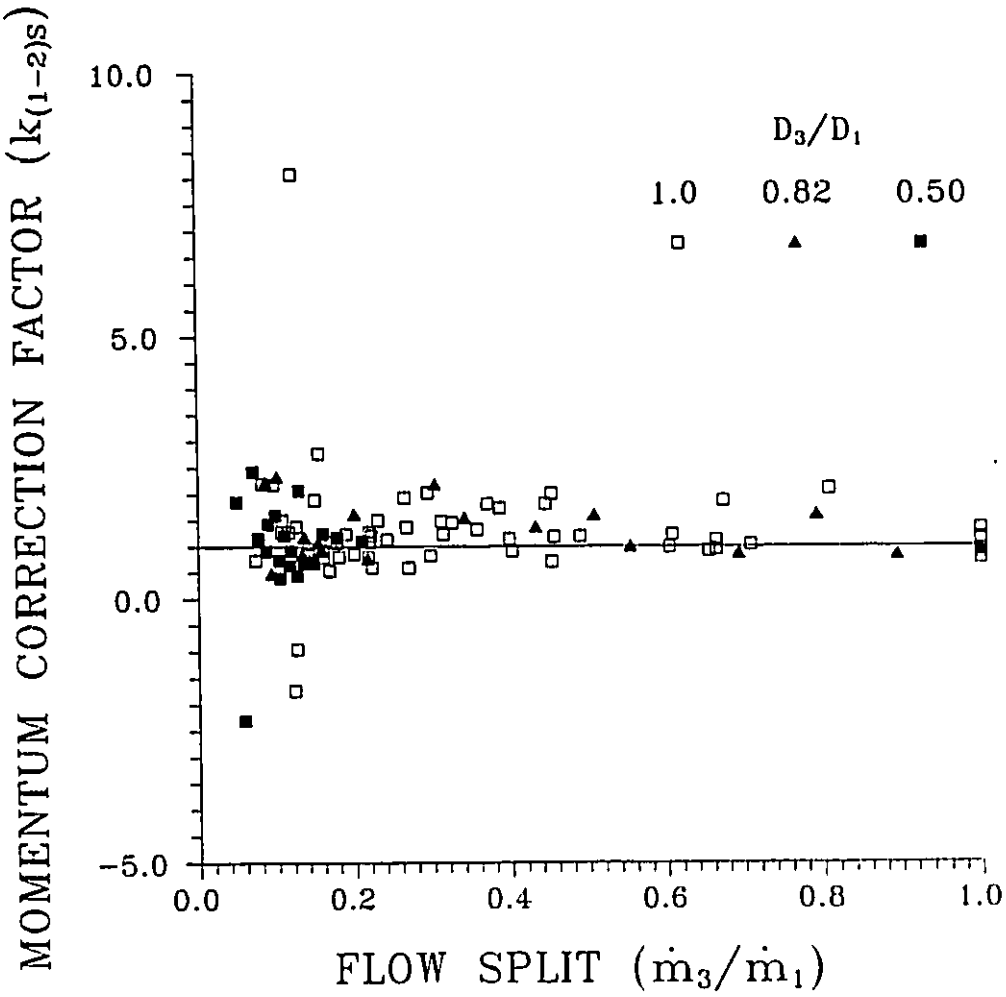

Figure 5.8 Separated Flow Momentum Correction Factor ($k_{(1-2)S}$) vs. Flow Split - Effect of Branch Diameter

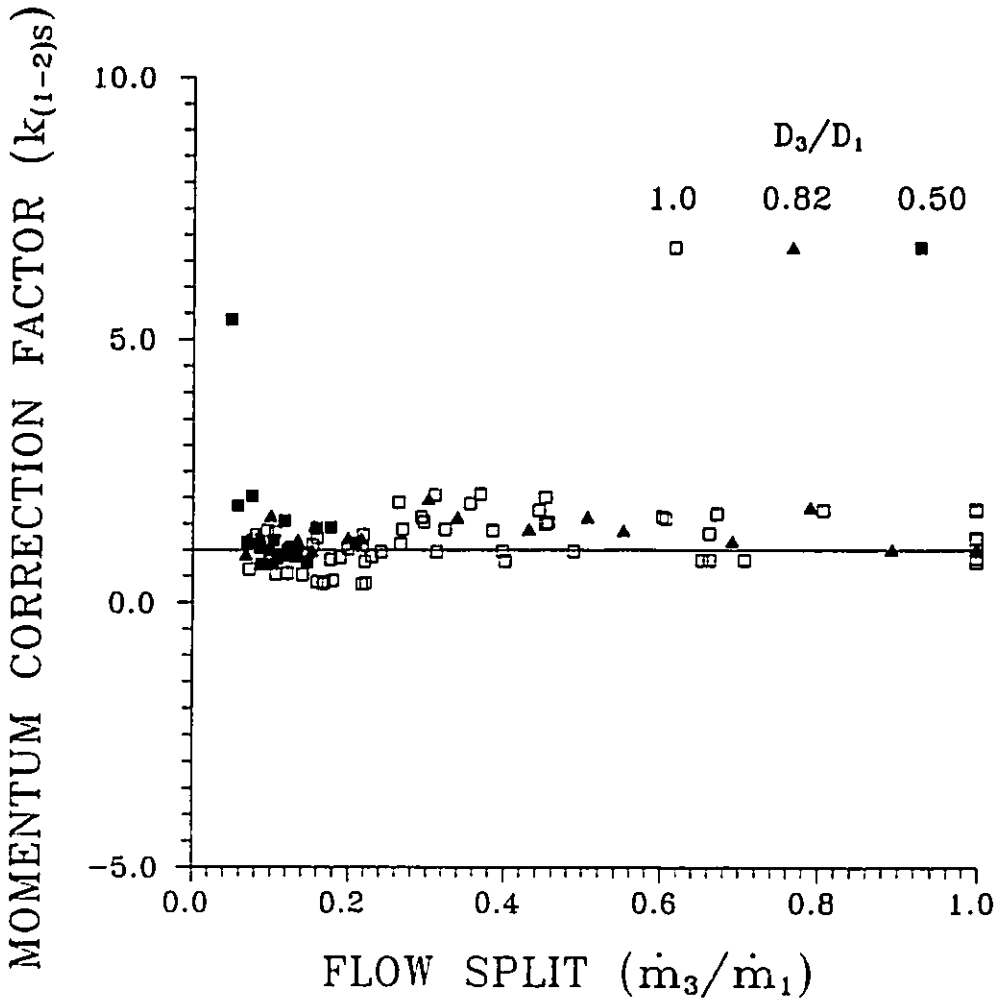

Figure 5.9 Separated Flow Momentum Correction Factor ($k_{(1-2)S}$) with Void Correlations - All Data

5.2.2 Branch Pressure Change

The branch pressure change data obtained in the present work were reduced to a homogeneous two-phase multiplier (Φ_H) in terms of the homogeneous flow mechanical energy balance model given by [2.25], i.e.,

$$(\Delta P_{1\text{-}3})_J = \frac{\rho_{H3}}{2}\left[\frac{G_3^2}{\rho_{H3}^2} - \frac{G_1^2}{\rho_{H1}^2}\right] + k_{1\text{-}3}\frac{G_1^2}{2\rho_L}\Phi_H \,. \tag{5.12}$$

The first term on the r.h.s of equation [5.12] represents the reversible portion of the total pressure change between the inlet and branch. The second term represents the irreversible portion modelled in terms of a two-phase multiplier (Φ_H) acting on the single-phase liquid irreversible loss for the junction at the same mass flux and flow split.

Figures 5.10 and 5.11 show plots of typical results obtained for (Φ_H) with a junction having equal branch and inlet diameters, a fixed inlet mass flux and varying inlet qualities. The results indicate a multiplier that is dependent on both flow split and inlet quality. Saba and Lahey (1984) suggested a homogeneous two-phase multiplier be used with Equation [5.12] of the form,

$$\Phi_H = \frac{\rho_L}{\rho_{H1}}, \tag{5.13}$$

which is independent of flow split, except for pressure effects, and demonstrated limited agreement with the measured data. The homogeneous multiplier suggested by Reimann and Seeger (1986), i.e.,

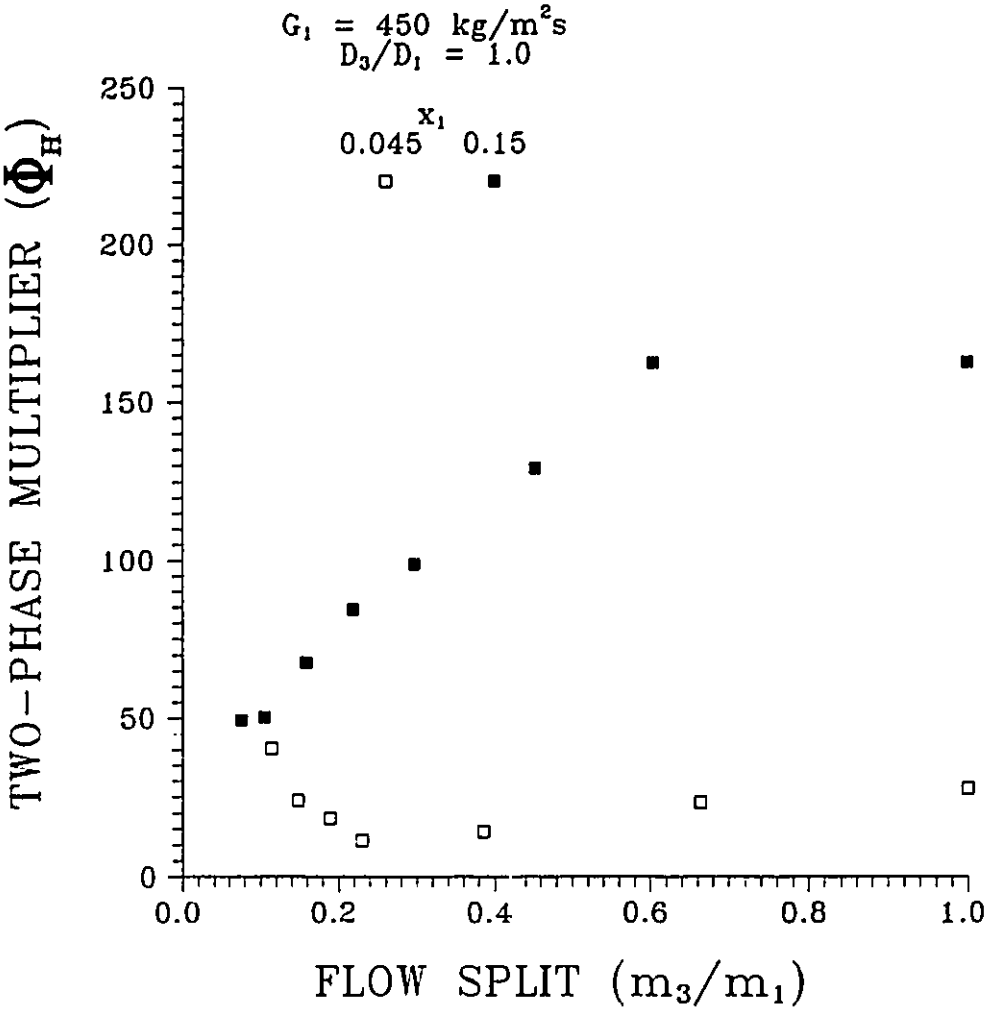

Figure 5.10 Homogeneous Two-Phase Multiplier (Φ_H)

G_1= 450 kg/m^{2}s, D_3/D_1= 1.0

x_1= 0.045 and 0.15

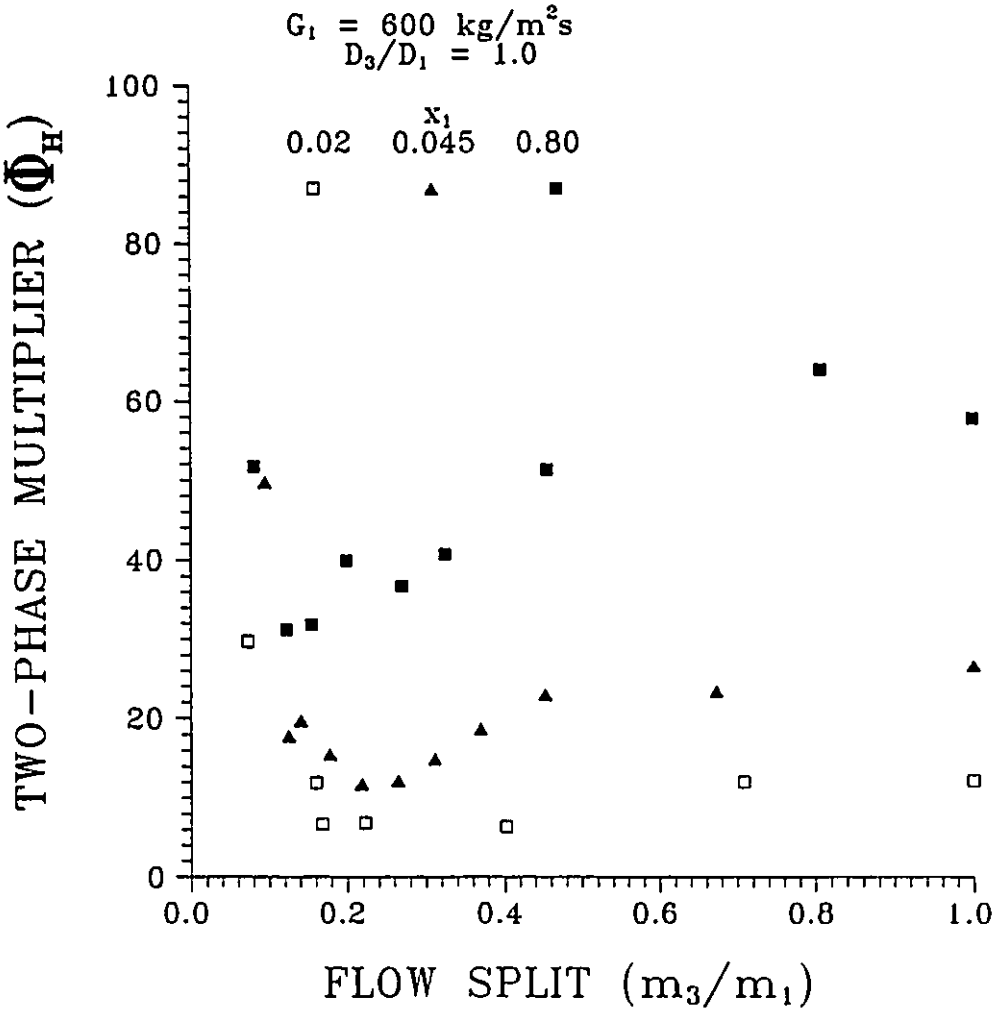

Figure 5.11 Homogeneous Two-Phase Multiplier (Φ_H)

G_1= 600 kg/m^{2}s, D_3/D_1= 1.0

x_1= 0.02, 0.045 and 0.80

$$\Phi_H = \frac{\rho_L \rho_{H3}}{\rho_{H1}^2} , \tag{5.14}$$

is more strongly dependent on the flow split (i.e. phase separation) through the branch homogeneous density (ρ_{H3}). This form of the homogeneous two-phase multiplier showed improved agreement with the measured data.

The data collected was also reduced in terms of the separated flow model given by Saba and Lahey (1984), i.e.,

$$(\Delta P_{1-3})_j = \frac{\rho_{H3}}{2}\left[\frac{G_3^2}{(\rho_3''')^2} - \frac{G_1^2}{(\rho_1''')^2}\right] + k_{1-3}\frac{G_1^2}{2\rho_L}\Phi_S . \tag{5.15}$$

Here, k_{1-3} is the single-phase loss coefficient for the junction, Φ_S is a separated flow two phase multiplier and the cnergy density (ρ''') is defined by

$$\frac{1}{(\rho''')^2} = \left[\frac{x^3}{\rho_G^2\alpha^2} + \frac{(1-x)^3}{\rho_L^2(1-\alpha)^2}\right] . \tag{5.16}$$

Typical results obtained with the separated flow model for the junction with equal inlet and branch diameters are shown in Figures 5.12 and 5.13. The loss multiplier is again shown to be dependent on the flow split and inlet conditions. Both the homogeneous and separated flow loss multipliers (Φ_H and Φ_S) approach the same value as the flow split approaches 1.0. Under these conditions, the reversible loss in both models (the first term on the r.h.s. of [5.12] and [5.15]) approaches zero. Both two-phase multipliers act on identical terms in the models yielding similar results at higher flow splits.

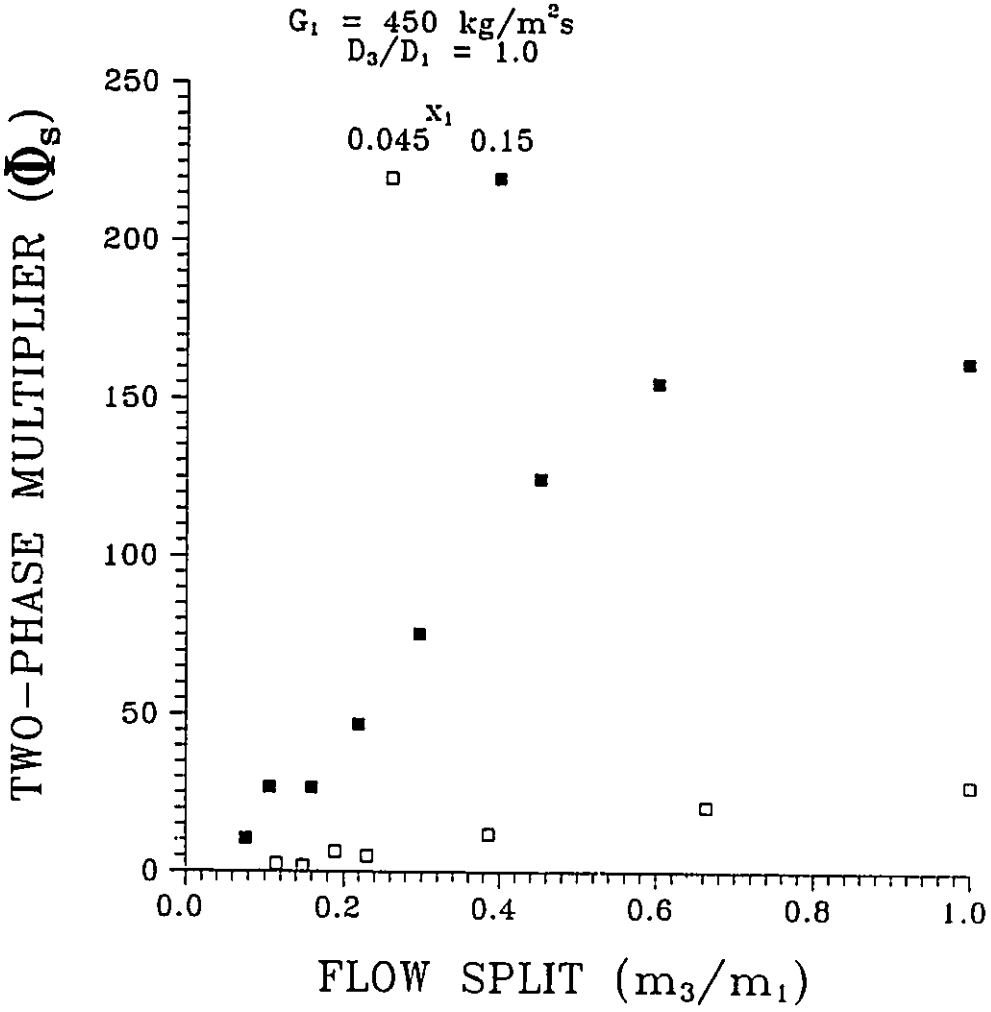

Figure 5.12 Separated Flow Two-Phase Multiplier (Φ_S)

G_1= 450 kg/m^{2}s, D_3/D_1= 1.0

x_1= 0.045 and 0.15

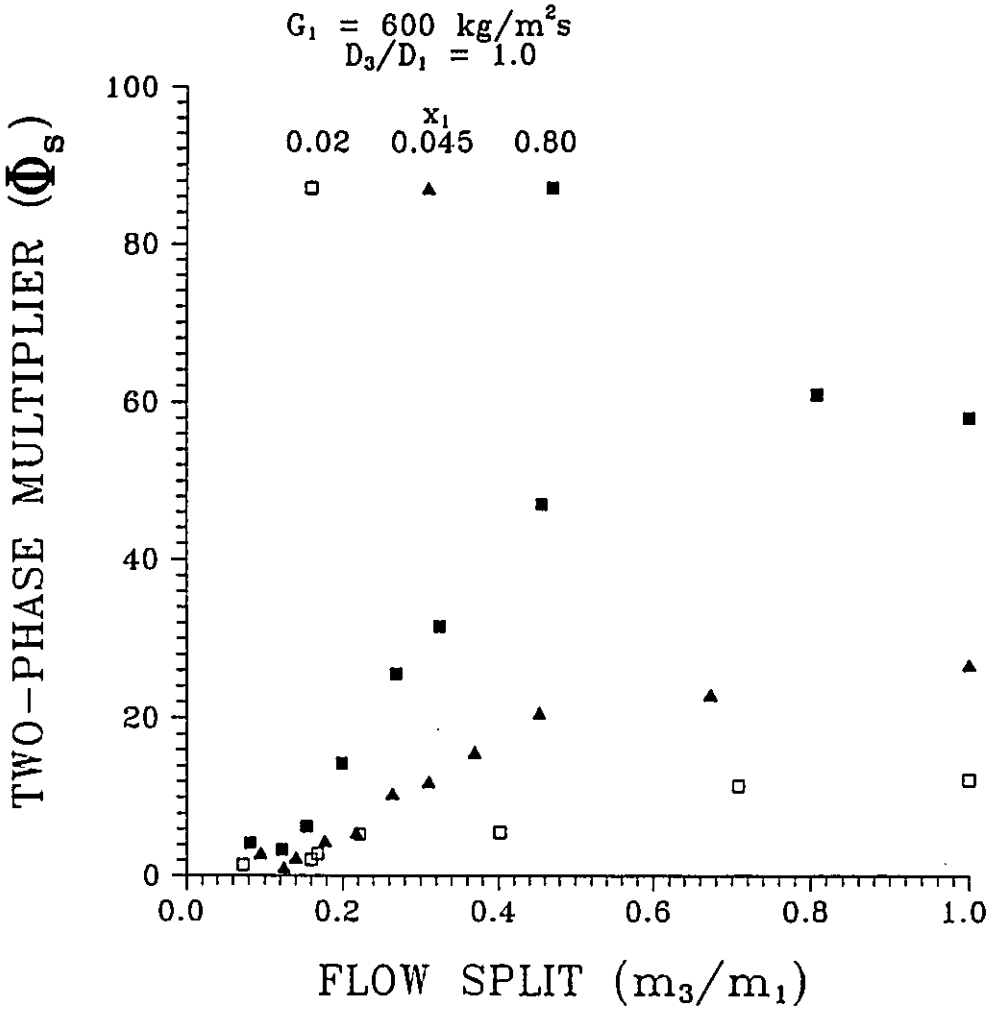

Figure 5.13 Separated Flow Two-Phase Multiplier (Φ_s)

G_1= 600 kg/m^{2}s, D_3/D_1= 1.0

x_1= 0.02, 0.045 and 0.80

All of the inlet conditions analyzed in this study were within the annular flow regime as shown in Section 3.3.5. As such, the structure of the flow at the inlet was similar for all tests, particularly the higher quality cases ($x_1 > 0.04$). Yet, both models presented yielded loss multipliers that were strongly dependent on the inlet conditions. One of the reasons for this was the inability of the mechanical energy balance models, as formulated by [5.12] and [5.15], to correctly account for the inlet dynamic head of the branching flow. This results in an inconsistent estimate of the reversible pressure change in both models which in turn affects the two-phase multipliers.

The model can be improved by more accurately accounting for this term. The mechanical energy balance model presented here is based on dividing the branch pressure change, $(\Delta P_{1-3})_j$, into reversible and irreversible components as in the previous two models. The flow is first assumed to be discontinuously divided into two streams just before the junction, one stream for the run and one for the branch as shown in Figure 5.14. If it is further assumed that no exchange of mass or momentum takes place across the boundaries between the two streams, the reversible pressure change between the inlet and branch can be modelled by way of a Bernoulli-type equation, as shown by Lahey and Moody (1977), of the form

$$(P_{1J}-P_{3J})_{rev} \frac{\dot{m}_3}{\rho_{H3}} = \frac{1}{2}\dot{m}_{G3}(u_{G3}^2 - u_{G1}^2) + \frac{1}{2}\dot{m}_{L3}(u_{L3}^2 - u_{L1}^2) \; . \tag{5.17}$$

The phasic velocities are then assumed to be characterized by

$$u_G = \frac{Gx}{\alpha\rho_G} \qquad \text{and} \qquad u_L = \frac{G(1-x)}{(1-\alpha)\rho_L} \; . \tag{5.18}$$

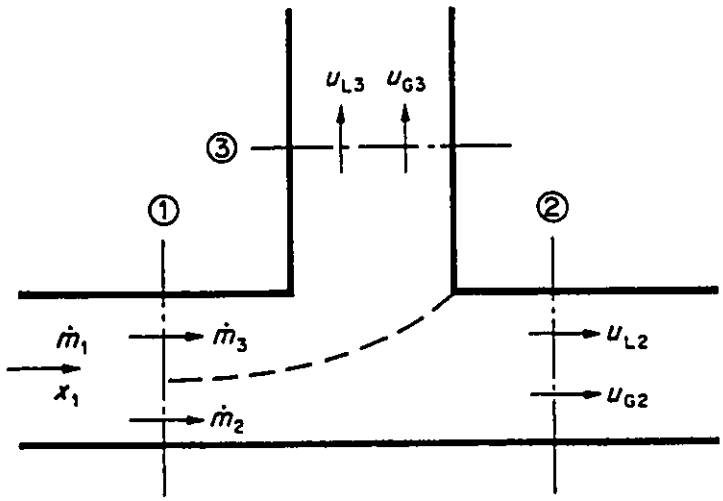

Figure 5.14 Junction Model for Branch Pressure Change

By substituting equations [5.18] into [5.17], the reversible pressure change may be written as

$$(\Delta P_{3\text{-}1})_{rev} = \frac{\rho_{H3}}{2}\left\{G_3^2\left[\frac{x_3^3}{\rho_G\alpha_1} + \frac{(1-x_3)^3}{\rho_L(1-\alpha_1)}\right] - G_1^2\left[\frac{x_1^2x_3}{\rho_G^2\alpha_1^2} + \frac{(1-x_1)^2(1-x_3)}{\rho_L^2(1-\alpha_1)^2}\right]\right\}. \quad (5.19)$$

The first term between square brackets in [5.19] contains the branch energy density (ρ_3''') defined earlier by [2.22] and [5.16]. The second term between square brackets contains an equivalent inlet density of the branching flow, defined as ρ_1^*, which is consistent with the present model assumptions. Applying these definitions Equation [5.19] can then be written as

$$(P_{1j} - P_{3j})_{rev} = \frac{\rho_{H3}}{2}\left(\frac{G_3^2}{(\rho_3''')^2} - \frac{G_1^2}{(\rho_1^*)^2}\right) \quad (5.20)$$

where ρ_3''' is defined by [2.22] and [5.16] and ρ^* is defined by

$$\frac{1}{(\rho_1^*)^2} = \frac{x_1^2x_3}{\rho_G^2\alpha_1^2} + \frac{(1-x_1)^2(1-x_3)}{\rho_L^2(1-\alpha_1)^2}. \quad (5.21)$$

By assuming $\rho_1^* = \rho_1'''$ (i.e. $x_3 = x_1$, equal separation) equation [5.20] reduces to the reversible portion of [5.15] as used by Saba and Lahey (1984). The formulation for the equivalent inlet density (ρ_1^*) in Equation [5.21] accounts for the fact that the branching flow, before being extracted, has phasic velocities that are characteristic of the inlet section and a quality

characteristic of the branch. Only for an assumption of equal phase distribution ($x_3 = x_1$) is $\rho_1^* = \rho_1'''$.

Following a procedure analogous to that of the single-phase case, i.e. defining the irreversible junction pressure loss in terms of the inlet dynamic head, it is appropriate to use the equivalent inlet density (ρ_1^*) to determine the loss multiplier. The total branch pressure change then becomes,

$$(\Delta P_{1-3})_j = \frac{\rho_{H3}}{2}\left[\frac{G_3^2}{(\rho_3''')^2} - \frac{G_1^2}{(\rho_1^*)^2}\right] + k_{1-3}\frac{\rho_{H3}\, G_1^2}{2\,(\rho_1^*)^2}\Phi^*, \qquad (5.22)$$

from which a new two-phase multiplier, Φ^*, is defined.

All of the data obtained were reduced in terms of [5.22] to calculate the two-phase multiplier, Φ^*, using the measured void fractions. Figure 5.15 shows the results obtained for the test section having equal branch and inlet diameters with various values of inlet mass flux and quality. The results show that, for a given junction geometry, the two-phase multiplier as formulated by [5.22] was independent of the inlet conditions for the range of data tested. The strong dependence of the multipliers obtained by way of the previous formulations is completely accounted for through the use of an equivalent inlet density term (ρ_1^*) which is compatible with the mechanical energy balance model assumptions. This result is what is expected from a consistent formulation of the mechanical energy balance model with similar flow structures at the inlet section.

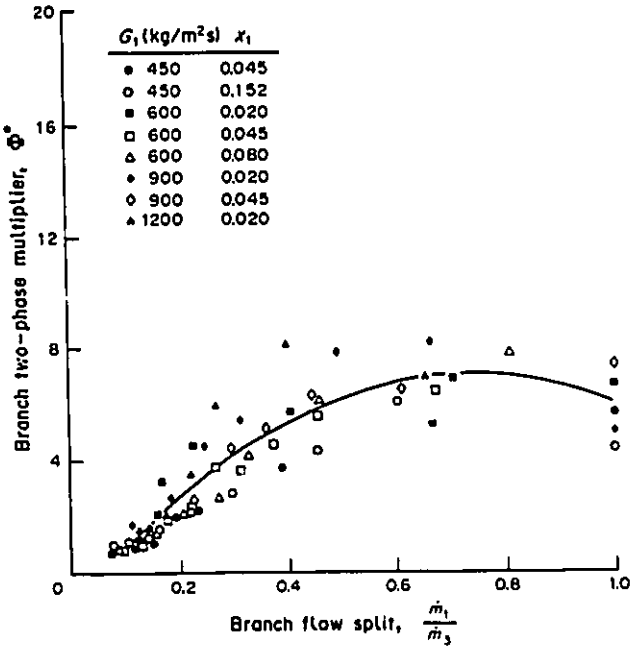

Figure 5.15 Separated Flow Two-Phase Multiplier (Φ^*)

D_3/D_1 = 1.0, Effect of Inlet Conditions

5.2.1-1 The Effect of Branch Diameter

Figure 5.16 shows the results obtained for all data from the three test sections having different branch to inlet diameter ratios. The data presented here again represents various inlet conditions. The multiplier, Φ^*, is seen to be a unique function of the flow split ($\dot{m}_3/\dot{m}_1$) independent of both the inlet mass flux and inlet quality for a given junction geometry. The two-phase multiplier shows a strong dependence on the junction geometry, similar to that shown by the single-phase loss coefficient (k_{1-3}), increasing with decreasing diameter ratio. For annular inlet flow, the data collected was used to obtain the following empirical correlations;

$$\Phi^* = -1.28 + 22.61 \frac{\dot{m}_3}{\dot{m}_1} - 15.21\left(\frac{\dot{m}_3}{\dot{m}_1}\right)^2 \qquad (5.23)$$

for $\dot{m}_3/\dot{m}_1 > 0.1$ and $D_3/D_1 = 1.0$, by

$$\Phi^* = -1.85 + 36.06 \frac{\dot{m}_3}{\dot{m}_1} - 26.00\left(\frac{\dot{m}_3}{\dot{m}_1}\right)^2 \qquad (5.24)$$

for $\dot{m}_3/\dot{m}_1 > 0.1$ and $D_3/D_1 = 0.82$ and by

$$\Phi^* = -16.05 + 297.02 \frac{\dot{m}_3}{\dot{m}_1} - 249.38\left(\frac{\dot{m}_3}{\dot{m}_1}\right)^2 \qquad (5.25)$$

for $0.075 < \dot{m}_3/\dot{m}_1 < 0.2$ and $D_3/D_1 = 0.5$. The data showed similar trends when empirical void fraction correlations (Smith (1969)) were used with [5.22] as shown in Figure 5.17.

For both single-phase and two-phase flow, the branch pressure

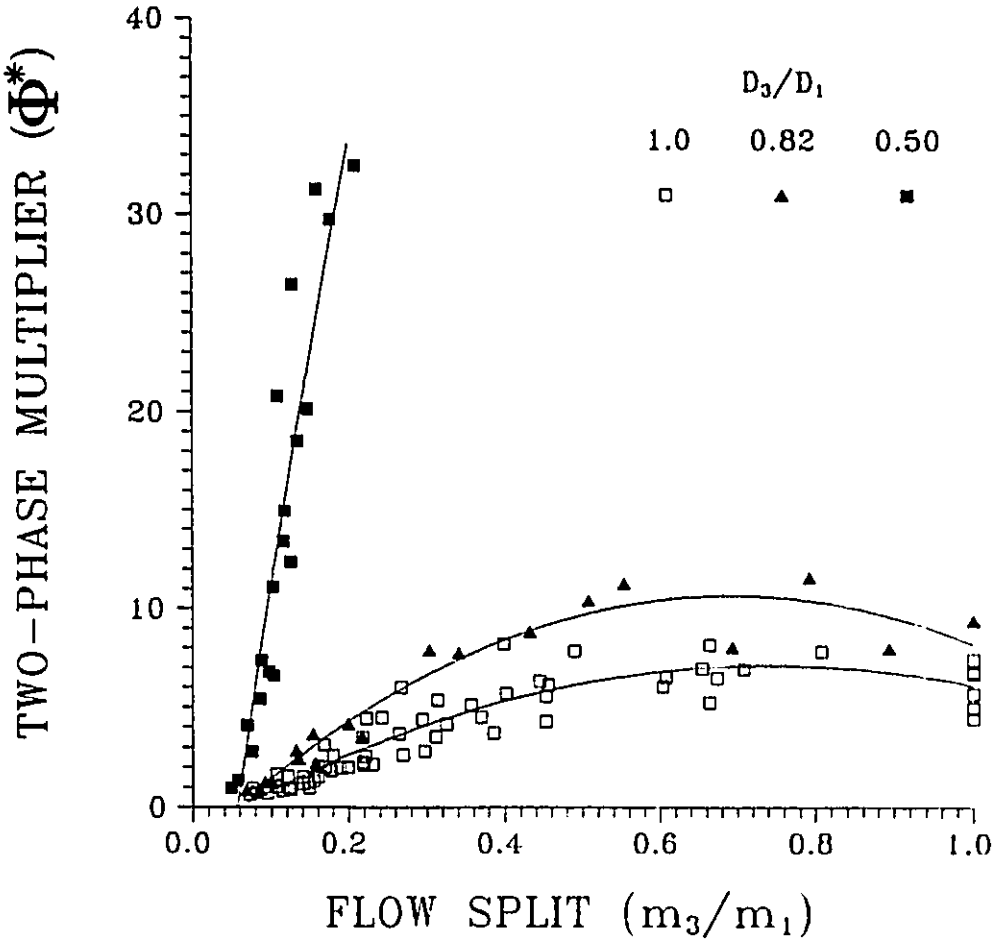

Figure 5.16 Separated Flow Two-Phase Multiplier (Φ^*)

Effect of Branch Diameter

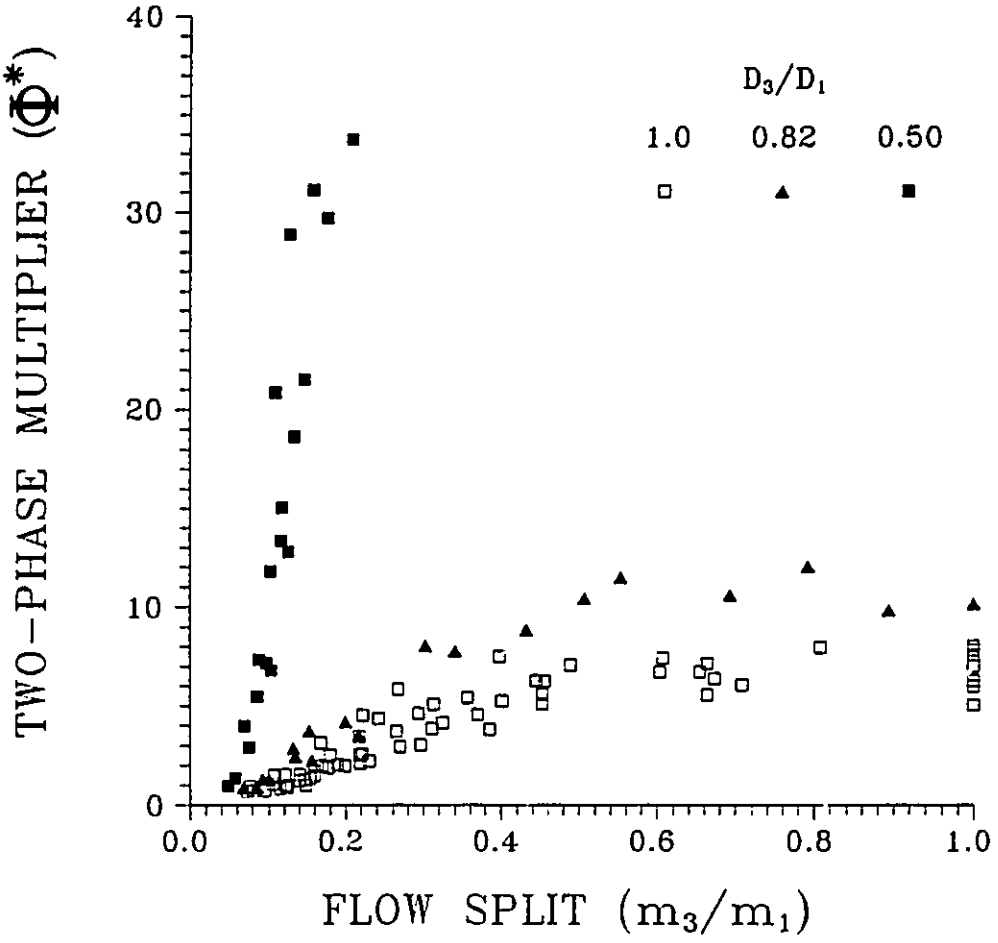

Figure 5.17 Separated Flow Two-Phase Multiplier (Φ^*)

With Void Correlations - All Data

change, $(\Delta P_{1-3})_j$, approaches zero as $G_3/G_1 \to 0$. Therefore, the limit of both k_{1-3} and Φ^* is 1.0 as $G_3/G_1 \to 0$. Equations [5.23] to [5.25] represent a least squares fit over a limited data range and as a result do not demonstrate this limiting trend.

The results presented have been for annular inlet flow conditions. The value of Φ^* as formulated by Equation [5.22] will also be dependent upon the inlet flow regime and geometrical parameters other than branch diameter (branch orientation, take-off angle, etc.). For single-phase liquid or vapour in the inlet section, Equation [5.22] reduces to the single-phase mechanical energy balance model (i.e. equation [2.20]) for $\Phi^* = 1.0$. Therefore, in the limit as x_1 approaches 0 or 1.0, Φ^* should approach unity.

As discussed in Section 4.1.1, at low flow splits the branch quality was seen to be below the inlet quality. At sufficiently reduced flow splits the branch quality can approach zero as the flow is removed from the liquid film intercepted by the branch opening alone and no vapour is extracted. As the branch carries a smaller portion of the inlet vapour, the two-phase effects on the branch pressure change will be reduced. This is indicated in Figure 5.15 by a reduction in the two-phase multiplier which approaches unity for low branch quality conditions. Appropriately, for a branch quality approaching zero and a multiplier of unity, Equation 6 reduces to the single phase mechanical energy balance for the liquid between the inlet and the branch, i.e.;

$$(\Delta P_{1-3})_j = \frac{\rho_L}{2}\left(u_{L3}^2 - u_{L1}^2\right) + k_{1-3}\frac{\rho_L}{2}u_{L1}^2 \quad . \tag{5.26}$$

CHAPTER 6

PHASE SEPARATION MODEL

6.1 Introduction

The results of the present study and those of Seeger et al. (1986) and Reimann and Seeger (1986) have shown that the phase and pressure distributions for steam/water flows have characteristics similar to those demonstrated in previous air/water studies. This similarity has also been identified by Hwang et al. (1986). It is therefore unlikely that condensation and flashing have a significant effect on the separation process. The dominant mechanisms for separation in single component two-phase flow are then a result of the flow dynamics. For this reason, the dynamics of the flow will be considered first in the development of a predictive model with a result that is applicable to both one and two-component mixtures. Discrepancies between steam-water and air-water results may then be considered in terms of the different thermodynamic processes.

The proposed model follows the format outlined in Section 2.3.1. That is, of the 8 prescribed parameters (x_1, x_2, x_3, G_1, G_2, G_3, $(\Delta P_{2-1})_j$ and $(\Delta P_{1-3})_j$), three are specified as boundary conditions requiring five independent equations to obtain a solution. Again, the equations typically used have been one form or another of;

i) The mixture continuity equation

ii) The vapour phase continuity equation

iii) A run pressure change correlation

iv) A branch pressure change correlation

v) A closure relationship.

The first two equations are used as presented previously i.e.

$$\dot{m}_1 = \dot{m}_2 + \dot{m}_3 \tag{6.1}$$

and

$$\dot{m}_1 x_1 = \dot{m}_2 x_2 + \dot{m}_3 x_3 \ . \tag{6.2}$$

The first equation is the mixture continuity equation, the second is the vapour phase continuity equation, assuming that no flashing and condensation takes place within the junction volume being considered.

The separated flow axial momentum balance model defined by Equation 5.11,

$$(\Delta P_{2\text{-}1})_j = k_{(1\text{-}2)S} \left[\left(\frac{G_1^2 x_1}{\rho_G \alpha_1} + \frac{G_1^2 (1-x_1)^2}{\rho_L (1-\alpha_1)} \right) - \left(\frac{G_2^2 x_2}{\rho_G \alpha_2} + \frac{G_2^2 (1-x_2)^2}{\rho_L (1-\alpha_2)} \right) \right], \tag{6.3}$$

with the momentum correction factor ($k_{(1\text{-}2)S}$) set to 1.0 is used for the run pressure change correlation in all model calculations.

For the branch pressure change correlation, the mechanical energy balance model as developed in Section 5.2.2 is used,

$$(\Delta P_{1\text{-}3})_j = \frac{\rho_{H3}}{2} \left(\frac{G_3^2}{(\rho_3''')^2} - \frac{G_1^2}{(\rho_1^*)^2} \right) + k_{1\text{-}3} \frac{\rho_{H3} G_1^2}{2 (\rho_1^*)^2} \Phi^* . \tag{6.4}$$

Appropriate correlations for the single-phase loss coefficient (k_{1-3}) and the two-phase multiplier (Φ^*) are used from Equations [5.8] - [5.10] and [5.23] - [5.25] respectively for the various branch diameters.

The closure relationship is only required prior to complete vapour extraction. Once complete vapour extraction has been reached, a mass balance shows the branch quality is given by

$$x_3 = (\dot{m}_1/\dot{m}_3)x_1. \tag{6.5}$$

6.2 The Closure Relationship

6.2.1 Introduction

The closure relationship must relate the degree of phase separation (or branch quality) to one or more of the flow and geometric parameters. The proposed method is related to previous models (e.g. Azzopardi and Whalley, 1982, and Hwang et. al., 1986) which are based on defining the portions of the inlet tube from which the branching flows of each phase are extracted. At any level within the junction, the branching flow of each flow component (vapour, liquid film and entrained droplets) is assumed to be separated from the run flow by a dividing streamline. All flow of a component on the branch side of the associated dividing streamline is assumed extracted through the branch with the remaining flow passing through the run. Determining the location of the dividing streamline at all levels within the junction volume at the inlet will define the area of the inlet tube from which each phase is extracted. This concept is represented schematically in Figure 6.1

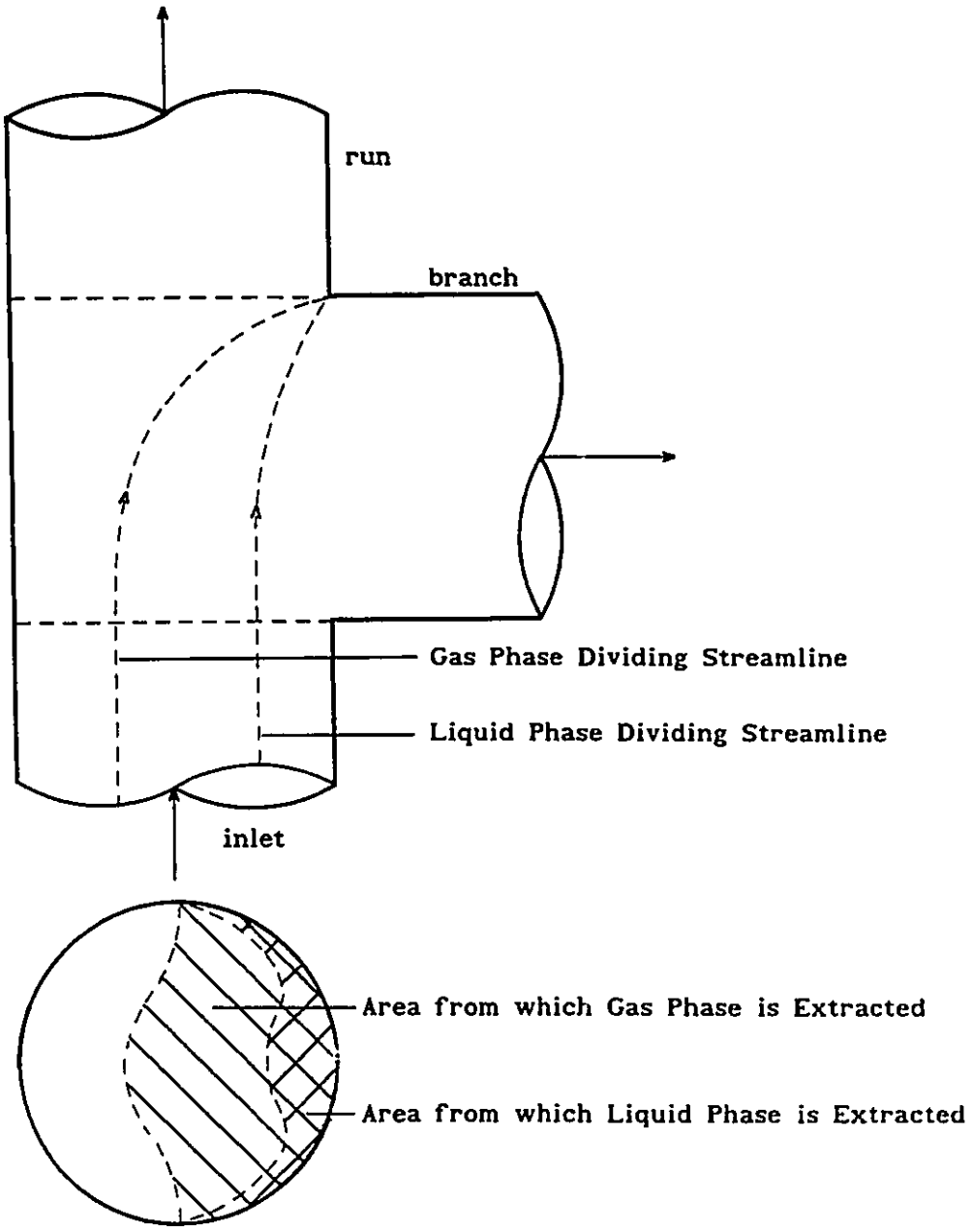

Figure 6.1 Schematic Representation of Dividing Streamlines

6.2.2 Model development ($D_3/D_1 = 1.0$)

In the present model, the junction volume is defined by the intersection of two horizontal equal diameter (2R) cylinders at right angles. Rectangular coordinates are used with the x-axis defined by the axis of the inlet cylinder, the y-axis by the axis of the branching cylinder and the z-axis by the vertical. Both the x and y-axis are positive in the direction of flow.

The local forces acting on a fluid element within the junction volume are:

i) viscous forces

ii) pressure forces

iii) inertia forces

iv) gravity forces

v) interfacial drag forces.

In dividing horizontal annular two-phase flow, the phasic velocities are typically high and the pressure gradients are large. Accordingly, for a first approximation, the inertia and pressure forces can be assumed to dominate the viscous and gravity forces. Although the interfacial drag effects of the vapour on the liquid film can be significant, these effects are minimized in a T junction with equal branch and inlet diameters. Under these conditions, the mean branching velocity of the gas phase is lowest minimizing the interfacial drag. Neglecting these interfacial forces greatly simplifies the problem such that it may be solved in terms of a balance

between pressure and inertia. This assumption is most reasonable for separated two-phase flows (annular and stratified), as in the present case, but may not be applicable to dispersed or intermittent flows.

Consider a volume element within a dividing T-junction as shown in Figure 6.2. Since the pressure is increasing through the run of the T ($\partial p/\partial x>0$) and decreasing through the branch ($\partial p/\partial y<0$), there exists a net resultant pressure force (F_{res}) on the element towards the inlet and branch as shown. The magnitude of the acceleration of the fluid within the volume in response to this pressure force will depend on the fluid density. As a result, the low density fluid (gas) has a higher acceleration towards the branch than does the liquid. This will result in some degree of phase separation that is dependent upon the initial velocities, densities and distribution of the two phases.

For typical inlet conditions considered in the experimental program, the relative momentum flux (ρu^2) between the gas, liquid film and entrained droplets is approximately 1:20:1250 (assuming no slip between the gas phase and entrained droplets). It has been suggested that the momentum flux represents a measure of the fluids resistance to being diverted to the branch (Azzopardi and Whalley, 1982). This is consistent with the experimental results of this study and the present model assumptions. It is then unlikely that the entrained droplets can contribute significantly to the branching flow prior to complete vapor extraction and will be neglected.

In any plane normal to the z-direction, the dividing streamline for either of the remaining flow components (liquid film and gas core) is defined as that streamline which, under the influence of the junction pressure field,

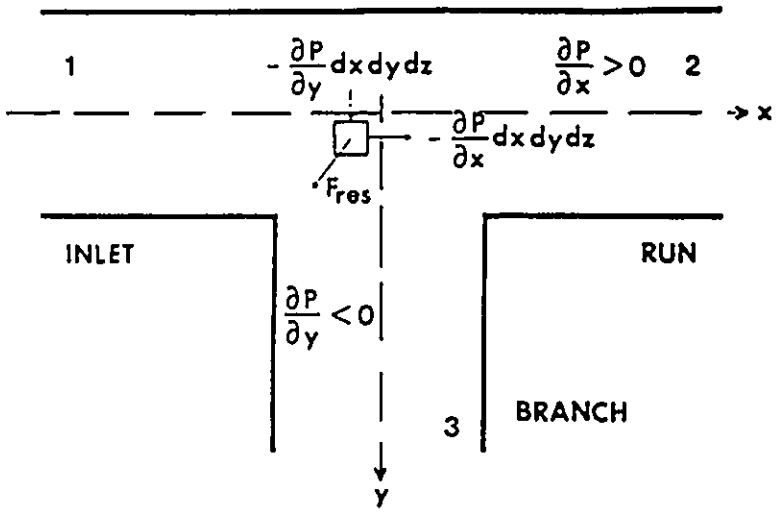

Figure 6.2 Junction Pressure Forces

would pass through the downstream intersection of the inlet and branch tubes (point D) as shown schematically in Figure 6.3. Since gravity forces and pressure gradients in the z-direction have been neglected, the flow is assumed to be two-dimensional. At any elevation within the junction volume, the coordinates of point D (x_D and y_D) and the x-coordinate of the dividing streamline at the junction volume inlet (x_0) can be determined geometrically as functions of the height (z) within the junction and the test section radius (R), i.e.

$$x_0(z) = -(R^2-z^2)^{1/2} \tag{6.6}$$

$$x_D(z) = (R^2-z^2)^{1/2} \tag{6.7}$$

$$y_D(z) = (R^2-z^2)^{1/2} \tag{6.8}$$

If the shape of the dividing streamlines for each flow component were known at every elevation within the junction, they would define two surfaces separating the run and branch flow of each phase. Also, the y-components at the inlet ($y_{0L}(z)$ and $y_{0G}(z)$) could be determined. Looking along the x-axis from the run to the inlet, the dependence of y_{0L} and y_{0G} on z may appear as shown schematically in Figure 6.4. Flows of each phase entering the volume with a y position greater than the associated y_0 value are assumed to be extracted through the branch, the remaining flow then passes through the run. The area of each phase assumed extracted through the branch (A_{GE} and A_{LE}) is then determined by superimposing the $y_0(z)$ functions on the inlet flow distribution and calculating the areas of each phase bounded by the inlet tube wall and the appropriate $y_0(z)$ function. This is shown schematically in Figure 6.4. Determining the appropriate areas requires the distribution of the phases in the inlet pipe to be known.

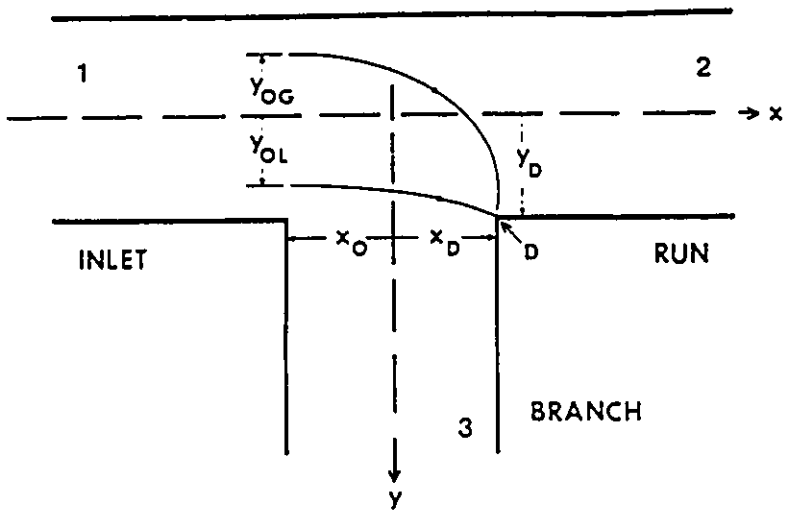

Figure 6.3 Gas Core and Liquid Film Dividing Streamlines

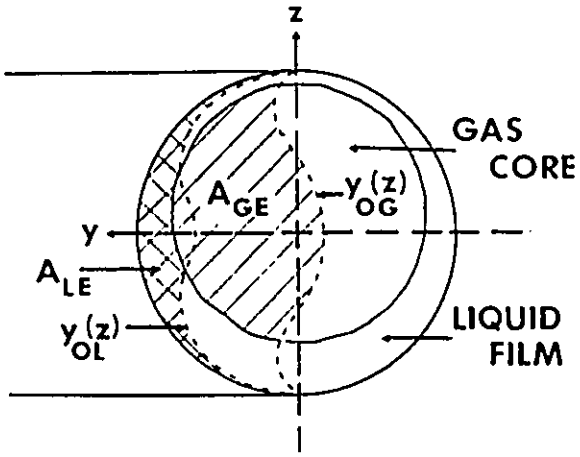

Figure 6.4 Schematic Representation of the Area of Gas Extracted (A_{GE}) and the Area of Liquid Extracted (A_{LE})

It has been assumed that the interfacial forces are not the dominant forces acting on the fluids in the junction volume and these forces have been neglected. It has also been assumed that no phase changes take place within the junction. The gas and liquid phase momentum equations are then uncoupled and can be solved independently. Since pressure and inertia are assumed to be the dominant forces, a potential flow solution for the dividing streamlines is appropriate. Continuity, conservation of x-directed and y-directed momentum and an assumption of irrotational flow then yields

$$\frac{\partial u}{\partial x} + \frac{\partial v}{\partial y} = 0 \tag{6.9}$$

$$u \frac{\partial u}{\partial x} + v \frac{\partial u}{\partial y} = - \frac{1}{\rho} \frac{\partial p}{\partial x} \tag{6.10}$$

$$u \frac{\partial v}{\partial x} + v \frac{\partial v}{\partial y} = - \frac{1}{\rho} \frac{\partial p}{\partial y} \tag{6.11}$$

$$\frac{\partial v}{\partial x} - \frac{\partial u}{\partial y} = 0 \ . \tag{6.12}$$

These can be re-arranged to give

$$\frac{\partial u}{\partial x} = \left(\frac{u}{u^2 + v^2} \right) \left(\frac{v}{u\rho} \frac{\partial p}{\partial y} - \frac{1}{\rho} \frac{\partial p}{\partial x} \right) \tag{6.13}$$

$$\frac{\partial v}{\partial y} = - \frac{\partial u}{\partial x} \tag{6.14}$$

$$\frac{\partial v}{\partial x} = \left(- \frac{1}{\rho} \frac{\partial p}{\partial y} - v \frac{\partial v}{\partial y} \right) \frac{1}{u} \tag{6.15}$$

$$\frac{\partial u}{\partial y} = \frac{\partial v}{\partial x} \tag{6.16}$$

The path of the dividing streamlines at any height within the junction can be determined from a shooting method type solution of Equations [6.13] - [6.16], i.e.

$$u_{I+1,J+1} = u_{I,J} + \frac{\partial u}{\partial x}\Delta x + \frac{\partial u}{\partial y}\Delta y \tag{6.17}$$

$$v_{I+1,J+1} = v_{I,J} + \frac{\partial v}{\partial x}\Delta x + \frac{\partial v}{\partial y}\Delta y \tag{6.18}$$

provided the inlet coordinates (x_0 and y_0), the corresponding inlet velocities (u_0 and v_0) and the pressure distribution are all known.

The value of x_0 is determined geometrically from the tube diameter (2R) and the height (z) within the junction as

$$x_0 = -(R^2 - z^2)^{1/2} , \tag{6.19}$$

which is the same for both phases at any level within the junction. The flow is assumed to be axial at the junction inlet such that the initial y-component of velocity (v_0) is zero for both phases, i.e.

$$v_{0G} = v_{0L} = 0 \tag{6.20}$$

For the gas phase, a uniform x-component of velocity is assumed at the inlet given by the mean vapour velocity, i.e.

$$u_{0,G} = \frac{Gx}{\rho_G \alpha} . \tag{6.21}$$

The inlet liquid phase velocity is assumed uniform and equal to the average film velocity (u_f) determined from the definition of void fraction (α), i.e.

$$\alpha = \frac{A_G}{A_G + A_d + A_f} \tag{6.22}$$

where A represents the time averaged cross-sectional area occupied by the flow components and subscripts G, d and f refer to the gas, entrained droplets and liquid film respectively. Assuming no slip between the entrained droplets and gas core (i.e., $u_d = u_G$), Equation [6.22] may be written as

$$\alpha = \frac{\dot{m}_G/\rho_G u_G}{\dot{m}_G/\rho_G u_G + \dot{m}_f/\rho_L u_f + \dot{m}_d/\rho_L u_G} \quad . \tag{6.23}$$

Since,

$$\dot{m}_G = \dot{m}x \ , \quad \dot{m}_d = \dot{m}(1-x)E \quad \text{and} \quad \dot{m}_f = \dot{m}(1-x)(1-E),$$

where E represents the equilibrium entrainment ratio, the film velocity is given by

$$u_{0,L} = u_f = \left[\frac{\rho_G u_G (1-x)(1-E)}{\rho_L x} \right] \left[\frac{1}{\alpha} - 1 - \frac{\rho_G E(1-x)}{\rho_L x} \right]^{-1} . \tag{6.24}$$

Little is known about the pressure distribution within the junction volume. Most experimental investigations have been concerned with the determination of the extrapolated junction pressure changes ($(\Delta P_{2-1})_j$ and $(\Delta P_{1-3})_j$) where only the fully developed pressure profiles in each leg are

required. As a first approximation, the pressure in the x-direction through the run of the T is assumed to increase linearly from the junction inlet (i.e. from x = -R). A development length through the run (DLX) is then defined in terms of the run pressure change as

$$P(DLX,0) - P(-R,0) = (\Delta P_{2\text{-}1})_j , \tag{6.25}$$

such that the pressure gradient in the x-direction is given by

$$\frac{\partial P}{\partial x} = \frac{(\Delta P_{2\text{-}1})_j}{(DLX + R)} . \tag{6.26}$$

It is expected that the pressure gradient in the y-direction will be steeper at the branch opening than it is at the opposite tube wall. For this reason, a parabolic profile is assumed. A development length (DLY) is again defined in terms of the branch pressure change as

$$P(0,-R) - P(0,DLY) = (\Delta P_{1\text{-}3})_j . \tag{6.27}$$

As a first approximation, the pressure gradient is assumed flat at a point in the junction volume furthest from the branch opening, i.e.

$$\frac{\partial P}{\partial y} \Big|_{y=-R} = 0. \tag{6.28}$$

The pressure gradient in the y-direction is then given by

$$\frac{\partial P}{\partial y} = -2(\Delta P_{1\text{-}3})_j \frac{(R + y)}{(R + DLY)^2}. \tag{6.29}$$

The assumed pressure gradient at any point in the junction volume is then dependent only on the junction pressure changes ($(\Delta P_{2\text{-}1})_j$ and $(\Delta P_{1\text{-}3})_j$) and the run and branch development lengths (DLX and DLY).

A solution requires information concerning the liquid film distribution and equilibrium entrainment ratio at the inlet. Since the angular distribution of liquid film in the inlet section was not measured in the present work, an experimental film thickness profile from Lin et. al. (1985) was used. The profile, shown in Figure 6.5, is a plot of film thickness (h) vs. angular displacement from the vertical (θ). To account for the different film flow areas between the distribution from Lin et. al. and the present experimental cases, the published data was normalized in terms of the bottom film thickness ($h(\pi)$). Several values for the relative film thickness ($h'(\theta)=h(\theta)/h(\pi)$) were extracted from the graph and used along with a cubic spline interpolator to obtain the values of $h'(\theta)$ at any angle. If R_f is defined as the radial distance from the centre of the inlet tube to the film surface, then the time averaged area occupied by the liquid film may be defined as

$$A_f = 2 \int_0^{\pi} \int_{R_f}^{R} r \, dr \, d\theta \quad . \tag{6.30}$$

Noting that $R_f = R - h(\theta)$ and that $h(\theta) = h(\pi)h'(\theta)$, Equation [6.30] may be written as

$$A_f = 2Rh(\pi)\int_0^{\pi} h'(\theta) \, d\theta - h(\pi)^2\int_0^{\pi} h'(\theta)^2 \, d\theta \quad . \tag{6.31}$$

The time averaged area occupied by the liquid film may also be determined from the present experimental measurements as

$$A_f = \frac{\dot{m}_f}{\rho_L u_f} = \frac{(1-E)(1-x)\dot{m}}{\rho_L u_f} \tag{6.32}$$

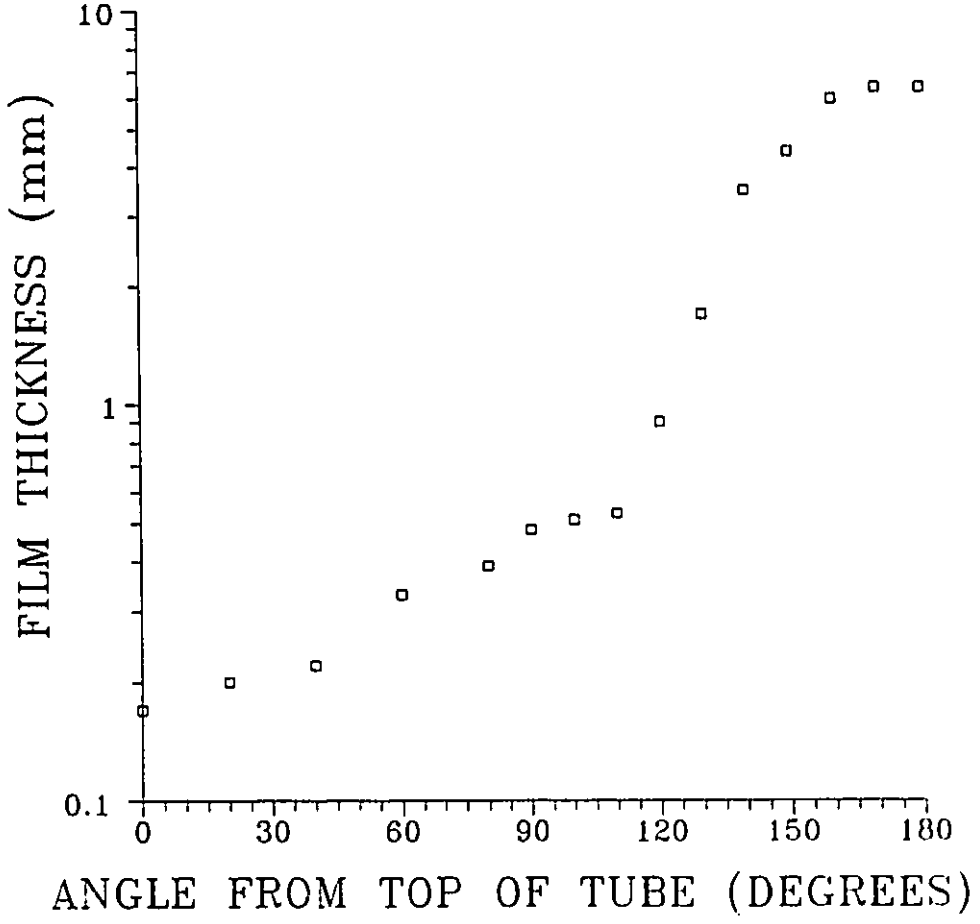

Figure 6.5 Experimental Liquid Film Distribution (from Lin et. al., 1985)

where the film velocity (u_f) is given by Equation [6.24]. The integrals in Equation [6.31] were solved numerically using Simpsons rule and the cubic spline approximation for $h'(\theta)$. When the average film area (A_f) is substituted from [6.32], the resulting quadratic can be solved for the bottom film thickness ($h(\pi)$). The assumed film thickness profile can then be determined from $h(\theta) = h'(\theta)h(\pi)$ for any known inlet conditions.

The problem can now be solved provided estimates of the run and branch development lengths are available. A solution is obtained by specifying the experimental inlet conditions ($\dot{m}_1$, x_1, α_1 and system pressure, P_1) averaged from the experimental values for a given set of inlet conditions. A branch flow split (i.e. $\dot{m}_3$) is then assumed and from continuity (Equation [6.1]) the run flow rate, $\dot{m}_2$, is calculated. The inlet velocities for both phases were then determined from Equations [6.20], [6.21] and [6.24] and the film distribution from Equations [6.31] and [6.32]. The fluid properties were determined from the correlations shown in Appendix A (from Shoukri, 1980).

To begin the calculation, an initial value of branch quality (x_3) was assumed such that initial values of the run quality (x_2) and the pressure changes ($(\Delta P_{2\text{-}1})_j$ and $(\Delta P_{1\text{-}3})_j$) could be determined from Equations [6.2], [6.3] and [6.4] respectively. Initial values of y_0 were assumed for both phases and the path of the dividing streamlines determined by iterating on Equations [6.13] through [6.18] using [6.26] and [6.29]. Once the y_0 values for each phase had been determined at several levels within the junction, the area of gas extracted and area of liquid extracted (A_{GE} and A_{LE}, see Figure 6.4) were determined by numerical integration using the junction geometry and

film distribution (h(θ)). An updated value of the branch quality was then calculated from

$$x_3 = \frac{A_{GE} A_f x_1}{A_1 \alpha_1 A_{LE} (1-x_1)(1-E_1) + A_{GE} x_1 A_f} \tag{6.33}$$

where A_1 represents the cross-sectional area of the inlet pipe and A_f the total film flow area from Equation [6.32]. The new value of branch quality was used to update the pressure changes $((\Delta P_{2-1})_j$ and $(\Delta P_{1-3})_j)$ and the process was iterated to convergence on the branch quality (x_3). The size of the spatial grid in the x, y and z directions was reduced until grid independent solutions were achieved.

6.3 Comparison of Model Predictions and Experimental Measurements

In the present experiments, the equilibrium entrainment ratio (E) was not measured. As discussed in Section 4.1.2, for most inlet conditions the amount of equilibrium entrainment is expected to be insignificant. Therefore, at this point in the analysis, the effects of net entrainment are neglected (i.e. E = 0).

In all cases from the present work, the measured void fraction in the inlet section was used in the model calculations. Where the void fraction was not measured, the correlation of Smith (1969) was used.

By specifying only the run and branch development lengths (DLX and DLY), a predicted curve for x_3/x_1 vs. flow split can be generated. This is done by iterating to convergence on x_3, as outlined above, for the range of measured flow splits. Figure 6.6 shows a typical pressure distribution

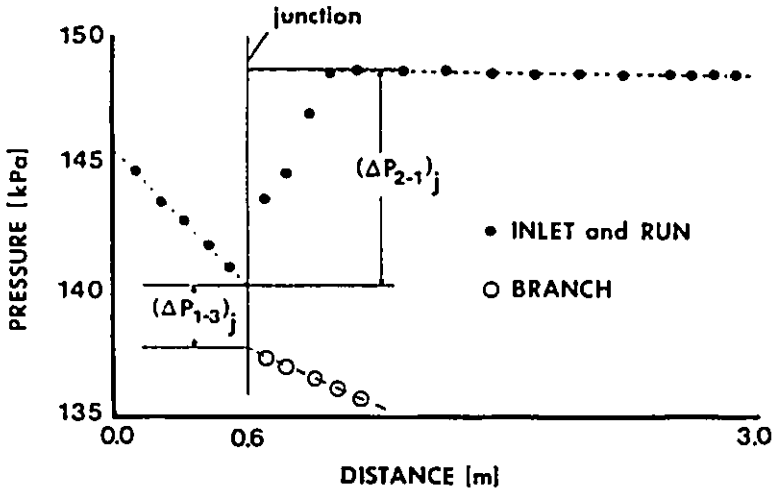

Figure 6.6 A Typical Pressure Distribution in Dividing Two-Phase Flow

(G_1= 600 kg/m^{2}s, x_1= 0.049, m_3/m_1= 0.31 and D_3/D_2= 1.0)

obtained in the experimental program (G_1= 600 kg/m^{2}s, x_1= 0.049, m_3/m_1= 0.31 and D_3/D_2= 1.0). Most of the data collected for D_3/D_1= 1.0 showed the pressure in the run peaking at approximately 10 tube diameters downstream of the junction. Consequently, DLX was fixed at 10 diameters for all calculations. As is the case in Figure 6.6, the pressure gradient in the branch was generally fully developed at the first measurement station such that a development length could not be estimated. As a result, DLY was used as a parameter to correlate the measured data. Varying the development lengths affected only the level of separation predicted. The model always maintained the experimentally observed parametric trends.

For all model predictions presented herein, single values are used for each of the run and branch development lengths along with the assumed pressure profiles as outlined above. The assumed run and branch pressure distribution, normalized with respect to the associated total pressure change, is then the same for all cases. In this way, the predicted model trends are not confounded by simultaneously varying many parameters.

Figure 6.7 shows the experimental and predicted results based on these assumptions with DLY fixed at 0.63D_1 for steam-water flow at approximately 0.15 MPa,G_1= 600 kg/m^{2}s and x_1= .045 and 0.08. The model predicts well the level of separation measured and the point of complete vapour extraction. Figure 6.8 shows the results for an inlet mass flux of 450 kg/m^{2}s and qualities of 0.045 and 0.15. Here, DLY was again fixed at 0.63D_1. The level of separation and point of complete vapour extraction are again reasonably well predicted.

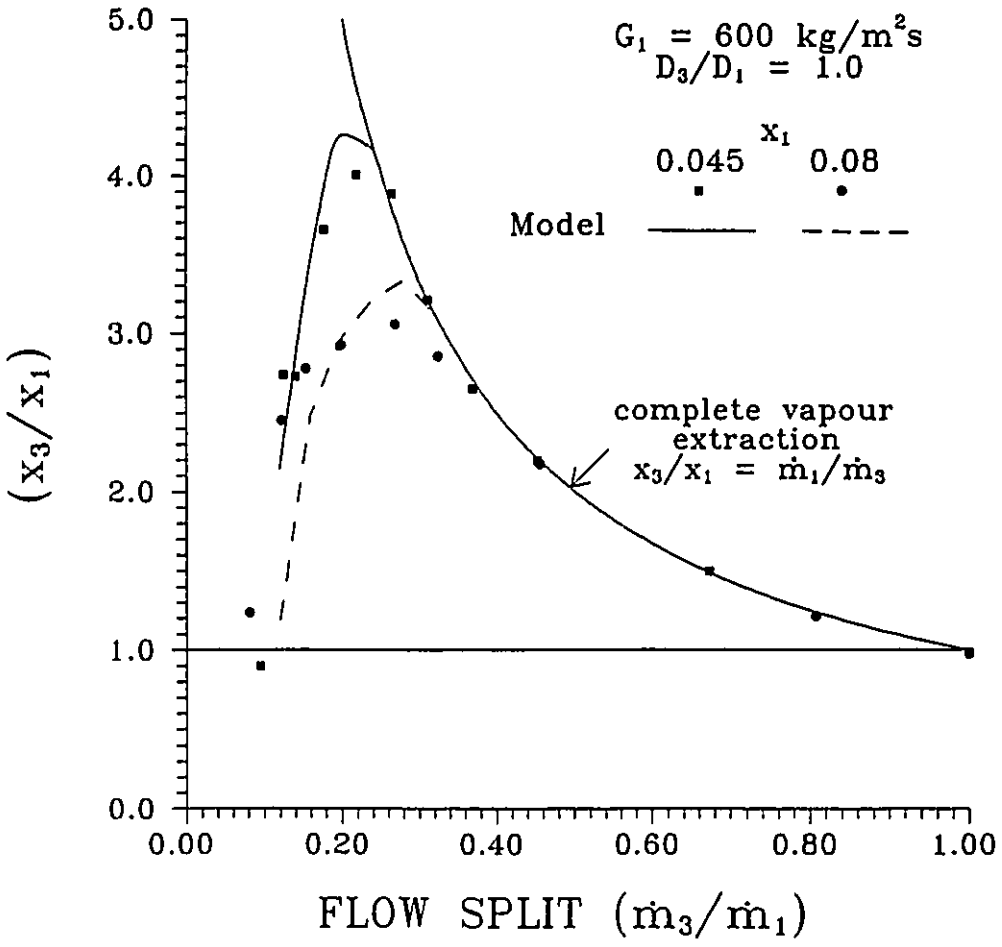

Figure 6.7 Comparison Between Measured and Predicted Values for Steam-Water Flow: P = 0.15 MPa, G_1= 600 kg/m^{2}s, E = 0.0, x_1= 0.045 and 0.08

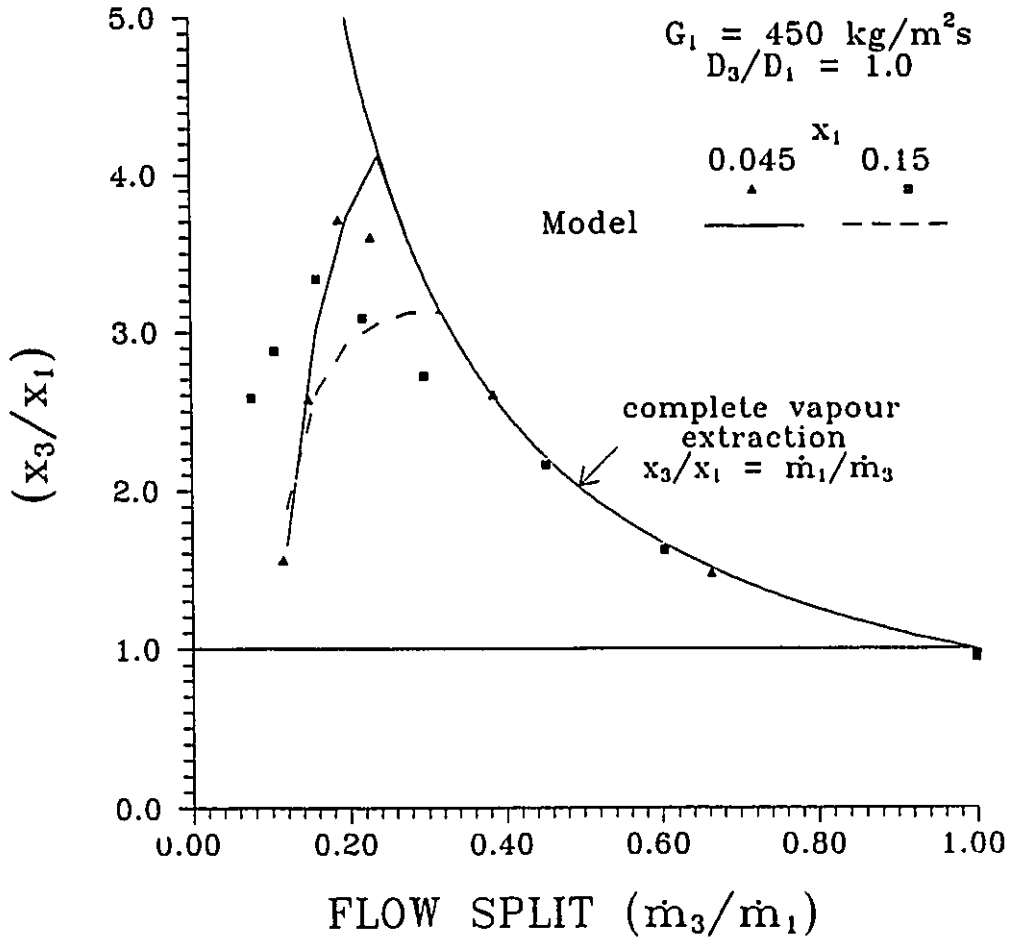

Figure 6.8 Comparison Between Measured and Predicted Values for Steam-Water Flow: P = 0.15 MPa, G_1= 450 kg/m^{2}s, E = 0.0, x_1= 0.045 and 0.15

The model underpredicts the level of separation for the higher inlet quality case (Figure 6.8, x_1 = 0.15). This condition represents the highest superficial gas velocity of all the measured data ($j_G \cong 70$ m/s). Under these conditions, the equilibrium entrainment can become significant. As discussed in Section 4.1.2, the correlation of Wallis (1968) predicts that almost 40% of the liquid is carried as entrained droplets. Figure 6.9 shows a comparison of the model predictions for this case with assumed equilibrium entrainment rates of 0.0 and 0.40. The parametric effect of increased entrainment is shown to increase separation and move the model predictions closer to the measured data.

The model, as developed, tends to overpredict the extent of phase separation for the lowest inlet qualities (x_1= 0.02). For these cases, the inlet flow parameters mapped very close to the slug/annular transition zone on the flow regime map of Mandhane et al. (1974). This was also confirmed by visual observation at the test section inlet. Under these conditions, an assumption that the dominant forces are pressure and inertia may not be valid. With a slower moving liquid film and a very thick layer of water on the bottom of the tube, gravity forces may become important, particularly at low flow splits where the pressure changes are small. Due to the geometry of a horizontal junction, gravity forces can divert a portion of the liquid film below the mid-plane to the branch. For low inlet qualities, much of the liquid flow is located below the mid-plane. This effect will tend to reduce the branch quality and is not accounted for in the model.

As the flow characteristics become more typical of slug flow, the model assumption neglecting phasic interactions also becomes less valid. For

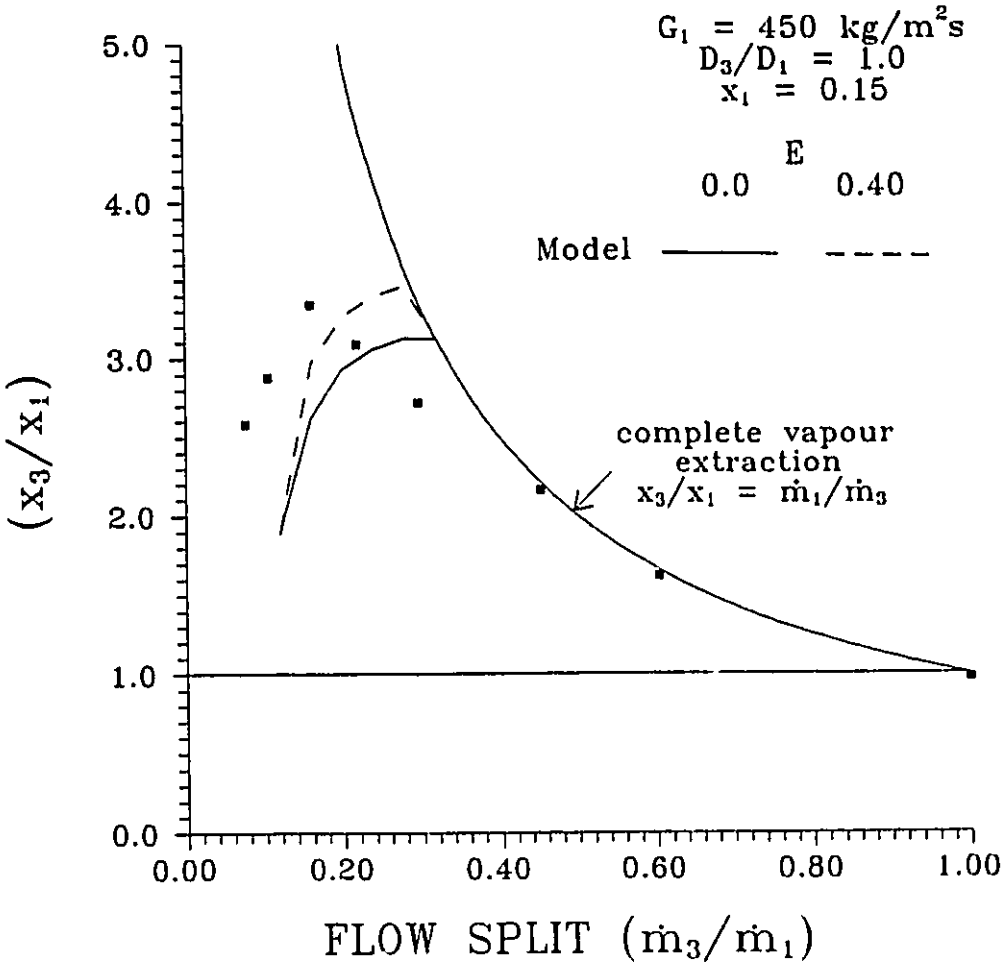

Figure 6.9 Comparison Between Measured and Predicted Values for Steam-Water Flow: P = 0.15 MPa, G_1 = 450 kg/m^{2}s, x_1 = 0.15, E = 0.0 and 0.40

mixed inlet flows, the liquid entrained by the branching gas flow can become significant. This also reduces the branch quality and is unaccounted for in the model.

The model predictions are also compared with experimental data obtained by other investigators for air-water and steam-water annular flow in dividing T-junctions with equal inlet and branch diameters. In all comparisons, the development lengths through the run and branch where kept constant at 10 and .65 diameters respectively. Figure 6.10 shows the present model predictions and experimental data of Seeger at al. (1986). These data are for air-water flow at a higher pressure than used in the present work ($P_I \cong$ 0.7 MPa). For these experiments, the superficial liquid velocity (j_L) is held constant at 1.0 m/s while the superficial gas velocities (j_G) were 40, 21 and 15 m/s. Agreement between the model predictions and measured values is best when an assumption of uniform film distribution is applied. These inlet conditions represent generally higher qualities and pressures than those used in the development of the model. Increasing the pressure and inlet quality will enhance the film distribution mechanisms discussed in Section 4.1.2 resulting in a more even liquid film. The level of phase separation is again predicted by the model as well as the parametric effect of superficial gas velocity.

Figure 6.11 shows a comparison of the model predictions and the experimental measurements of Seeger et al. (1986) as presented by Lahey (1987). For this data set the superficial gas and liquid velocities are both held constant (j_G= 15 m/s and j_L= 1 m/s) as the inlet pressure is varied between 1 and 5 MPa. As the pressure is increased, the gas phase density

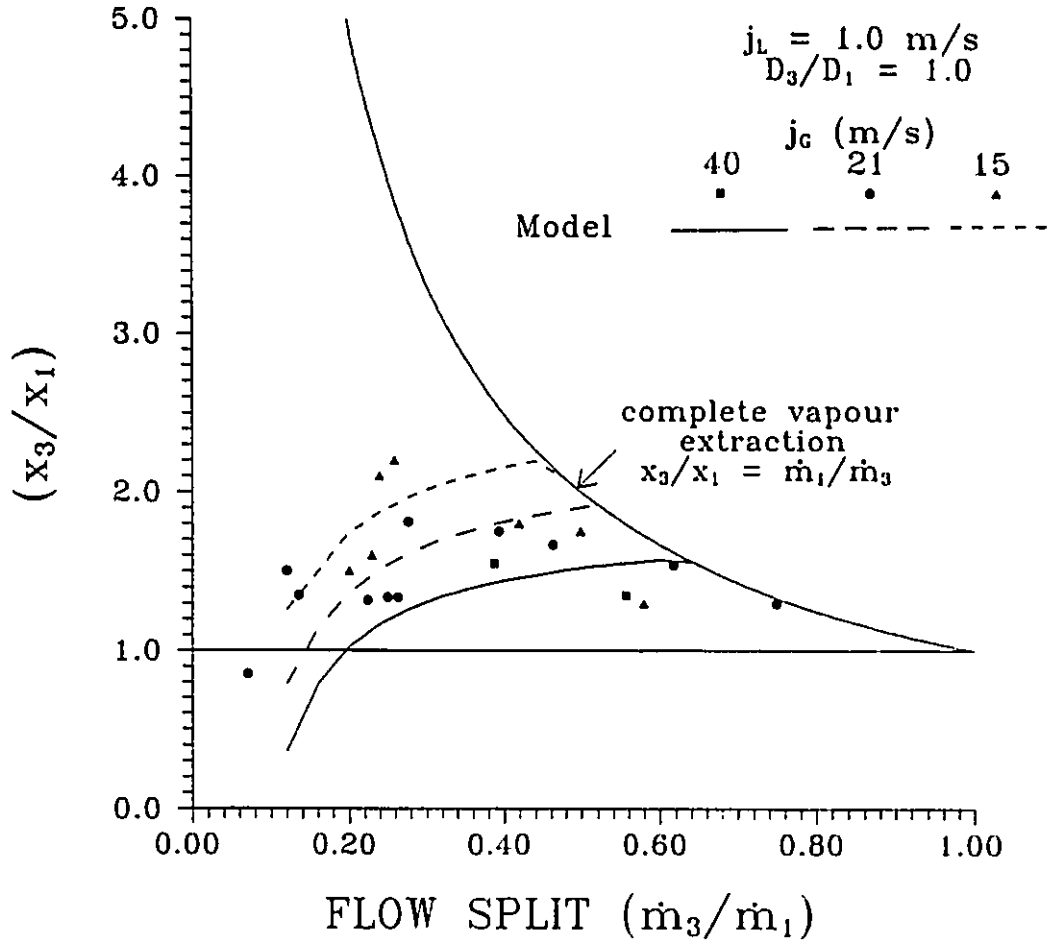

Figure 6.10 Comparison Between Measured and Predicted Values for Air-Water Flow From Seeger et al. (1986):

P = 0.7 MPa, j_L = 1.0 m/s, j_G = 40, 21 and 15 m/s

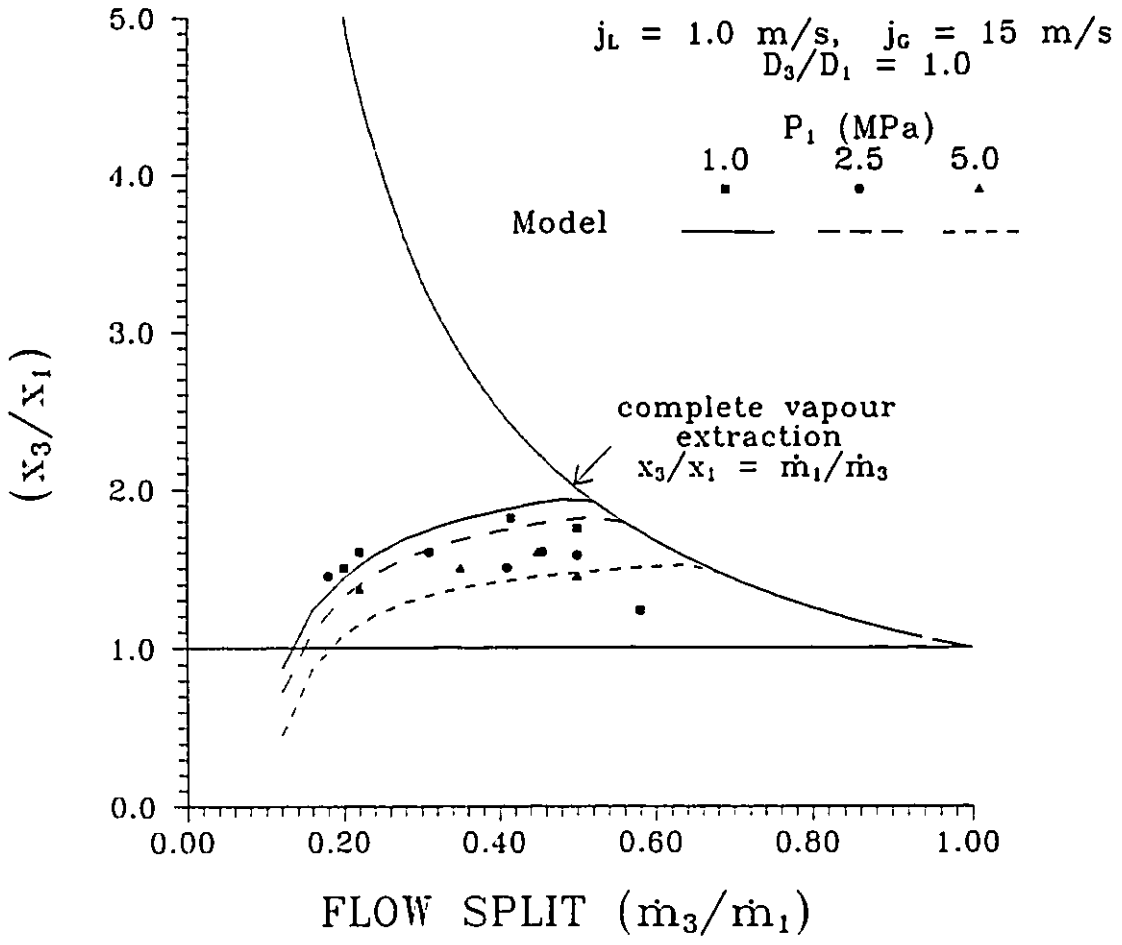

Figure 6.11 Comparison Between Measured and Predicted Values for Steam-Water and Air-Water Flow From Seeger et al. (1986)

j_L = 1.0 m/s, j_G = 15 m/s, P_1 = 1, 2.5 and 5 MPa

and momentum flux (ρu^2) also increases. This enhances the resistance of the gas core to extraction through the branch and will tend to reduce the level of separation. This trend is demonstrated by the data. The model again predicts the level of separation as well as the parametric effect of inlet pressure.

A comparison between the model predictions and experimental data of Azzopardi (1984) is shown in Figure 6.12. These data are for air-water annular flow (P_1= 0.15 MPa) in a vertical T-junction with equal branch and inlet diameters and G_1= 135 kg/m^{2}s and x_1= 0.41. The film flow rate for identical inlet conditions was measured by Azzopardi and Whalley (1982) such that the equilibrium entrainment ratio is known (E = 0.31). For vertical inlet flow a uniform film distribution is assumed. The liquid phase momentum equation has been modified to account for gravitational forces, i.e. Equation [6.10] becomes:

$$u \frac{\partial u}{\partial x} + v \frac{\partial u}{\partial y} = - \frac{1}{\rho} \frac{\partial p}{\partial x} - \rho_L g. \qquad (6.34)$$

Figure 6.12 shows that the model generally over predicts the branch quality although agreement is typically with 30%. Due to the low mass flux, the use of pressure change correlations and development lengths from horizontal experiments cannot be justified. Agreement should improve when these values are established from vertical phase separation experiments.

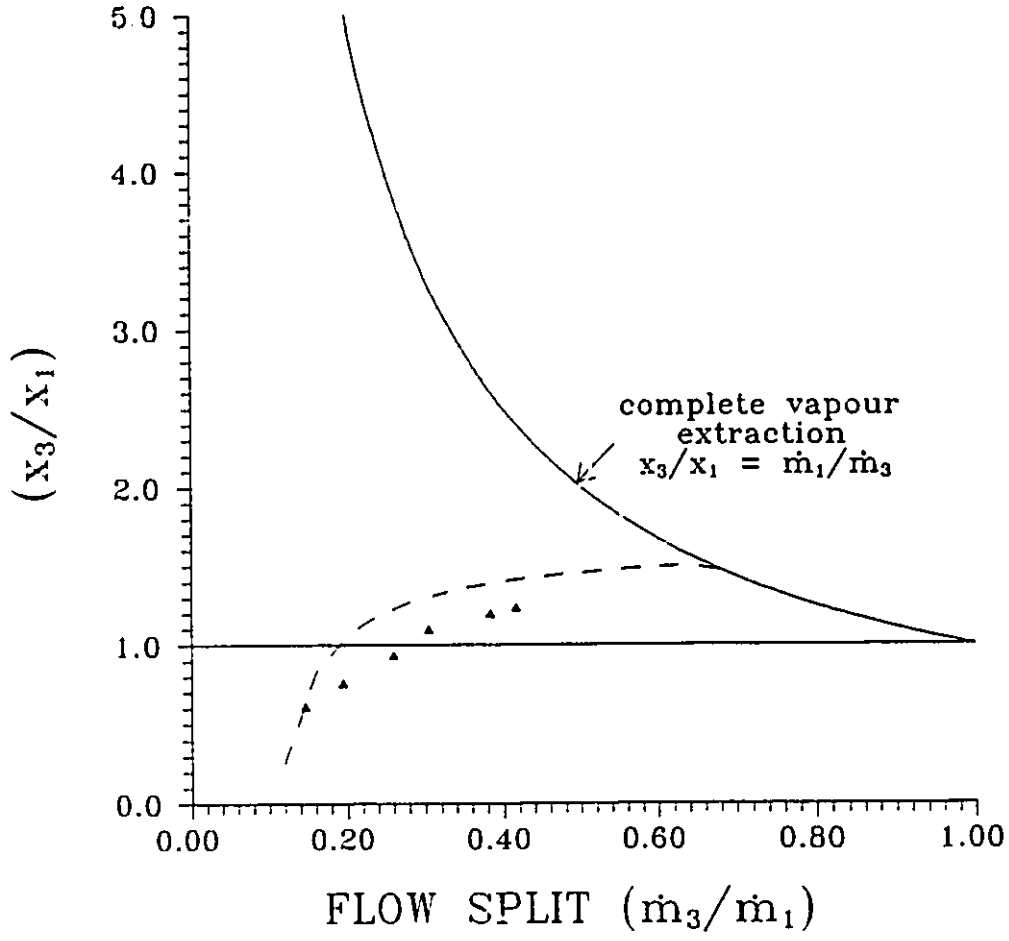

Figure 6.12 Comparison Between Measured and Predicted Values for Vertical Air-Water Flow From Azzopardi (1984):

P = 0.15 MPa, G_l= 135 kg/m^{2}s, x_l= 0.41 and E = 0.31

6.4 Effect of Branch Diameter

The model, as developed in the previous section, is applicable to T-junctions having equal branch and inlet diameters. The flow is assumed to be two-dimensional such that the vertical (z-component) velocities for both phases are zero. As the branch diameter is reduced, the flow becomes more three-dimensional as the liquid film flowing above and below the branch opening must be entrained into the branch. These effects are not accounted for in the model.

The model is applied to the smaller branch diameters by considering only the flow between the top and bottom of the branch opening. Again, the run and branch development lengths have been fixed at 10 and .65 diameters respectively. Figure 6.13 shows the model predictions and measured values for the three T-junctions (D_3/D_1= 1.0, 0.82 and 0.5) with G_1= 600 kg/m^{2}s and x_1= 0.045. The model correctly predicts the parametric trend of increased phase separation with smaller branch diameters although the level of separation does not match the measured data. In order to improve the model predictions for smaller branch diameters, the phasic interactions must also be modeled.

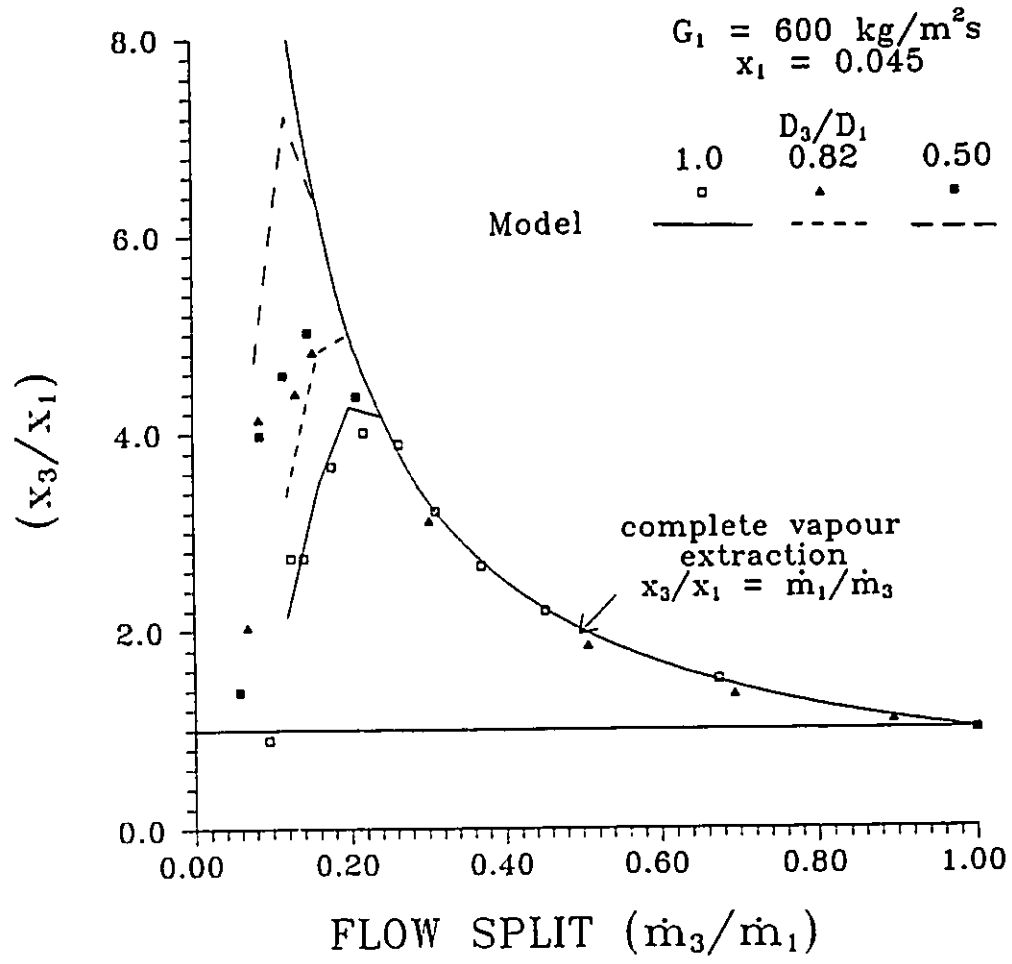

Figure 6.13 Comparison Between Measured and Predicted Values for Steam-Water Flow: P = 0.15 MPa, G_1= 600 kg/m^{2}s, E = 0.0, x_1= 0.045

D_3/D_1= 1.0, 0.82, 0.50

CHAPTER 7

CONCLUSIONS AND RECOMMENDATIONS

Extensive data for steam-water annular flow in horizontal T-junctions with a horizontal branch were obtained. Different conditions of inlet mass flux, inlet quality, branch flow split and branch to inlet diameter ratio were considered. The data covered a range of operating conditions which has not been examined previously. Included in the experimental measurements are detailed phase separation and pressure distribution characteristics within the test section. A unique feature of the experiments was the measurement of the void fraction profiles along the three legs of the junction.

For the flow conditions considered, separation effects were seen to be severe with the gas phase preferentially entering the branch. The ease of vapour extraction is associated with its relatively low momentum flux in the inlet section. An assumption of complete vapour extraction closely approximated the measured data when more than 30% of the total inlet flow was removed through the branch. Below 30% removal, the degree of phase separation was strongly dependent upon the flow split ratio, inlet quality, and to a lesser extent the inlet mass flux.

Phase separation effects became more severe as the branch diameter was reduced. This results from the reduced portion of liquid film that can

be directly extracted through the branch as the branch diameter is reduced.

Through the set of measurements made in the experimental program, the phase separation and pressure distribution characteristics were shown to be strongly interdependent. With the support of these measurements, a physical model describing the phase separation mechanism is presented.

Based on the data obtained in the present work, the use of a separated flow axial momentum balance is recommended for modelling the axial pressure rise through the run. Under the conditions tested herein, the value of the separated flow momentum correction factor, $k_{(1-2)S}$, was approximately unity independent of inlet flow conditions and junction geometry (branch diameter). This indicates that the axial momentum associated with the branching flow is insignificant relative to the momentum change across the junction.

A consistent model, based on a balance of mechanical energy for the branching flow, was introduced to correlate the pressure changes through the branch. This model resulted in the definition of a new equivalent inlet density of the branching flow, ρ^*, and a new branch two-phase multiplier, Φ^*, accounting for the branch irreversible losses. Based on the present data, the two-phase multiplier was found to be dependent only on the flow split ratio for a given junction geometry. The data were used to empirically correlate the two-phase branch loss multiplier with the flow split ratio and branch to inlet diameter ratio..

A model to predict the phase separation characteristics in dividing annular two-phase flow has also been presented. The model consists of the vapour phase continuity equation, the mixture continuity equation, the run and branch pressure change correlations and a newly developed closure

relationship. The closure relationship links the phase redistribution characteristics with the junction geometry and flow characteristics. This relationship is based on an assumption that pressure and inertia are the dominant forces within the junction volume. In the model, the degree of phase separation is also dependent upon a well defined inlet flow distribution. These assumptions are consistent with the experimentally observed phenomena. The model is capable of predicting the observed phase separation characteristics from three independent experimental studies of annular two-phase flow division covering the ranges of; $135 \leq G_1 \leq 1325$ kg/m^{2}s, $0.045 \leq x_1 \leq 0.41$, and $0.72 \leq \rho_G \leq 25.3$ kg/m^{2}s.

The parametric effect of the reduction in branch diameter was also captured by the model. To better predict the degree of phase separation with reduced branch diameters, the model must be extended to include phasic interactions. This type of extension would also make the model better suited to more dispersed or intermittent two-phase flows.

There is considerable scope for future work related to phase separation in dividing two-phase flow. The effect of the branch angle of orientation w.r.t. the horizontal would be of particular interest for further model development and validation. Previous experiments with annular inlet flows (e.g. Seeger et al. (1986)) have shown that as the branch is rotated above or below the horizontal, the phase separation effects become respectively more and less severe. This has been attributed to the asymmetric film distribution for horizontal flows which have a thicker film on the bottom of the tube. The thicker film causes more water to be available for direct extraction from a downward facing branch. This effect is accounted for in the model as formulated here.

The effects of inlet flow regime can be investigated using test sections with larger inlet diameters. This allows measurable flow rates of steam and water to be combined in the mixer that would yield stratified and intermittent flows at the test section inlet.

Further model development requires information from supporting studies not directly related to the phase separation phenomena. These would include studies of phase distribution under flow conditions of interest and studies related to equilibrium entrainment for annular flow.

REFERENCES

Asali, J. C., Lemam, G. W. and Hanratty, T. J., 1985, Entrainment measurements and their use in design equations. PHC PhysicoChemical Hydrodynamics, 6, 1/2, pp. 207-221.

Azzopardi, B. J. and Freeman-Bell, G., 1983, The effect of side arm diameter on the two-phase flow split at a T-junction. Report AERE-M3290.

Azzopardi, B. J. and Whalley, P. B., 1982, The effect of flow patterns on two-phase flow in a T-junction. Int. J. Multiphase Flow 8, 491-507.

Azzopardi, B. J., 1988, Measurements and observations of the split of Annular flow at a vertical t-junction. Int. J. Multiphase Flow 14, 701-710.

Ballyk, J. D., 1986, On the characteristics of dividing steam-water flow in a horizontal T-junction. M.Eng Thesis, McMaster Univ., Hamilton, Ontario.

Ballyk, J. D., Shoukri, M. and Chan, A. M. C., 1987, Experimental investigation of steam-water annular flow in piping junctions. Presented at the ASME Winter Annual Meeting, Boston, Mass., Dec 13-18, 1987 (87-WA/NE-8)

Ballyk, J. D., Shoukri, M. and Chan, A. M. C., 1988, Steam water flow in a horizontal dividing t-junction. Int. J. Multiphase flow, 14, 265-285.

Butterworth, D., 1972, Air-water annular flow in a horizontal tube. Progress in Heat and Mass transfer 6, 235

Collier, J. G., 1976, Single-phase and two-phase flow behavior in primary circuit components. In Proceedings of NATO Advanced Institute on Two-phase flow and Heat Transfer, Vol. 1, pp. 313-365. Hemisphere, Washington, D. C.

Delhay, J. M., 1981, Singular pressure drops. In: Two-phase Flow and Heat Transfer in the Power and Process Industries, Chap. 4, (Edited by Bergles, A. E. et al.) Hemisphere, Washington, D. C.

Delhay, J. M., 1981, Instumentation. In: Two-phase Flow and Heat Transfer in the Power and Process Industries, Chap. 4 (Edited by Bergles, A. E. et al.) Hemisphere, Washington, D. C.

Fouda, A. E., 1975, Two-phase flow behaviour in manifolds and networks. Ph.D. Thesis, Dept. of Chem. Eng, Univ. of Waterloo, Ontario.

Fouda, A. E. and Rhodes, E., 1974, Two-phase annular flow stream division in a simple tee. Trans. Instn Chem. Engrs 52, 354-360

Henry, J. A. R., 1981, Dividing annular flow in a horizontal tee. Int. J. Multiphase flow 7, 343-355.

Hewitt, G. F., 1981, Annular flow. In: Two-phase Flow and Heat Transfer in the Power and Process Industries, Chap. 5 (Edited by Bergles, A. E. et al.) Hemisphere, Washington, D. C.

Hewitt, G. F. and Hall-Taylor N. S., 1970, Annular two-phase flow, Pergamon Pess Ltd., Oxford.

Hewitt, G. F. and Lacey, P. M. C., 1965, The break down of the liquid film in annular two-phase flow. Int. J. Heat Mass Transfer, 8, 781-791.

Hinze, J. O., 1967, Secondary currents in wall turbulence. Phys. Fluids (Suppl.) 10, 112-125.

Hong, K. C., 1978, Two-phase flow splitting at a pipe tee. J. Petrol. Technol. 290-296

Hwang, S. T., Soliman, H. M. and Lahey, R. T. Jr., 1988, Phase separation in dividing two-phase flow. Int. J. Multiphase flow 14, 439-458.

Hwang, S. T., Soliman, H. M. and Lahey, R. T. Jr., 1989, Phase separation in impacting wyes and tees. Int. J. Multiphase flow 15, 965-975.

James, P. W., Wilkes, N. S., Conkie, W. and Burns, A., 1987, Developments in the modelling of horizontal annular two-phase flow. Int. J. Multiphase flow 13, 173-198.

Johansen, S. E., 1979, Experimental study of gas-liquid flow in a pipe tee. M.Sc. Thesis, Univ. Tulsa,Okla.

Kalkach-Navarro, S., Lee, S-J and Lahey, R. T. Jr., 1988, The analysis of to-phase pressure drop in branching conduits using a two-fluid model. 1988 ANS Annual meeting, San Diago, California.

Kataoka, I., Ishii, M. and Mishima, K., 1983, Generation and size distribution of droplet in annular two-phase flow. Journal of Fluids Engineering, 105, June, 1983.

Lahey, R. T. Jr., 1987, Dividing flow in a tee junction. In: G. F. Hewitt et al., eds., Multiphase Science and Technology, Data Set No. 9, (Hemisphere, Washington, D.C., 1987).

Lahey, R. T. Jr., 1986, Current understanding of phase separation mechanisms in branching conduits, 1986, Nuclear Engineering and Design, 95, 145-161

Lahey, R. T. Jr and Moody, F. J., 1977, The thermal-hydraulics of boiling water reactors, ANS Monograph.

Laurinat, J. E., 1982, Studies of the effects of pipe size on horizontal annular two-phase flow. Ph.D. Thesis, University of Illinois at Urbana-Champaign, Urbana, Illinois.

Laurinat, J. E., Hanratty, T. J. and Jepson, W. P., 1985, Film thickness distribution for gas-liquid annular flow in a horizontal pipe. PCH PhysicoChemical Hydrodynamics, 6, 179-195.

Lemonnier, H and Hervieu, E., 1988, Theoretical modelling and experimental investigation of single-phase and two-phase flow division at a tee junction, ANS Proceedings of the National Heat Transfer Conference, July 1988, Houston, Texas. (HTC-Vol. 3).

Lin, T. F., Jones, O. C., Lahey R. T. Jr, Block, R. C. Jr and Murase, M., 1985, Film thickness measurements and modelling in horizontal annular flow. PHC PhysicoChemical Hydrodynamics, 6, 1/2, pp. 197-206.

Maciaszek, T. and Micaelli, J. C., 1988, A phase separation model for tee junctions application to a pwr safety code. ANS Proceedings of the National Heat Transfer Conference, July 1988, Houston, Texas. (HTC-Vol. 3).

Madden, J. M. and St Pierre, C. S., 1969/70, Two-phase air-water flow in a slot-type distributor. Proc. Instn mech. Engrs, 184/3C, 175.

Mandhane, J. M., Gregory, G. A. and Aziz, K, 1974, A flow pattern map for gas-liquid flow in horizontal pipes. Int. J. Multiphase Flow, 1, 537-553.

McNown, J. S., 1954, Mechanics of manifold flow Trans. ASCE 2714 119, 1103-1142.

Muller, U. and Reimann, 1991, Redistribution of two-phase flow in branching conduits, Proceeding of the International Conference on Multiphase Flows '91-Tsukuba, September 24 - 27, 1991, Tsukuba Japan.

Oranje, L., 1973, Condensate behavior in gas pipelines is predictable, Oil Gas J. 39-44.

Reimann, J. and Seeger, W., 1986, Two-phase flow in a T-junction with a horizontal inlet-Part II: pressure differences, Int. J. Multiphase Flow, 12, 587-608.

Seeger, W.,Reimann, J. and Muller, U., 1986, Two-phase flow in a T-junction with a horizontal inlet-Part I: phase separation, Int. J. Multiphase Flow, 12, 575-585.

Rubel, M., 1986, Experimental investigation of phase distribution in a horizontal tee junction, M.Sc. Thesis Univ. of Manitoba, Winnipeg.

Rubel, M. T., Soliman, H. M. and Sims, G. E., 1988, Phase distribution during steam-water flow in a horizontal t-junction, Int. J. Multiphase flow, 14, 425-438.

Saba, N. and Lahey, R. T. Jr ,1982, Phase separation phenomena in branching conduits, Report NUREG/CR-2590.

Saba, N. and Lahey, R. T. Jr, 1984, The analysis of phase separation phenomena in branching conduits. Int. J. Multiphase Flow, 10, 1-20.

Seeger, W., Reimann, J. and Müller, U., 1986, Two-phase flow in a T-junction with a horizontal inlet-Part I: phase separation, Int. J. Multiphase Flow, 12, 575-585.

Shoham, O., Brill, J. P. and Taitel, Y., 1987, Two-phase flow splitting in a Tee - experiment and modelling, Chemical Engineering Science. Vol 42. No. 11. pp. 2667-2676.

Shoham, O., Arirachakaran, S. and Brill, J. P., 1989, Two-phase flow splitting in a horizontal reduced pipe tee, Chemical Engineering Science, Vol 44. No. 10. pp. 2388-2391.

Shoukri, M., Ballyk, J. D. and Chan, A. M. C., 1987, On the characteristics of two-phase flow in network branches, Canadian Electrical Association (CEA) Report 325G430.

Shoukri, M., 1980, The effect of heat addition on the pressure drop in two-phase flow systems, Canadian Electrical Association (CEA) Report 000G104

Smith, S. L., 1969, Void fractions in two-phase flow. A correlation based on an equal velocity head model. Proc. Inst. Mech. Engrs. 184, Pt 1, (36) 647-664

Steen, D. A. and Wallis, G. B., AEC Rept. NYO-3114-2, 1964.

Tsuyama, M. and Taga, M., 1959, On the flow of the air-water mixture in the branch pipe, I. Experiment on the horizontal branch pipe which is equal to the main one in diameter,

Wallis, G. B., One-dimensional two-phase flow, 1969, New York: (McGraw Hill, Inc.).

APPENDIX A

SATURATED WATER AND STEAM PROPERTIES

The empirical equations listed below were obtained by the least square method using standard steam tables for pressures ranging from 1 to 10 bar (Shoukri (1980)). The equations are dimensional and SI units are used, i.e. $v = m^3/kg$, $p = bar$, $\mu = Ns/m^2$, $\sigma = N/m$, $T = {}^{\circ}C$, $C_p = kJ/kg{}^{\circ}C$.

$$v_f = 0.99453 \times 10^{-3} + 48.7443 \times 10^{-6}(P)^{0.43503}$$

$$v_g = 3.6305672 \times 10^{-2} + 1.674019/P$$

$$v_{fg} = v_g - v_f$$

$$h_{fsat} = -127.422 + 545.254(P)^{0.21265}$$

$$h_{fg} = 2474.56 - 217.561(P)^{0.32378}$$

$$C_{pf} = 4.11784 + 39.205 \times 10^{-4}(P)^{0.75965}$$

$$T_{sat} = -44.0965 + 143.7725(P)^{0.19246}$$

$$\mu_f = 2.72737 \times 10^{-4} - 5.5749 \times 10^{-5}\ln(P)$$

$$\mu_g = 1.195 \times 10^{-5} + 1.314 \times 10^{-6}\ln(P)$$

$$\sigma = 7.5448 \times 10^{-2} - 1.3017 \times 10^{-4}T_{sat} - 3.5056 \times 10^{-7}T_{sat}^{2}$$

APPENDIX B

EXPERIMENTAL DATA

TABLE B.1

SINGLE-PHASE DATA FOR $D_3/D_1 = 1.0$

$\frac{\dot{m}_3}{\dot{m}_1}$	G_1 (kg/m^{2}s)	$(\Delta P_{2-1})_J$ (Pa)	$(\Delta P_{1-3})_J$ (Pa)
0.098	451.4	26.6	4.0
0.305	448.4	64.5	0.3
0.504	447.5	81.7	16.9
0.702	451.7	87.8	44.4
0.905	451.6	78.8	95.5
1.000	449.4	75.8	127.3
0.103	597.2	44.7	6.0
0.301	599.8	113.4	-10.2
0.500	599.8	149.4	22.0
0.700	596.4	150.0	86.5
0.903	599.4	140.3	163.0
1.000	598.1	128.3	217.0
0.100	900.4	106.0	9.8
0.300	896.6	253.3	-12.5
0.502	900.1	327.2	,55.6
0.702	898.6	330.2	187.6
0.904	897.9	306.5	375.7
1.000	896.9	285.7	472.7
0.098	1213.6	176.6	13.0
0.299	1196.5	437.2	-3.3
0.504	1195.6	571.5	88.8
0.702	1181.8	573.9	326.6

TABLE B.2

SINGLE-PHASE DATA FOR D_3/D_1= 0.82

$\frac{\dot{m}_3}{\dot{m}_1}$	G_1 (kg/m^{2}s)	$(\Delta P_{2-1})_J$ (Pa)	$(\Delta P_{1-3})_J$ (Pa)
0.127	454.1	29.1	-4.1
0.299	449.1	54.2	11.8
0.491	452.9	73.8	58.0
0.704	449.6	76.9	130.9
0.916	450.3	73.0	241.4
1.000	450.7	68.6	293.5
0.100	601.2	44.1	-4.2
0.304	604.7	102.4	24.3
0.503	603.8	131.1	108.1
0.696	605.0	147.4	249.8
0.908	602.2	127.5	407.5
1.000	597.9	119.1	507.6
0.102	901.4	95.9	-9.4
0.303	898.7	224.8	48.9
0.501	901.2	295.4	227.9
0.702	900.0	309.45	538.4
0.896	899.6	282.1	942.0
1.000	902.4	273.3	1145.3
0.102	1197.3	165.1	-18.3
0.300	1199.6	397.7	85.4
0.500	1198.2	517.3	401.4
0.704	1197.1	530.2	957.4
0.914	1196.1	474.6	1737.6
1.000	1197.9	458.9	1992.8

TABLE B.3

SINGLE-PHASE DATA FOR $D_3/D_1 = 0.50$

$\frac{\dot{m}_3}{\dot{m}_1}$	G_1 (kg/m^{2}s)	$(\Delta P_{2-1})_J$ (Pa)	$(\Delta P_{1-3})_J$ (Pa)
0.100	451.7	22.4	23.6
0.301	450.7	55.0	217.7
0.501	447.7	69.2	589.5
0.699	452.0	73.7	1155.9
0.904	450.4	68.4	1893.5
0.999	450.6	70.3	2296.2
0.101	600.2	46.3	37.9
0.298	598.2	94.8	362.4
0.501	599.7	124.1	1014.5
0.699	598.9	130.9	1936.6
0.900	600.2	127.8	3429.1
1.000	598.4	119.1	4256.2
0.099	899.1	116.6	73.7
0.298	900.2	216.1	799.9
0.499	899.0	281.8	2228.9
0.701	900.4	300.8	4707.2
0.901	901.4	284.9	7870.5
1.000	898.1	268.3	9595.7
0.102	1200.0	214.1	146.8
0.298	1200.2	405.9	1455.2
0.498	1198.2	505.9	4152.9
0.700	1197.7	534.6	8318.5
0.902	1200.2	500.5	13957.1
1.000	1164.9	444.8	16028.8

TABLE B.4

TWO-PHASE DATA FOR $D_3/D_1 = 1.0$

$\frac{\dot{m}_3}{\dot{m}_1}$	G_1 (kg/m^{2}s)	x_1	$\frac{\dot{x}_3}{\dot{x}_1}$	α_1	α_2	α_3	$(\Delta P_{2-1})_j$ (kPa)	$(\Delta P_{1-3})_j$ (kPa)	P_1
0.115	445.9	0.051	1.56	0.884	0.892	0.867	0.685	-0.068	128
0.149	439.9	0.049	2.57	0.866	0.894	0.886	1.009	0.041	119
0.189	431.9	0.051	3.71	0.879	0.874	0.918	1.532	0.660	111
0.230	450.5	0.046	3.60	0.854	0.865	0.923	1.488	0.589	141
0.386	451.7	0.044	2.60	0.851	0.059	0.917	3.273	1.306	117
0.664	459.0	0.043	1.47	0.908	0.120	0.846	3.075	2.168	123
1.000	450.7	0.046	0.95	0.907	-----	0.898	2.340	3.598	137
0.077	446.8	0.151	2.58	0.977	0.977	0.957	2.693	0.004	185
0.105	454.4	0.152	2.88	0.991	0.992	0.968	4.877	0.379	169
0.160	447.5	0.153	3.34	0.976	0.949	0.982	8.241	2.489	130
0.220	454.6	0.153	3.09	0.981	0.976	0.976	9.755	4.921	132
0.297	452.4	0.152	2.72	0.988	0.976	0.969	11.580	7.302	148
0.453	450.6	0.152	2.16	0.987	0.948	0.984	11.023	11.923	171
0.603	442.7	0.152	1.62	0.979	0.039	0.979	11.303	14.999	184
1.000	411.1	0.148	0.97	0.983	-----	0.955	9.580	17.694	203
0.073	601.5	0.019	0.78	0.804	0.801	0.909	0.240	-0.120	130
0.160	583.8	0.023	2.73	0.806	0.816	0.895	0.546	0.271	117
0.168	588.4	0.021	4.32	0.790	0.685	0.901	0.609	0.494	112
0.222	593.6	0.025	4.35	0.808	0.739	0.909	0.810	1.027	117
0.402	620.6	0.018	2.47	0.804	0.187	0.860	1.839	1.015	114
0.708	583.4	0.025	1.41	0.803	0.080	0.813	2.096	1.984	125
1.000	602.2	0.022	1.02	0.816	-----	0.848	2.071	2.837	139

TABLE B.4 (Continued)

TWO-PHASE DATA FOR $D_3/D_1 = 1.0$

$\frac{\dot{m}_3}{\dot{m}_1}$	G_1 (kg/m^{2}s)	x_1	$\frac{\dot{x}_3}{\dot{x}_1}$	α_1	α_2	α_3	$(\Delta P_{2-1})_J$ (kPa)	$(\Delta P_{1-3})_J$ (kPa)	P_1
0.095	598.7	0.042	0.90	0.861	0.873	0.921	0.963	-0.184	152
0.125	596.1	0.044	2.74	0.878	0.885	0.933	1.419	-0.016	137
0.141	591.8	0.046	2.73	0.886	0.852	0.906	1.532	0.201	132
0.178	598.9	0.045	3.66	0.879	0.867	0.923	2.143	0.839	118
0.218	598.1	0.044	4.00	0.874	0.766	0.989	3.641	1.332	119
0.264	597.5	0.045	3.88	0.890	0.067	0.966	7.708	2.178	126
0.311	609.0	0.050	3.21	0.926	0.072	0.840	8.459	2.544	142
0.370	594.6	0.047	2.65	0.905	0.045	0.932	8.156	2.845	126
0.453	593.5	0.048	2.20	0.889	0.020	0.927	8.090	3.626	131
0.673	596.0	0.045	1.50	0.865	0.031	0.903	6.478	4.172	141
1.000	610.1	0.044	0.98	0.883	-----	0.927	4.560	6.360	164
0.081	600.6	0.079	1.23	0.889	0.903	0.850	1.613	-0.351	194
0.122	593.5	0.080	2.45	0.876	0.935	0.931	2.689	0.057	163
0.154	597.1	0.079	2.78	0.908	0.942	0.940	4.099	0.782	145
0.200	596.6	0.082	2.92	0.944	0.898	0.948	5.541	2.381	123
0.269	598.1	0.084	3.06	0.975	0.875	0.946	8.339	4.300	138
0.325	594.1	0.081	2.86	0.925	0.878	0.967	8.343	5.920	145
0.456	601.3	0.078	2.17	0.940	0.104	0.946	9.265	8.469	155
0.808	596.6	0.080	1.21	0.864	0.037	0.919	9.873	11.903	189
1.000	599.9	0.078	0.97	0.935	-----	0.942	9.250	13.459	206

TABLE B.4 (Continued)

TWO-PHASE DATA FOR $D_3/D_1 = 1.0$

$\frac{\dot{m}_3}{\dot{m}_1}$	G_1 (kg/m^{2}s)	x_1	$\frac{\dot{x}_3}{\dot{x}_1}$	α_1	α_2	α_3	$(\Delta P_{2-1})_j$ (kPa)	$(\Delta P_{1-3})_j$ (kPa)	P_1
0.107	901.6	0.021	1.39	0.749	0.781	0.860	0.806	0.362	158
0.140	892.4	0.020	3.38	0.780	0.781	0.939	1.216	0.266	143
0.180	907.5	0.019	4.17	0.787	0.787	0.921	1.346	0.731	128
0.242	901.9	0.019	4.00	0.779	0.060	0.914	4.144	1.465	137
0.314	907.6	0.019	3.01	0.776	0.131	0.926	4.579	1.940	130
0.490	896.6	0.020	2.07	0.784	0.086	0.882	4.815	3.354	134
0.664	906.9	0.019	1.53	0.784	0.076	0.835	3.952	3.969	147
1.000	898.1	0.019	0.97	0.807	-----	0.845	3.538	4.852	180
0.125	873.0	0.044	2.04	0.831	0.922	0.892	2.048	0.030	192
0.147	901.2	0.044	2.27	0.911	0.901	0.874	2.720	0.380	182
0.222	888.8	0.043	3.07	0.888	0.900	0.942	4.792	2.478	128
0.294	890.7	0.043	3.40	0.824	0.220	0.956	11.930	5.027	143
0.357	905.9	0.043	2.76	0.913	0.122	0.936	13.815	5.892	150
0.445	902.9	0.043	2.21	0.864	0.154	0.921	13.265	6.913	161
0.608	883.8	0.043	1.62	0.905	0.185	0.900	11.401	8.145	176
1.000	826.6	0.043	1.00	0.869	-----	0.898	7.210	10.928	212
0.122	1189.4	0.019	1.90	0.780	0.852	0.880	1.249	0.488	199
0.169	1194.2	0.020	3.03	0.809	0.847	0.906	1.722	0.829	165
0.218	1191.2	0.020	3.64	0.772	0.799	0.935	2.159	2.021	136
0.267	1189.5	0.020	3.57	0.769	0.062	0.921	8.534	3.981	133
0.398	1198.5	0.020	2.42	0.778	0.111	0.901	7.695	5.511	147
0.655	1196.7	0.020	1.55	0.779	0.053	0.894	6.453	6.402	181

TABLE B.5

TWO-PHASE DATA FOR $D_3/D_1 = 0.82$

$\frac{\dot{m}_3}{\dot{m}_1}$	G_1 (kg/m^{2}s)	x_1	$\frac{\dot{x}_3}{\dot{x}_1}$	α_1	α_2	α_3	$(\Delta P_{2-1})_j$ (kPa)	$(\Delta P_{1-3})_j$ (kPa)	P_1
0.100	426.6	0.152	3.20	0.970	0.975	0.982	4.884	1.088	163
0.157	447.0	0.158	3.57	0.988	0.983	0.984	9.666	6.213	132
0.217	449.9	0.156	3.00	0.980	0.934	0.983	8.608	10.103	148
0.433	428.4	0.149	2.21	0.937	0.084	0.969	8.290	20.291	192
0.553	411.5	0.143	1.85	0.967	0.113	0.961	7.034	23.862	197
0.068	596.3	0.045	2.04	0.866	0.892	0.939	0.636	-0.095	150
0.085	569.6	0.042	4.15	0.898	0.905	0.951	1.558	0.025	141
0.132	608.1	0.047	4.40	0.897	0.846	0.961	2.263	1.762	120
0.153	590.1	0.046	4.82	0.878	0.793	0.958	2.760	2.349	123
0.303	619.9	0.046	3.12	0.861	0.143	0.931	7.765	5.833	141
0.507	596.1	0.045	1.85	0.879	0.061	0.922	5.736	7.117	153
0.693	606.2	0.044	1.36	0.911	0.108	0.947	4.096	8.483	169
0.894	598.3	0.043	1.09	0.892	0.047	0.918	3.275	9.124	189
1.000	602.7	0.042	0.98	0.880	-----	0.922	3.439	10.323	187
0.092	604.6	0.087	3.13	0.953	0.926	0.925	2.296	0.730	147
0.135	595.8	0.087	3.85	0.925	0.890	0.975	5.796	3.858	130
0.200	602.0	0.080	3.73	0.917	0.914	0.970	6.542	6.741	144
0.340	599.1	0.081	2.71	0.908	0.218	0.955	8.885	11.588	181
0.792	582.1	0.073	1.21	0.913	0.054	0.907	8.337	18.331	209

TABLE B.6

TWO-PHASE DATA FOR $D_3/D_1 = 0.50$

$\frac{\dot{m}_3}{\dot{m}_1}$	G_1 (kg/m^{2}s)	x_1	$\frac{\dot{x}_3}{\dot{x}_1}$	α_1	α_2	α_3	$(\Delta P_{2-1})_j$ (kPa)	$(\Delta P_{1-3})_j$ (kPa)	P_1
0.098	483.2	0.043	4.23	0.844	0.839	0.950	1.283	3.618	123
0.058	596.2	0.046	1.39	0.858	0.909	0.923	1.406	0.339	150
0.086	593.7	0.044	3.98	0.883	0.830	0.937	1.668	3.839	132
0.116	591.2	0.048	4.58	0.906	0.813	0.953	1.816	10.153	160
0.147	595.2	0.048	5.01	0.882	0.734	0.853	1.815	15.425	191
0.210	579.2	0.045	4.36	0.850	0.161	0.877	2.743	19.868	224
0.104	589.1	0.081	4.04	0.966	0.896	0.980	3.182	13.208	155
0.126	561.5	0.080	4.02	0.958	0.870	0.984	2.882	18.437	192
0.069	896.8	0.019	4.56	0.764	0.763	0.900	1.892	1.502	146
0.088	901.5	0.021	5.21	0.789	0.773	0.945	1.900	3.629	138
0.109	905.6	0.019	6.59	0.768	0.725	0.923	1.926	8.367	166
0.128	898.0	0.023	6.81	0.733	0.701	0.905	3.010	13.668	193
0.159	893.9	0.022	5.67	0.783	0.134	0.902	4.227	14.492	207
0.177	897.6	0.021	5.03	0.797	0.089	0.893	4.379	13.560	207
0.118	868.5	0.044	4.32	0.893	0.791	0.960	4.508	17.697	196
0.134	882.7	0.045	3.90	0.880	0.756	0.945	3.402	21.893	220
0.049	1158.8	0.018	2.25	0.768	0.737	0.866	2.195	0.073	214
0.075	1163.4	0.021	1.15	0.798	0.743	0.904	2.730	2.565	206
0.102	1200.3	0.022	4.99	0.815	0.719	0.968	3.206	9.787	174